Studies on the Photocatalytic Conversion of CO_2 in and by H_2O over Heterogeneous Photocatalysts

Zheng Wang

2015

Preface

It is widely accepted that the increasing of atmospheric CO_2 owing to various human activities such as energy production and transport, is the major cause of global warming. Since the Kyoto protocol ratification by many countries, the development of adequate methods to remove CO_2 from the atmosphere has become more and more important in order to control climate change. There are several methods to reduce CO_2: the capture and geological storage of the gas to form stable carbonates, absorption into various functionalized materials, and large-scale forestation. However, those solutions are in fact energy intensive and costly. One alternative method, artificial conversion of CO_2 to other useful chemical compounds using the abundant solar energy, has attracted much attention.

As we all know, plant photosynthesis has been employed for both conversion of CO_2 to organics and conversion of solar energy to chemical energy. This means plants can store the solar energy, especially visible light energy, in the form of chemical bonds and utilize water as the reductant to produce O_2. Therefore, artificial photosynthesis for the CO_2 conversion and utilization should achieve these essential features in plant photosynthesis. The photocatalytic conversion of CO_2 using H_2O as the electron donor over heterogeneous photocatalysts is one potential approach as artificial photosynthesis.

In this thesis, the author found that the photocatalytic conversion of CO_2 in and by water could proceed over Zn-modified Ga_2O_3, $ZnGa_2O_4$, $La_2Ti_2O_7$, and SrO-modified Ta_2O_5 photocatalysts, which were loaded with Ag metal as a cocatalyst. CO was evolved as the main product for the reduction of CO_2 and H_2 production from

overall water splitting was largely suppressed. The simultaneous evolution of O_2 in a stoichiometric ratio proved that H_2O could function as an electron donor during the photocatalytic conversion of CO_2 in water. Among all the photocatalysts, Zn-modified Ga_2O_3 and $ZnGa_2O_4$ exhibited the highest activity and selectivity towards CO evolution. According to the investigation, we demonstrated that the photocatalytic activity and selectivity for the conversion of CO_2 in and by H_2O largely depends on the crystallization and the surface modification of photocatalysts. High crystallinity can facilitate the migration and separation of photogenerated charges, thus improve the photocatalytic activity. The surface modification with metal oxides on the photocatalysts is an effective method to suppress the competition reaction of overall water splitting and promote the reduction of CO_2. The introduction of Ag cocatalyst also affects both the activity and selectivity. Furthermore, the addition of various salts and alkalis into reaction solution plays an important role for the photocatalytic conversion of CO_2 in and by H_2O.

The studies presented in this thesis were performed at Department of Molecular Engineering, Graduate School of Engineering, Kyoto University from 2011 to 2014 under the supervision of Professor Tsunehiro Tanaka and Professor Kentaro Teramura. The author wishes to express his sincere gratitude to Professor Tsunehiro Tanaka for his precise guidance and valuable suggestions in the work and his paternal encouragements and cares in the life of staying in Japan. Special acknowledgements are made to Professor Kentaro Teramura who gave the author the conscientious and patient direction, the insightful discussions and the best supports for the research. The author is deeply grateful to Professor Tetsuya Shishido of Tokyo Metropolitan University for his fruitful advices and continual stimulations. Cordial thanks are given to Dr. Saburo Hosokawa

for his effective discussions and considerate help. The author appreciates the significant assistances and discussions from Dr. Tomoyuki Kitano, Mr. Hiroyuki Asakura, Dr. Shinya Furukawa and Dr. Osamu Tomita.

Meanwhile, the author shows gratitude to Prof. Yoshihisa Sakata of Yamaguchi University who kindly supplied the materials for the research in Chapter 1. The author is indebted to Mr. Akira Yamamoto, Ms. Lidan Deng, and Mr. Shoji Iguchi for their kindhearted help and discussions in the experiments. The author had a pleasurable collaboration with Mr. Hiroyuki Tatsumi on the studies of photocatalytic conversion of CO_2 by H_2O using Ta_2O_5-based and Ga_2O_3-based materials, thanks a lot for his smart thinking and diligent working. The author is also grateful to every student in the laboratory of Professor Tsunehiro Tanaka because of their impressive friendship and help. Special thanks are conveyed to Secretary Ms. Ayako Tanaka and Ms. Mami Nishio for their aids in official affairs.

Finally, the author sincerely thanks his parents, his wife and his family members for their understanding and encouragement.

Zheng Wang

Kyoto
2014

CONTENTS

General Introduction

Principle of Photocatalytic conversion of CO_2

The photocatalytic conversion of CO_2 over photocatalysts is triggered by the light irradiation. Absorption of light by a photocatalyst electrode or particles causes the transition of an electron from the valence band (VB) to the conduction band (CB) leaving a hole in the valence band. Both an excited electron (e^-) and a hole (h^+) are generated simultaneously in the CB and VB, respectively.[1,2] The photogenerated electron with sufficient reduction potential would be transferred to adsorbed CO_2 and used for CO_2 reduction. Because protons can easily receive the excited electron, hydrogen evolution often competes with the reduction of CO_2, and this is one of the most serious problems in the field. On the other hand, the photogenerated hole is consumed by electron donors such as water, organic molecule, hydrogen and so on. In order to utilize water as a reductant, the top of the VB must be positioned more positively than the oxidation potential of water. However, very few photocatalysts could make use of water as a reductant for the photocatalytic conversion of CO_2.

Taking the thermodynamics into consideration, CO_2 is one of the most stable molecules among carbon compounds. The molecule consists of a linear connection of a carbon and two oxygen atoms (O=C=O) and it does not have a dipole moment. Therefore, in comparison of Gibbs free energy for the desired carbon compounds (ΔG_f^o = −51 kJ mol^{-1} for CH_4, ΔG_f^o = −137 kJ mol^{-1} for CO and ΔG_f^o = −166 kJ mol^{-1} for CH_3OH), the energetic stability of the CO_2 molecule (ΔG_f^o = −394 kJ mol^{-1}) appears to be a strong limitation.[3] This fact makes CO_2 reduction a highly endothermic process, even more difficult than the water splitting reaction (ΔG_f^o = −228 kJ mol^{-1} for liquid

H_2O).

Regarding the electronic mechanism of the reduction of CO_2, CO_2 can be reduced by receiving one or several electrons to become the corresponding reduced forms. Equation (1) indicates that the one-electron transfer to form $\bullet CO_2^-$ (at pH 7 in an aqueous solution, vs NHE[4]) is highly endothermic and unfavorable. However, formation of $\bullet CO_2^-$ may be the first step for the photoreduction of CO_2. The experimental data revealed that adsorbed CO_2 was photocatalytically reduced to form the carbonate anion radical ($\bullet CO_2^-$),[5-7] it is suggested that the special interaction between the photocatalyst surface and CO_2 is very important. Afterwards, the carbonate anion radical ($\bullet CO_2^-$) is further reduced by receiving multiple electrons with protons, formate anion (HCO_2^-), carbon monoxide (CO), formaldehyde (HCHO), methanol (CH_3OH) and methane (CH_4) are obtained as the products of the photocatalytic reduction of CO_2, as shown in (2)~(6).

$$CO_2 + e^- \rightarrow CO_2^- \qquad E^o = -1.90\ V \qquad (1)$$

$$CO_2 + 2H^+ + 2e^- \rightarrow HCOOH \qquad E^o = -0.61\ V \qquad (2)$$

$$CO_2 + 2H^+ + 2e^- \rightarrow CO + H_2O \qquad E^o = -0.53\ V \qquad (3)$$

$$CO_2 + 4H^+ + 4e^- \rightarrow HCHO + H_2O \qquad E^o = -0.48\ V \qquad (4)$$

$$CO_2 + 6H^+ + 6e^- \rightarrow CH_3OH + H_2O \qquad E^o = -0.38\ V \qquad (5)$$

$$CO_2 + 8H^+ + 8e^- \rightarrow CH_4 + 2H_2O \qquad E^o = -0.24\ V \qquad (6)$$

Therefore, an efficient photocatalyst would have to overcome the important mechanistic challenges which involve (i) the adequate band gap energy for the reduction potential of CO_2; (ii) the suitable catalytic sites for the adsorption and activation of CO_2; (iii) the efficient multielectron transfer with protons (or hydrogen radicals).

At present, many reported photocatalysts are constructed with metal complexes, organic compounds, and semiconductors combined with various cocatalysts, such as

metal complexes, metal particles, and enzymes. Typically, the reported photocatalysts for the reduction of CO_2could be classified into two categories: homogeneous and heterogeneous systems. In this study, we focus on the heterogeneous photocatalysts. In 1979, Fujishima et al. examined the use of photocatalyst powders for CO_2 reduction.[8] These included TiO_2, ZnO, CdS, SiC and WO_3, suspended in CO_2-saturated water illuminated by a Xe lamp. Small amounts of formic acid, formaldehyde, methyl alcohol, and methane were produced. Since then, various other photocatalytic systems that employ heterogeneous photocatalysts have been studied. Although there remain many problems, such as low activity of catalysts and low selectivity of the products, further development of photocatalysts is an essential target.

TiO_2 and Titanium Based Photocatalysts

Since the earliest report of Fujishima and co-workers, TiO_2 and Ti-based materials have been studied deeply due to the low cost, stability and performance. In 1983, Halmann et al. evaluated the CO_2 reduction ability of TiO_2, $SrTiO_3$, and $CaTiO_3$ photocatalysts under natural sunlight illumination.[9] The light energy conversion efficiencies were estimated to be 0.001~0.016% only. The use of Cu and Ag as cocatalysts was reported by Wu et al,[10] moist CO_2 was photocatalytically reduced to methanol under UV irradiation. The UV-light induced reduction of CO_2 to CH_4 using various metal-deposited (Pd, Rh, Pt, Au, Cu, and Ru) TiO_2 particles in water has been investigated.[11] The Pd-deposited TiO_2 (Pd-TiO_2) was the most efficient photocatalyst in such systems. Photoreduction of gaseous CO_2 to CO with hydrogen over Rh-loading TiO_2 was investigated by Kohno et al.[12] When Rh in Rh/TiO_2 was strongly reduced to be in a fully metallic state, or the loading amount of Rh was raised, the activity was lowered and the main product shifted from CO to CH_4.

Nano-shaped TiO_2 with high surface area can facilitate efficient charge transfer and enhance the photocatalytic activity. Titania nanotubes[13,14] has been used for the photocatalyitc reduction of CO_2 and EPR spectroscopy indicated that the nanotube structure effectively facilitated the charge separation and enhanced the CO_2 reduction to CH_4. Grimes et al. reported efficient solar conversion of CO_2 with water vapor to CH_4 and other hydrocarbons was achieved using nitrogen-doped titania nanotube arrays.[15] Using outdoor global AM 1.5 sunlight, a hydrocarbon production rate of 111 $ppm \cdot cm^{-2} \cdot h^{-1}$, was obtained when the nanotube array samples were loaded with both Cu and Pt nanoparticles. Recently, a CuO-$TiO_{2-x}N_x$ hollow nanocube for the photocatalytic conversion of CO_2 into CH_4 under solar irradiation is reported by Schaak et al.[16] The catalytic performance of CuO-$TiO_{2-x}N_x$ hollow nanocube is also impressive.

Recently, Kudo et al. reported that Ag cocatalyst-loaded $ALa_4Ti_4O_{15}$ (A = Ca, Sr, and Ba) photocatalysts with layered perovskite structures showed excellent activities for CO_2 reduction to form CO and HCOOH by bubbling CO_2 gas into the aqueous suspension of the photocatalyst powder.[17] $BaLa_4Ti_4O_{15}$ showed higher photocatalytic activity for CO_2 reduction than $SrLa_4Ti_4O_{15}$ and $CaLa_4Ti_4O_{15}$. CO was the main reduction product rather than H_2 in an aqueous medium on the optimized $Ag/BaLa_4Ti_4O_{15}$ photocatalyst. The evolutions of H_2 CO and O_2 were in a stoichiometric ratio (H_2 + CO : O_2 = 2 : 1 in a molar ratio), which indicated that water was consumed as a reducing reagent (an electron donor) for the reduction of CO_2.

Other Oxide Photocatalyst

Besides the TiO_2 and titanium-based catalysts, various metal oxides are employed in the photocatalytic reduction of CO_2. ZrO_2 has been largely reported.[5,18-24] Sayama and Arakawa reported the use of 1% Cu-loaded ZrO_2 as a

catalyst for photocatalytic reduction of CO_2 to CO in an aqueous solution of $NaHCO_3$ under UV irradiation.[18] Although H_2, O_2 and CO were stoichiometrically produced over Cu-loaded ZrO_2, decomposition of H_2O was a main reaction in the aqueous solution.[18] In 1997, Kohno et al. reported that gaseous CO_2 was reduced to CO by hydrogen on a ZrO_2 photocatalyst without loading a cocatalyst under UV light irradiation.[23] They also found that the photocatalytic reduction of CO_2 with CH_4 proceeded over ZrO_2 at room temperature.[24] The yield of CO was originated not from CH_4, but from CO_2.

The photocatalytic reduction of CO_2 by H_2 was also examined on MgO.[25] Teramura et al. revealed that surface bidentate formate species can act as photocatalytically active species, which convert another CO_2 molecule to CO molecule upon photoirradiation.[7] Teramura et al. also reported that Ga_2O_3 promoted the photoreduction of CO_2 by H_2 to yield CO selectively.[26] The highest yield of CO was obtained when the amount of adsorbed H_2 reached saturation. The use of $ATaO_3$ (A = Li, Na, K) compound oxides for the photocatalytic reduction of CO_2 in the presence of H_2 was reported by Teramura et al. subsequently.[27] The activity for the generation of CO was in the order: $LiTaO_3$ > $NaTaO_3$ > $KTaO_3$. In addition, Teramura et al. used layered double hydroxides (LDHs) to obtain significant amounts of CO and O_2 gas in the photocatalytic conversion of CO_2 in water.[28] GC-Mass results of isotope labeled CO_2 reduction revealed that CO was produced from gaseous CO_2.

Large specific surface area of catalysts could enhance the photocatalytic activity due to the exposure of sufficient catalytic sites. Zou et al. reported that the mesoporous $ZnGa_2O_4$ showed good photocatalytic activity for converting CO_2 into CH_4 under UV light irradiation, because of strong gas adsorption and large specific surface

area.[29] They also synthesized single-crystalline Zn_2GeO_4 nanoribbons for the photocatalytic reduction of CO_2 into CH_4 in the presence of water vapor under UV irradiation.[30] Moreover, the ultrathin and uniform Bi_2WO_6 square nanoplates showed great potential in the utilization of visible light energy to the highly efficient reduction of CO_2 into CH_4.[31] They concluded that the ultralong and ultrathin geometry improves the specific surface area and facilitates the separation and transfer of the photogenerated electrons and holes. Although the photocatalytic reduction of CO_2 is still in its infancy, these results demonstrate a significant step toward making more efficient photocatalysts for CO_2 capture and reuse.

Nonoxide Photocatalyst

Due to the durability and high performance, metal oxides have been widely researched. Until now, there are only a few reports about nonoxide photocatalysts for photocatalytic CO_2 reduction, such as p-SiC[8,32], p-GaP[33], ZnS[34], CdS[35,36], $Cd_xZn_{1+x}S$[37] and so on. Cook et al. reported the reduction of CO_2 to CH_4, C_2H_4, and C_2H_6 as a function of electrolyte pH using a mixture of p-SiC and Cu particles.[32] CdS can be used as a visible-light-driven photocatalyst for the reduction of CO_2 to CO in a DMF solution containing TEA as a reductant.[35] Sulfur vacancies on the surface of the CdS nanocrystallites played an important role in the CdS-DMF system. ZnS also worked as a photocatalyst for CO_2 reduction to formic acid using TEA as a reductant.[34] The addition of Cd^{2+} enhanced the photocatalytic ability of ZnS, the highest quantum efficiency of production was twice as large as that obtained on bare ZnS microcrystals.[37]

Hybrid System

In recent years, novel photocatalytic CO_2 reduction systems, which combine

semiconductors and other functional units, have been reported. Heterostructured CdSe quantum dots-sensitized Pt/TiO_2 catalyst was used for the photocatalytic reduction of CO_2 under visible light illumination (λ>420nm).[38] When quantum confinement shifts the conduction band of CdSe quantum dots to higher energy, electron transfer from CdSe quantum dots to TiO_2 occured. Therefore, visible light irradiation of the $CdSe/Pt/TiO_2$ hybrid catalyst in an aqueous solution gives the primary product CH_4, with CH_3OH, H_2, and CO as secondary products. A newly-designed two-step photoexcitation system for the reduction of CO_2 and the oxidation of H_2O was established.[39] The hybrid photocatalyst for the selective reduction of CO_2 was a combination of an indium phosphide (InP), p-type semiconductor, and ruthenium complex polymer electrocatalyst(MCE). The photoreduction of CO_2 to $HCOO^-$ using H_2O as an electron donor and proton source was performed by functionally conjugating the InP/[MCE] photocatalyst for the reduction of CO_2 with a Pt/TiO_2 photocatalyst for the oxidation of H_2O. The conversion efficiency from solar energy to chemical energy was 0.03~0.04% which approaches that for photosynthesis in a plant.

Perspective

Recently, the number of reports about the reduction of CO_2 using various photocatalysts has been increasing rapidly. Most metal oxide photocatalysts have advantages in the durability and the use of water as a reductant. However, the conversion efficiency of the reduction of CO_2 remains quite low, mainly due to the competition with H_2 production from water splitting. The development of effective photocatalysts and photocatalytic systems for the reduction of CO_2 using H_2O as the electron donor should be promoted and the details of mechanism behind this reaction remain to be uncovered. Moreover, the visible-light-driven photocatalysts for the

photocatalytic reduction of CO_2 need to be exploited, because a large portion of solar light on earth is visible light. It should be noted that, in many cases, the carbon source of the products has not been identified. Since the organic contaminants can be both carbon sources and reductants of the reaction products in photocatalytic reduction of CO_2 using TiO_2,[40] careful experiments should always be carried out to clarify the origin of products for CO_2 conversion, such as isotopic labeled experiments using $^{13}CO_2$.

Outline of the Present Thesis

This thesis focuses on the photocatalytic conversion of CO_2 using H_2O as the reductant over Zn-modified Ga_2O_3, $ZnGa_2O_4$, $La_2Ti_2O_7$, and SrO-modified Ta_2O_5 photocatalysts, which were loaded with Ag metal as a cocatalyst. CO was evolved as the main product for the reduction of CO_2 together with O_2 production from the oxidation of H_2O in all the cases. This thesis consists of six chapters.

Chapter 1 describes that Ga_2O_3 photocatalysts exhibit the high conversion of CO_2, modification of Zn species onto Ga_2O_3 supresses the H_2 evolution derived from overall water splitting, and consequently, Ag-loaded Zn-modified Ga_2O_3 exhibits higher selectivity toward CO evolution than does Ag-loaded bare Ga_2O_3. Stoichiometric amounts of O_2 was observed being evolved together with CO. Mass spectrometry clarified that the carbon source of CO evolved was not the residual carbon species on the photocatalyst surface but was the CO_2 introduced in the gas phase.

Chapter 2 further found that the selectivity towards CO evolution between CO and H_2 over the Ag-loaded Zn-modified Ga_2O_3 photocatalyst gradually increased with the increment of Zn addition whereas the evolution of CO was not affected. XRD, XAFS and XPS revealed that the formation of $ZnGa_2O_4$ layer on the surface of Ga_2O_3

obstructs the reduction of protons in the photocatalytic conversion of CO_2 in and by H_2O.

In Chapter 3, the effect of various additives on the photocatalytic conversion of CO_2 by H_2O over the Ag-loaded Zn-modified Ga_2O_3 photocatalyst was investigated. It was found that the major carbon species in the aqueous solutions of weak acid salts and alkalis was HCO_3^- during the photocatalytic reaction, which was related to the high activity for CO evolution. Moreover, the maintenance of the equilibrium between the dissolved CO_2 molecules and the HCO_3^- species was very important for the photocatalytic conversion of CO_2 with H_2O in the presence of weak acid salt and alkaline additives.

Chapter 4 shows the high activity and selectivity for the photocatalytic conversion of CO_2 by H_2O using Ag-loaded $ZnGa_2O_4$ photocatalyst. The maximum photocatalytic activity of $ZnGa_2O_4$ was achieved by making a balance between the crystallinity and the surface area. Furthermore, the formation of metallic Ag particles with different sizes and dispersions on the surface of $ZnGa_2O_4$ also influenced the evolution of CO.

Chapter 5 reported that Ag-modified $La_2Ti_2O_7$ with a layered perovskite structure exhibits activity for the photocatalytic conversion of CO_2 to CO in pure water. Maximization of the photocatalytic activity of $La_2Ti_2O_7$ was accomplished by making a trade-off between the crystallite size and surface area. In addition, the loading amount and modification method of the Ag cocatalyst also influenced the amount of CO evolved.

In Chapter 6, we found that addition of alkaline earth metal oxides into Ag-loaded Ta_2O_5 (Ag/Ta_2O_5) suppresses the H_2 production derived from overall water

splitting for the photocatalytic conversion of CO_2 by H_2O as an electron donor. It was demonstrated that the tiny amount of SrO dramatically changed the selectivity toward to CO evolution. In addition, we confirmed that Ag cocatalyst also influences on the selectivity toward to CO evolution and relatively small Ag nanoparticles indicate the high effecency.

Reference:

[1] A. Fujishima, K. Honda, *Nature* **1972**, *238*, 37.

[2] Y. Shiraishi, T. Hirai, *J. Photochem. Photobiol. C.* **2008**, *9*, 157.

[3] A. Kubacka, M. Fernández-García, G. Colón, *Chem. Rev.* **2012**, *112*, 1555.

[4] V. P. Indrakanti, J. D. Kubicki, H. H. Schobert, *Energy. Environ. Sci.* **2009**, *2*, 745.

[5] Y. Kohno, T. Tanaka, T. Funabiki, S. Yoshida, *Phys. Chem. Chem. Phys.* **2000**, *2*, 2635.

[6] J. H. Lunsford, J. P. Jayne, *J. Phys. Chem.* **1965**, *69*, 2182.

[7] K. Teramura, T. Tanaka, H. Ishikawa, Y. Kohno, T. Funabiki, *J. Phys. Chem. B* **2004**, *108*, 346.

[8] T. Inoue, A. Fujishima, S. Konishi, K. Honda, *Nature* **1979**, *277*, 637.

[9] M. Halmann, M. Ulman, B. Aurian-Blajeni, *Sol. Energy* **1983**, *31*, 429.

[10] J. C. S. Wu, T. H. Wu, T. Chu, H. Huang, D. Tsai, *Top. Catal.* **2008**, *47*, 131.

[11] O. Ishitani, C. Inoue, Y. Suzuki, T. Ibusuki, *J. Photochem. Photobiol. A* **1993**, *72*, 269.

[12] Y. Kohno, H. Hayashi, S. Takenaka, T. Tanaka, T. Funabiki, S. Yoshida, *J. Photochem. Photobiol. A* **1999**, *126*, 117.

[13] K. Schultea, P. DeSariob, K. Gray, *Appl. Catal. B* **2010**, *97*, 354.

[14] B. Vijayan, N. M. Dimitrijevic, T. Rajh, K. Gray, *J. Phys. Chem. C* **2010**, *114*,

12994.

[15] O. Varghese, M. Paulose, T. LaTempa, C. Grimes, *Nano. Lett.* **2009**, *9*, 731.

[16] S. I. In, D. Vaughn II, R. Schaak, *Angew. Chem.* **2012**, *124*, 3981.

[17] K. Iizuka, T. Wato, Y. Miseki, K. Saito, A. Kudo, *J. Am. Chem. Soc.* **2011**, *133*, 20863.

[18] K. Sayama, H. Arakawa, *J. Phys. Chem.* **1993**, *97*, 531.

[19] C. C. Lo, C. H. Hung, C. S. Yuan, J. F. Wu, *Sol. Energy. Mater. Sol. Cells.* **2007**, *91*, 1765.

[20] T. Tanaka, Y. Kohno, S. Yoshida, *Res. Chem. Intermed.* **2000**, *26*, 93.

[21] Y. Kohno, T. Tanaka, T. Funabiki, S. Yoshida, *Phys. Chem. Chem. Phys.* **2000**, *2*, 5302.

[22] Y. Kohno, T. Tanaka, T. Funabiki, S. Yoshida, *J. Chem. Soc. Faraday. Trans.* **1998**, *94*, 1875.

[23] Y. Kohno, T. Tanaka, T. Funabiki, S. Yoshida, *Chem. Commun.* **1997**, 841.

[24] Y. Kohno, T. Tanaka, T. Funabiki, S. Yoshida, *Chem. Lett.* **1997**, 993.

[25] Y. Kohno, H. Ishikawa, T. Tanaka, T. Funabiki, S. Yoshida, *Phys. Chem. Chem. Phys.* **2001**, *3*, 1108.

[26] K. Teramura, H. Tsuneoka, T. Shishido, T. Tanaka, *Chem. Phys. Lett.* **2008**, *467*, 191.

[27] K. Teramura, S. Okuoka, H. Tsuneoka, T. Shishido, T. Tanaka, *Appl. Catal. B.* **2010**, *96*, 565.

[28] K. Teramura, S. Iguchi, Y. Mizuno, T. Shishido, T. Tanaka, *Angew. Chem. Int. Ed.* **2012**, *51*, 8008.

[29] S. Yan, S. Ouyang, J. Gao, M. Yang, J. Feng, X. Fan, L. Wan, Z. Li, J. Ye, Y. Zhou,

Z. Zou, *Angew. Chem. Int. Ed.* **2010**, *49*, 6400.

[30] Q. Liu, Y. Zhou, J. Kou, X. Chen, Z. Tian, J. Gao, S. Yan, Z. Zou, *J. Am. Chem. Soc.* **2010**, *132*, 14385.

[31] Y. Zhou, Z. Tian, Z. Zhao, Q. Liu, J. Kou, X. Chen, J. Gao, S. Yan, Z. Zou, *Appl. Mater. Interfaces.* **2011**, *3*, 3594.

[32] R. L. Cook, R. C.Macduff, A. F.Sammells, *J. Electrochem. Soc.* **1988**, *135*, 3069.

[33] E. E. Barton, D. M. Rampulla, A. B. Bocarsly, *J. Am. Chem. Soc.* **2008**, *130*, 6342.

[34] M. Kanemoto, H. Hosokawa, Y. Wada, K. Murakoshi, S. Yanagida, T. Sakata, H. Mori, M. Ishikawa, H. Kobayashi, *J. Chem. Soc. Faraday. Trans*. **1996**, 92, 2401.

[35] H. Fujiwara , H. Hosokawa , K. Murakoshi , Y. Wada , S. Yanagida, *J. Phys. Chem. B* **1997**, *101*, 8270.

[36] B. J. Liu, T. Torimoto, H. Yoneyama, *J. Photochem. Photobiol. A* **1998**, *113*, 93.

[37] H. Inoue, H. Moriwaki, K. Maeda, H. Yoneyama, *J. Photochem. Photobiol. A* **1995**, *86*, 191.

[38] C. J. Wang, R. L. Thompson, J. Baltrus, C. Matranga, *J. Phys. Chem. Lett.* **2010**, *1*, 48.

[39] S. Sato, T. Arai, T. Morikawa, K. Uemura, T. M. Suzuki, H. Tanaka, T. Kajino, *J. Am. Chem. Soc.* **2011**, *133*, 15240.

[40] C. C. Yang, Y. H. Yu, B. Linden, J. C. S. Wu, G. Mul, *J. Am. Chem. Soc.* **2010**, *132*, 8398.

Chapter 1

Highly Selective Photocatalytic Conversion of CO_2 with H_2O over Ag-loaded Zn-modified Ga_2O_3

Abstract

Photocatalytic conversion of CO_2 to reduction products such as CO, HCOOH, HCHO, CH_3OH, and CH_4 is one of the most attractive propositions for producing green energy by artificial photosynthesis. Herein, we found that Ga_2O_3 photocatalysts exhibit the high conversion of CO_2, modification of Zn species into Ga_2O_3 supresses the H_2 evolution derived from overall water splitting, and consequently, Ag-loaded Zn-modified Ga_2O_3 exhibits higher selectivity toward CO evolution than does Ag-loaded bare Ga_2O_3. We observed stoichiometric amounts of O_2 being evolved together with CO. Mass spectrometry clarified that the carbon source of CO evolved was not the residual carbon species on the photocatalyst surface but was the CO_2 introduced in the gas phase. Modification of the photocatalyst with Zn is expected to establish the surface property that CO_2 can be adsorbed easily.

Introduction

Artificial photosynthesis has been drawing a lot of attention as one of the most attractive new-generation energy production systems.[1] Plants carry out photosynthesis using sunlight and water to obtain energy required for their own growth. Humans, on the other hand, are looking to generate liquid fuel for our various needs from inexhaustible sunlight and water by artificial photosynthesis. Artificial photosynthesis replicates the natural process of photosynthesis and comprises four steps: (1) light-harvesting, (2) charge transfer, (3) oxidation of H_2O, and (4) fuel production (the protons and electrons generated during water splitting can subsequently be used to reduce carbon dioxide to storable fuels such as CO, HCOOH, HCHO, CH_3OH, and CH_4). Various water-splitting methods have been investigated previously. However, the use of heterogeneous photocatalysts to split water into stoichiometric amounts of H_2 and O_2 (overall water splitting) is of particular interest because of its simplicity (all the four steps can be carried out in the same system) and low cost of operation. Many research groups have already made significant progress in the field of water splitting to produce pure H_2 and O_2; in contrast, studies on the photocatalytic conversion of CO_2 using H_2O as a reductant are very few. This is because in such systems, overall water splitting occurs together with the reduction of CO_2, resulting in H_2 being the main product. Thus, it is very important to control the reduction of protons in the presence of both CO_2 and H_2O in order to achieve the reduction of CO_2 by H_2O.

Kudo and colleagues reported that $ALa_4Ti_4O_{15}$ (A = Ca, Sr, and Ba), known as an effective photocatalyst for overall water splitting, when loaded with Ag as a cocatalyst exhibited good selectivity to CO evolution (i.e., CO was the main reduction product rather than H_2) during the photocatalytic conversion of CO_2 in water.[2] To the

best of our knowledge, this is the only the report stating that stoichiometric amounts of CO, H_2, and O_2 were generated in water and that the selectivity towards CO evolution was higher than that towards H_2 evolution derived from overall water splitting. On the other hand, we have previously reported that ZrO_2[3], MgO[4], $ATaO_3$ (A = Li, Na, and K)[5], and Ga_2O_3[6], exhibit photocatalytic activity in the conversion of CO_2 in the presence of H_2, of which Ga_2O_3 exhibited the highest conversion of CO_2: 7.8% over 48 h of photoirradiation). Unfortunately, these bare metal oxides do not function as photocatalysts for the conversion of CO_2 in the presence of H_2O. However, it is known that overall water splitting occurs over a bare Ga_2O_3 photocatalyst.[7] Recently, Kang *et al.* reported that highly porous Ga_2O_3 exhibits a higher activity for CO and CH_4 evolutions than typical Ga_2O_3[8]; however, the amounts of CO and CH_4 evolved were tiny, and no evolution of O_2 was observed. We previously demonstrated that Ga_2O_3 modified with Zn was one of the best photocatalysts for overall water splitting under UV irradiation. Formation rates of 21.0 mmol h^{-1} for H_2 and 10.5 mmol h^{-1} for O_2 were achieved over Zn-modified Ga_2O_3 loaded by $Rh_{0.5}Cr_{1.5}O_3$ as a cocatalyst under UV irradiation.[9] In this study, we found that Zn-modified Ga_2O_3 exhibits a higher conversion of CO_2 compared to several photocatalysts reported previously. In addition, we revealed that the photocatalytic conversion of CO_2 by H_2O proceeds in priority to the overall water splitting over Zn-modified Ga_2O_3 in the presence of CO_2, resulting in high selectivity towards CO evolution.

Experimental Section

Zn-modified Ga_2O_3 was fabricated as reported previously.[9] Two kinds of Ga_2O_3 precursors were used in this study: a commercial sample supplied by High Purity Chemical and a homemade sample obtained by the hydrolysis of $Ga(NO_3)_3$ with

aqueous NH_3. The amount of Zn species was fixed at 3 mol% against the total amount of metal species (Ga atoms and Zn atoms). The photocatalytic conversion of CO_2 in H_2O, including modification of the photocatalysts, if any, was carried out using a quartz inner-irradiation-type reaction vessel (1.0 L) in a quasi-flowing batch system. The fabricated photocatalysts (1.0 g) were modified with 1 wt% of a Ag co-catalyst by a typical *in situ* photodeposition method. To do this, the photocatalysts—Ga_2O_3 and Zn-modified Ga_2O_3—were dispersed in an aqueous solution of $AgNO_3$ and then illuminated for 4 h. Inductively coupled plasma (ICP) analysis clarified that 2.3% of $AgNO_3$ introduced (2.16 μmol) still remained in the solution. Then, $NaHCO_3$ (0.1 mol L^{-1}) was added to the same solution, and the suspension was irradiated under a 400 W high-pressure mercury lamp via a quartz filter equipped with a cooling water system. CO_2 gas (99.999%) was bubbled into the water at a flow rate of 30 mL min^{-1}. The products such as CO, H_2, and O_2 were analyzed by thermal conductivity detector-gas chromatography (TCD-GC) using a GC-8A chromatograph (Shimadzu Corp.) equipped with an Molecular Sieve 5A column (carrier gas: Ar) and by flame ionization detector-gas chromatography (FID-GC) using a methanizer and a Shincarbon ST column (carrier gas: N_2). In an isotopic experiment using $^{13}CO_2$, the formation of ^{13}CO and ^{12}CO were observed by mass spectroscopy using a quadrupole-type mass spectrometer (BEL Japan, Inc., BEL Mass).

Results and discussions

CO was evolved as the main product during the photocatalytic conversion of CO_2 over 1 wt% Ag-loaded Zn-modified Ga_2O_3 under UV irradiation, as shown in Figure 1. H_2 was simultaneously generated as the reduction product similar to CO, although the amount of H_2 evolved was tiny as compared to that of CO. Expectedly, the

evolution of O_2 was observed together with those of CO and H_2, although most of the research groups did not succeed using their photocatalysts. We confirmed that no CH_4 was generated in the gas phase. Other products in the solution, such as HCOOH, HCHO, and CH_3OH, were not detected by HPLC. After 7 h of photoirradiation, we obtained 815 μmol of CO, 65.7 μmol of H_2, and 479 μmol of O_2. The reaction could be carried out stably over three times, indicating that Ag-loaded Zn-modified Ga_2O_3 is very stable in water and under photoirradiation. The recycled photocatalyst exhibited the same activity (Figure 2). The XRD pattern of Ag-loaded Zn-modified was similar before and after the reaction (Figure 3). The pH of the solution, which could be monitored during the reaction, did not change much, and remained between 6.7 and 6.8

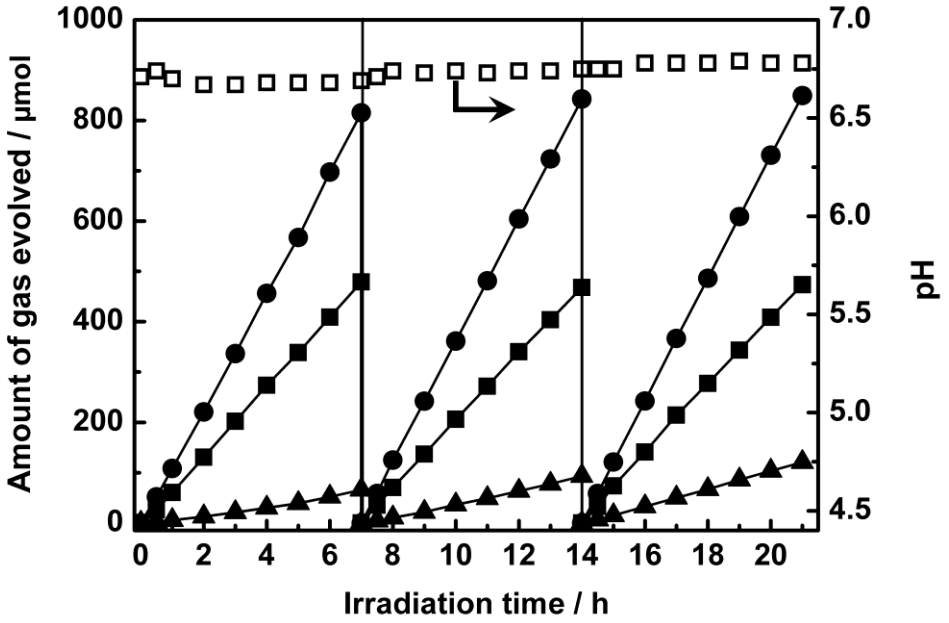

Figure 1 Time course of CO (circle), H_2 (triangle), and O_2 (square) evolved for the photocatalytic conversion of CO_2 by H_2O over Ag-loaded Zn-modified Ga_2O_3. Amount of catalyst under photoirradiation using a 400 W high-pressure mercury lamp: 1.0 g, volume of water: 1.0 L, CO_2 flow rate: 30 mL min^{-1}, additve: $NaHCO_3$ (0.1 mol L^{-1}).

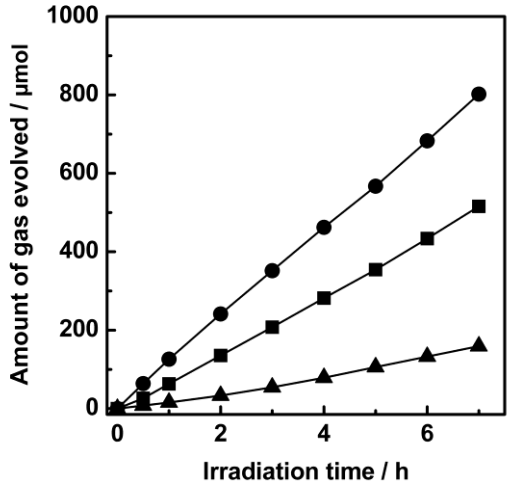

Figure 2 Time course of CO (circle), H_2 (triangle), and O_2 (square) evolved for the photocatalytic conversion of CO_2 by H_2O over recycled Ag-loaded ZnO-modified Ga_2O_3.

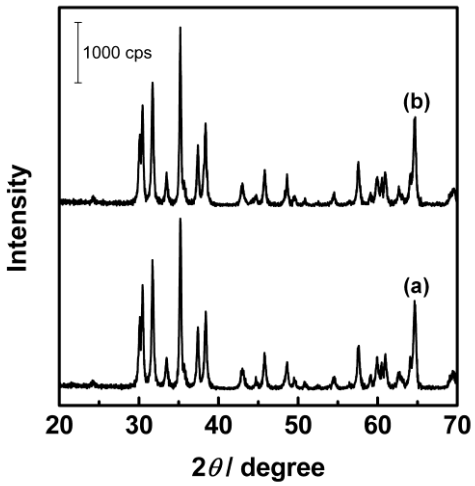

Figure 3 XRD patterns of Zn-doped Ga_2O_3 (a) before the reaction and (b) after the reaction.

because CO_2 was continuously supplied to the solution. We believe that Ag-loaded Zn-modified Ga_2O_3 is one of the most valuable photocatalysts as it exhibits a high conversion of CO_2 and selective evolution of CO in the presence of H_2O. 1g of the photocatalyst contains 93.6 μmol of Ag metal as a cocatalyst, and the turnover number (TON) was approximately 8.7 after 7 h, indicating that the conversion of CO_2 to CO proceeds photocatalytically presumably with Ag metal particles on the surface functioning as sites for the reduction of CO_2.

To achieve highly selective conversion to CO, all the following components of the system—(a) Ag-loaded Zn-modified Ga_2O_3 photocatalyst, (b) photoirradiation, (c) CO_2 bubbling, (d) an Ag cocatalyst, and (e) a $NaHCO_3$ additive, are necessary. We carried out the five blank tests in the absence of each component and handled the reaction without any carbon sources as shown in Figure 4. Justifiably, the reactions did

not proceed without a Ga_2O_3 photocatalyst or photoirradiation (Figures 4(a) and (b)). When inert Ar gas was flowed into the reactor instead of CO_2, H_2 was evolved exponentially in comparison to CO, which was derived from the bicarbonate (HCO_3^-) of $NaHCO_3$ that added as an additive (Figure 4(c)). The rate of CO evolved steadily decreased with photoirradiation time because HCO_3^- was consumed in the solution. On the other hand, the amount of O_2 evolved rose linearly. This means that the reduction of HCO_3^- takes place in competition with the reduction of protons (H^+) to H_2. Bubbling of CO_2 improved the selectivity towards CO evolution while suppressing that of H_2. The Ag cocatalyst is also a very important factor in achieving the photocatalytic conversion of CO_2 by H_2O selectively (Figure 4(d)). H_2 and O_2 were generated stoichiometrically with tiny amounts of evolved CO. Hori *et al*. reported that Ag functions as a good electrode for the electrochemical reduction of CO_2 into CO.[10] In addition, Kudo *et al.* pointed out the availability of the Ag cocatalyst for CO evolution in the photocatalytic conversion of CO_2.[2] The evolution of H_2 was suppressed by the introduction of the Ag cocatalyst, resulting in the dramatic enhancement in the selective evolution of CO. Accordingly, in our case, CO_2 would be reduced to CO on the surface of the Ag metal species, acting as a cocatalyst. The effect of various additives including $NaHCO_3$ was reported by Sayama *et al*.[11] The presence of HCO_3^- accelerated the rate of CO evolved and decelerated the rate of H_2 evolved under a flow of CO_2 (Figure 4(e)). On the other hand, we confirmed that CO was not deifinitely evolved without any carbon sources like CO_2 and $NaHCO_3$ (Figure 4(f)). In this case, nearly stoichiometric rates of H_2 and O_2 evolved were observed. Tiny amount of CO evolved was detected under a flow of CO_2, which means that CO_2 acts as an intert gas like Ar. Interestingly, the same time course was obtained as Figure 4(e) in case that $NaHCO_3$ was introduced

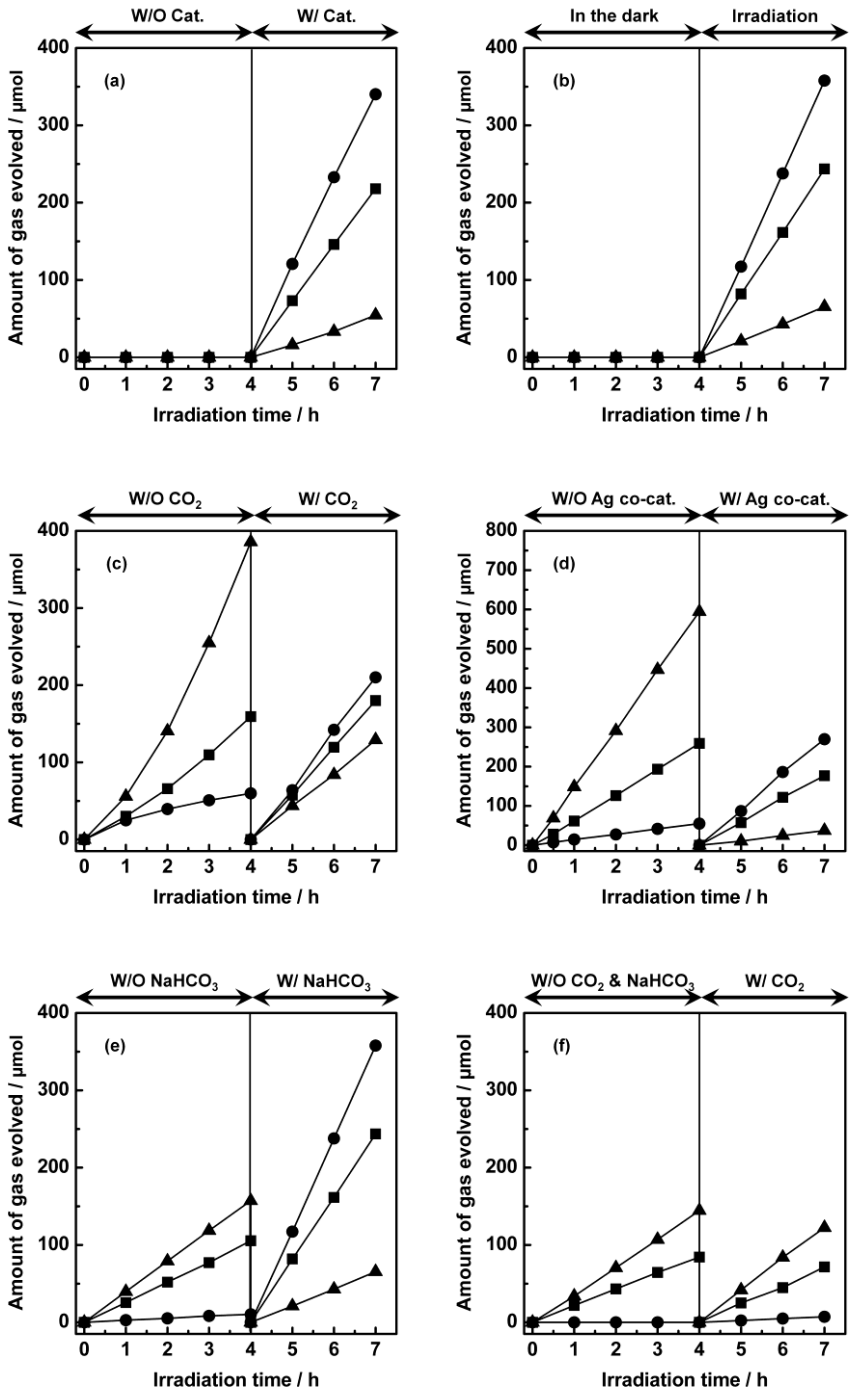

Figure 4 Time course of CO (circle), H_2 (triangle), and O_2 (square) evolved for the photocatalytic conversion of CO_2 by H_2O without (a) a Ag-loaded Zn-modified Ga_2O_3 photocatalyst, (b) photoirradiation, (c) CO_2 bubbling, (d) an Ag cocatalyst, (e) a $NaHCO_3$ additive, and (f) CO_2 and $NaHCO_3$. Amount of catalyst: 1.0 g, volume of water: 1.0 L, flow rate of CO_2: 30 mL min^{-1}, concentration of $NaHCO_3$: 0.1 mol L^{-1}.

to this suspension. Accordingly, it is concluded that $NaHCO_3$ plays an important role in this reaction; however, the details are under investigation.

The rate of evolutions of all the products reached a steady-state quickly (after approximately 2 h of photoirradiation). The steady-state formation rates are obtained by an exponential curve fitting as shown in Figure 5. Table 1 shows the steady-state formation rates of H_2, O_2, and CO evolved for the photocatalytic conversion of CO_2 in

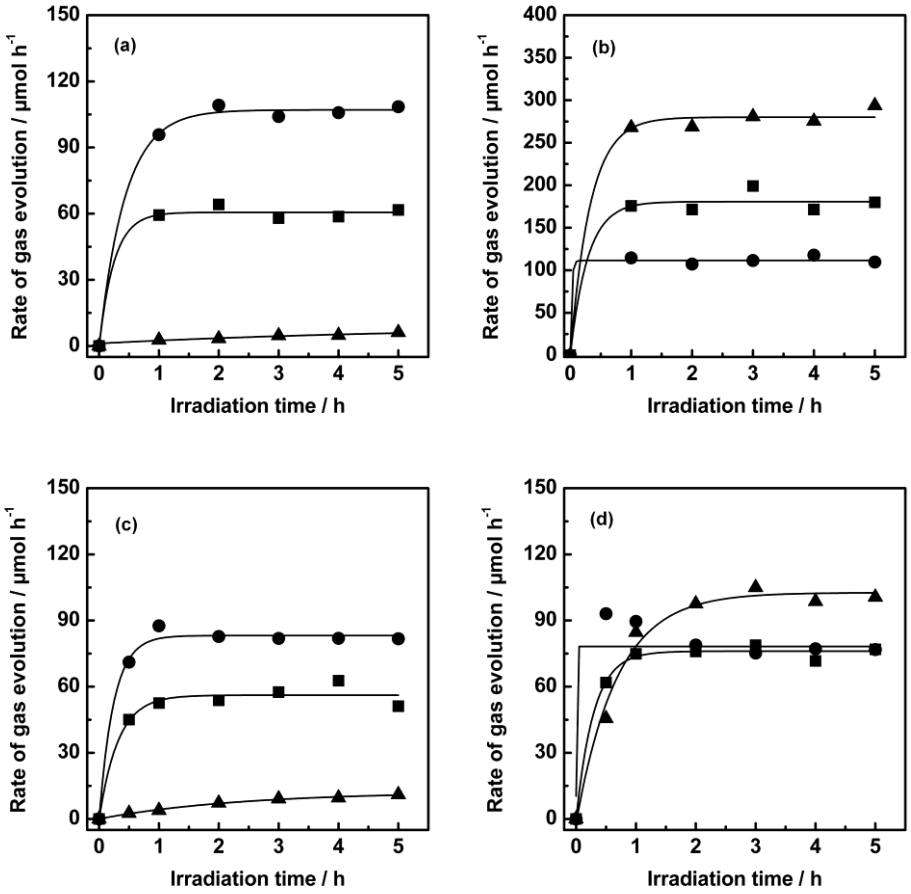

Figure 5 Time course of rate of CO (circle), H_2 (triangle), and O_2 (square) evolved for the photocatalytic conversion of CO_2 by H_2O over (a) Ag-loaded Zn-modified homemade Ga_2O_3, (b) Ag-loaded homemade Ga_2O_3, (c) Ag-loaded Zn-modified commercial Ga_2O_3, and (d) Ag-loaded commercial Ga_2O_3. Amount of catalyst: 1.0 g, volume of water: 1.0 L, CO_2 flow rate: 30 mL min^{-1}, additve: $NaHCO_3$ (0.1 mol L^{-1}).

H_2O over four Ga_2O_3-based photocatalysts. As described above, Ag-loaded Zn-modified Ga_2O_3 exhibits a higher conversion of CO_2 and selective evolution of CO. The rate of H_2 evolved was only 16.9 μmol h^{-1}; on the other hand, CO was generated from CO_2 at a rate of 117 μmol h^{-1} (Entry 1). Generally, holes and electrons are generated simultaneously in a photocatalytic reaction, indicating that oxidation should occur together with reduction (so-called, redox reaction). If H_2O did indeed work as a reductant in the photocatalytic conversion of CO_2, it should be possible to accurately determine the stoichiometric rate of O_2 evolved. In our case, 70.1 μmol h^{-1} of O_2 was generated nearly stoichiometrically against the evolutions of CO and H_2. It is expected that CO_2 is efficiently reduced by H_2O over an Ag-loaded Zn-modified Ga_2O_3 photocatalyst. Surprisingly, bare Ga_2O_3, which was fabricated in the same manner barring the Zn modification process, did not exhibit good selectivity towards CO evolution. It is easy to compare the rates of H_2 and CO evolved because both H_2 and CO are redox reaction products. When bare Ga_2O_3 was used as a photocatalyst, the stoichiometric reaction could not be observed. In this case, the rate of H_2 evolution (266 μmol h^{-1}) was higher than that of CO evolution (95.3 μmol h^{-1}) (Entry 2). This result indicates that modification by Zn affects the selectivity towards CO evolution. Zn modification of commercial Ga_2O_3 also enhanced the selectivity towards CO evolution for the photocatalytic conversion of CO_2 (Entry 3). Interestingly, in the case of bare commercial Ga_2O_3, H_2 evolution was dominant over CO evolution (Entry 4). Of special interest is that the selectivity towards CO evolution observed for Zn-modified commercial Ga_2O_3 was approximately consistent with that observed for Zn-modified homemade Ga_2O_3.

Table 1 Formation rate of H_2, O_2, and CO and consumption rate of generated electrons and holes for the photocatalytic conversion of CO_2 by H_2O[a]

Entry	Sample	Formation rate / μmol h^{-1}			Reacted electrons / μmol h^{-1}	Reacted holes / μmol h^{-1}	Sel.
		H_2	O_2	CO			
1	Zn-Ga_2O_3 (homemade)	8.9	60.6	108	234	242	92.4
2	Ga_2O_3 (homemade)	280	181	111	782	724	28.4
3	Zn-Ga_2O_3 (commercial)	14.4	56.1	82.0	192	224	85.1
4	Ga_2O_3 (commercial)	101	72.7	73.7	349	291	42.2

[a] Amount of catalyst: 1.0 g, volume of water: 1.0 L, flow rate of CO_2: 30 mL min^{-1}, concentration of $NaHCO_3$: 0.1 mol L^{-1}

Recently, the photocatalytic conversion of CO_2 in and by H_2O has attracted a great deal of attention from a number of scientists and engineers. Although many related articles have been published, very few research groups have investigated the origin of the carbon source of the reduction products such as CO using $^{13}CO_2$. In our opinion, it is necessary to confirm the origin of the carbon source of the products by mass spectrometry or ^{13}C NMR. Especially, Mul *et al.* insisted on the risk that we evaluate the formation of CO not from introduced CO_2 but residual carbon species on the surface of photocatalyst.[12] The utilization of $^{13}CO_2$ will prevent us from getting a false idea. Figure 6 shows mass spectra (m/z 28 and 29) during the photocatalytic conversion of $^{13}CO_2$ by H_2O over Ag-loaded Zn-modified Ga_2O_3. Sampling gases were introduced into a mass spectrometer after separation by a gas chromatograph. ^{13}CO was monitored at 5.3 min and m/z = 29. The peak position was consistent with that detected by GC.

The predominant product was ^{13}CO. Amount of ^{13}CO evolved estimated by the mass spectrometer was approximately consistent with amount of CO evolved determined by FID-GC. In conclusion, CO was generated from the CO_2 introduced in the gas phase. We succeeded in designing a highly selective photocatalytic conversion of CO_2 to CO using Ag-loaded Zn-modified Ga_2O_3. In particular, we highlight that O_2 was stoichiometrically evolved and that CO was derived from the introduced CO_2. It was found that the modification of bare Ga_2O_3 photocatalysts with Zn remarkably enhanced the selectivity towards CO evolution. Although the precise cause of it is not been well known as yet, we believe that the surface property has an effect on the selectivity towards CO evolution as well as the mobility of both electrons and holes.

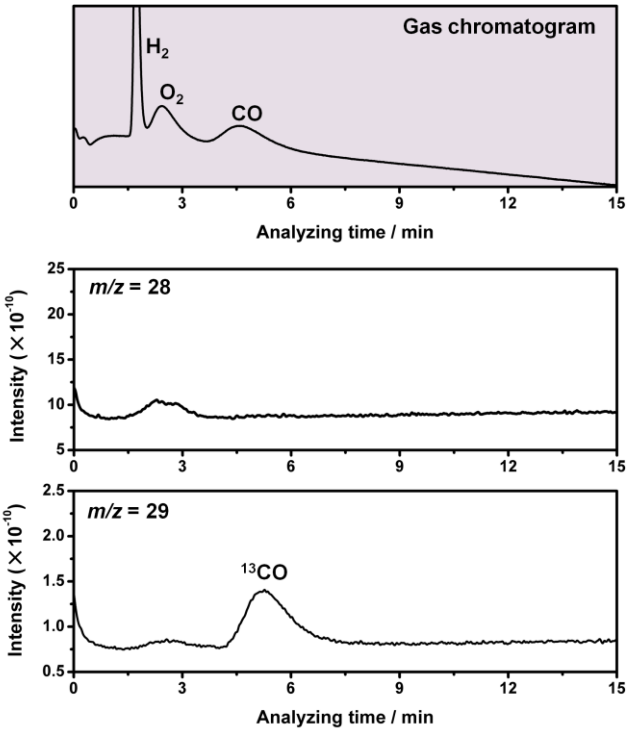

Figure 6 Gas chromatogram and mass spectra (m/z 28 and 29) during the photocatalytic conversion of $^{13}CO_2$ in water over Ag-loaded Zn-modified Ga_2O_3. Amount of catalyst: 1.0 g, volume of water: 1.0 L, CO_2 flow rate: 30 mL min^{-1}, concentration of $NaHCO_3$: 0.1 mol L^{-1}

Conclusion

We succeeded in designing a highly selective photocatalytic conversion of CO_2 to CO using Zn-modified Ga_2O_3. In particular, we highlight that O_2 was stoichiometrically evolved and that CO was derived from the introduced CO_2. It was found that the doping of bare Ga_2O_3 photocatalysts with Zn remarkably enhanced the selectivity towards CO evolution. Although the precise cause of it is not been well known as yet, we believe that the surface property has an effect on the selectivity towards CO evolution as well as the mobility of both electrons and holes.

Reference

[1] a) N. S. Lewis, D. G. Nocera, *Proc. Natl. Acad. Sci. USA* **2006**, *103*, 15729; b) H. Inoue, T. Shimada, Y. Kou, Y. Nabetani, D. Masui, S. Takagi, H. Tachibana, *ChemSusChem* **2011**, *4*, 173; c) O. Ishitani, *CSJ Current Review* **2010**, *2*, 81; d) K. Maeda, K. Domen, *J. Phys. Chem. Lett.* **2010**, *1*, 2655; e) A. Kudo, Y. Miseki, *Chem. Soc. Rev.* **2009**, *38*, 253.

[2] K. Iizuka, T. Wato, Y. Miseki, K. Saito, A. Kudo, *J. Am. Chem. Soc.* **2011**, *133*, 20863.

[3] a) Y. Kohno, T. Tanaka, T. Funabiki, S. Yoshida, *Chem. Commun.* **1997**, 841; b) Y. Kohno, T. Tanaka, T. Funabiki, S. Yoshida, *Chem. Lett.* **1997**, 993; c) Y. Kohno, T. Tanaka, T. Funabiki, S. Yoshida, *J. Chem. Soc. Faraday Trans.* **1998**, *94*, 1875; d) Y. Kohno, T. Tanaka, T. Funabiki, S. Yoshida, *Phys. Chem. Chem. Phys.* **2000**, *2*, 2635.

[4] a) Y. Kohno, H. Ishikawa, T. Tanaka, T. Funabiki, S. Yoshida, *Phys. Chem. Chem. Phys.* **2001**, *3*, 1108; b) K. Teramura, T. Tanaka, H. Ishikawa, Y. Kohno, T. Funabiki, *J.*

Phys. Chem. B **2004**, *108*, 346.

[5] K. Teramura, S.-i. Okuoka, H. Tsuneoka, T. Shishido, T. Tanaka, *Appl. Catal. B* **2010**, *96*, 565.

[6] H. Tsuneoka, K. Teramura, T. Shishido, T. Tanaka, *J. Phys. Chem. C* **2010**, *114*, 8892.

[7] T. Yanagida, Y. Sakata, H. Imamura, *Chem. Lett.* **2004**, *33*, 726.

[8] H.-a. Park, J. H. Choi, K. M. Choi, D. K. Lee, J. K. Kang, *J. Mater. Chem.* **2012**, *22*, 5304.

[9] a) Y. Sakata, Y. Matsuda, T. Yanagida, K. Hirata, H. Imamura, K. Teramura, *Catal. Lett.* **2008**, *125*, 22; b) Y. Sakata, Y. Matsuda, T. Nakagawa, R. Yasunaga, H. Imamura, K. Teramura, *ChemSusChem* **2011**, *4*, 181.

[10] Y. Hori, K. Kikuchi, S. Suzuki, *Chem. Lett.* **1985**, 1695.

[11] K. Sayama, H. Arakawa, *J. Photochem. Photobiol., A* **1996**, *94*, 67.

[12] C.-C. Yang, Y.-H. Yu, B. van der Linden, J. C. S. Wu, G. Mul, *J. Am. Chem. Soc.* **2010**, *132*, 8398.

Chapter 2

Tuning the selectivity toward CO evolution in the photocatalytic conversion of CO_2 by H_2O through the modification of Ag-loaded Ga_2O_3 with a $ZnGa_2O_4$ layer

Abstract

Stoichiometric evolutions of CO, H_2, and O_2 were achieved for the photocatalytic conversion of CO_2 by H_2O as an electron donor using Ag-loaded Zn-modified Ga_2O_3 that was calcined at high temperature. The selectivity toward the evolution of CO over H_2 can be controlled by varying the addition of Zn species in the Ag-loaded Zn-modified Ga_2O_3 photocatalyst. The production of H_2 gradually decreased with increasing amounts of Zn species from 0.1 to 10.0 mol%, whereas the evolution of CO was almost unchanged. The XRD, XAFS, and XPS measurements revealed that a $ZnGa_2O_4$ layer was generated on the surface of Ga_2O_3 by modification with the Zn species. The formation of the $ZnGa_2O_4$ layer eliminated the proton reduction sites on Ga_2O_3, although the morphology, surface area, and crystallinity of Ga_2O_3 did not change. In conclusion, we designed a highly selective photocatalyst for the conversion of CO_2 by H_2O as an electron donor using Ag (cocatalyst for the CO evolution), $ZnGa_2O_4$ (inhibitor of the H_2 production), and Ga_2O_3 (photocatalyst).

Introduction

Conversion of CO_2 into useful carbon sources such as CO, HCOOH, HCHO, CH_3OH, and CH_4 is currently attracting considerable interest because of the demand for methods to recycle CO_2 as a natural resource.[1-3] In order to achieve the reduction of CO_2, H_2 or CH_4 is usually fed as a reducing agent.[1,4] However, H_2O is the preferred reductant, because it is a rich source of hydrogen, harmless, and abundant. The photocatalytic conversion of CO_2 by H_2O over heterogeneous photocatalysts, regarded as artificial photosynthesis, is a promising route for sustainable energy development.[5-7] If H_2O does function as the electron donor then it is important to obtain a stoichiometric ratio between the amount of O_2 evolved and CO_2 reduced. Moreover, the reduction of H^+, released from H_2O molecules, usually competes with CO_2 reduction when several heterogeneous materials are used as photocatalysts in the presence of both CO_2 and H_2O for the reduction of CO_2 by H_2O. Generally, the production of H_2 via the reduction of H^+ is the dominant pathway.[5,8] Therefore, to achieve high selectivity in the photocatalytic conversion of CO_2 by H_2O, the electrons generated through the oxidation of H_2O must be controlled to selectively reduce CO_2.

Although various photocatalysts such as TiO_2,[9,10] $BiVO_4$,[11] $ZnGa_2O_4$,[12] and Zn_2GeO_4[13] have been reported for the reduction of CO_2 with H_2O under photoirradiation, the evolution of O_2 was not observed in these reactions. Therefore, the function of H_2O as an electron donor in this reaction is a controversial subject. Moreover, the synthesis gas (syngas for short, H_2 and CO), a raw feed material in the Fischer–Tropsch synthesis and other syngas-to-syncrude technologies, can be directly produced through the photocatalytic conversion of CO_2 using H_2O as an electron donor. The adjustment of synthesis gas composition (H_2:CO ratio) is essential for the

Fischer–Tropsch technology.[14] Thus, the selectivity between CO and H_2 in the photocatalytic conversion of CO_2 by H_2O needs to be finely tuned. Sayama *et al*. found that Cu-modified ZrO_2 could produce CO and H_2 with the evolution of O_2 in an aqueous solution of $NaHCO_3$.[15] However, the selectivity of the generated electrons for reducing CO_2 was quite low, indicating that the main reaction was still the reduction of H^+ into H_2. Recently, Kudo *et al*. reported that $ALa_4Ti_4O_{15}$ (A = Ca, Sr, and Ba) loaded with a Ag cocatalyst showed good activity for the stoichiometric evolution of CO, H_2, and O_2.[16] Therefore, modification of the catalyst's surface with Ag nanoparticles is effective for inhibiting the production of H_2 during the photocatalytic reduction of CO_2. In addition, $KCaSrTa_5O_{15}$ was reported to be active for the photocatalytic conversion of CO_2 to CO utilizing H_2O as an electron donor.[17] However, controlling the selectivity of the generated electrons for the reduction of CO_2 was difficult with $KCaSrTa_5O_{15}$. Previously, we found that the selectivity toward CO evolution surpasses 90% for the photocatalytic conversion of CO_2 by H_2O over Ag-loaded Zn-modified Ga_2O_3, although the production of H_2 proceeded preferentially over Ag-loaded Ga_2O_3.[18] Addition of the Zn species into the Ag-loaded Ga_2O_3 improved the selectivity for CO evolution because of the suppression of H_2 production. Therefore, understanding the role of the Zn species in the highly selective photocatalytic conversion of CO_2 by H_2O is necessary for further photocatalyst development. In this study, we characterized the Zn species using XAFS, XRD, and XPS measurements, and demonstrated the formation of a $ZnGa_2O_4$ structure on the surface of Ga_2O_3.

Experimental section

Ga_2O_3 was fabricated by the precipitation method as reported previously.[18]

$Ga(NO_3)_3 \cdot xH_2O$ (12 g, Kojundo, 99.999%) was first dissolved in distilled water (200 mL). Then an aqueous ammonia solution (28 wt%) was added dropwise to the aqueous solution of $Ga(NO_3)_3 \cdot xH_2O$ until a pH value of approximately 8.9 was reached. A white precipitate was centrifuged, washed extensively with distilled water (500 mL), and dried at 353 K in air to obtain the gallium hydroxide precursor. Ga_2O_3 was obtained by calcining the precursor at 1273 K for 6 h. Zn-modified Ga_2O_3 was synthesized by an impregnation method. The as-prepared Ga_2O_3 was dispersed in an aqueous solution containing various amounts of $Zn(NO_3)_2$ by ultrasonication. After drying under vacuum at room temperature, the solid mixture of Ga_2O_3 and $Zn(NO_3)_2$ was calcined at 1223 K for 6 h. The amount of Zn species varied from 0 to 10.0 mol% of the total amount of metal species (Ga atoms and Zn atoms).

A Ag cocatalyst (1 wt%) was loaded on the Zn-modified Ga_2O_3 and Ga_2O_3 by an *in-situ* photodeposition method. First, $AgNO_3$ (1 wt%) was added into the reaction suspension, and then the Ag co-catalyst was deposited on Zn-modified Ga_2O_3 and Ga_2O_3 under photoirradiation. The photocatalytic reaction was carried out in a flow system using an inner-irradiation-type reaction vessel at room temperature and ambient pressure. The photocatalyst (1.0 g) was dispersed in ultra-pure water (1.0 L) containing a $NaHCO_3$ additive (0.1 M), and CO_2 (99.999%) was bubbled into the solution at a flow rate of 30 mL min^{-1}. The suspension was irradiated under a 400 W high-pressure mercury lamp with a quartz filter connected to a cooling water system. Gaseous products such as H_2, O_2, and CO were analyzed by thermal conductivity detector-gas chromatography (TCD-GC) using a GC-8A chromatograph (Shimadzu Corp.) equipped with a Molecular Sieve 5A column (carrier gas: Ar), and by flame ionization detector-gas chromatography (FID-GC) using a methanizer and a Shincarbon ST

column (carrier gas: N_2).

The UV-Vis diffuse reflectance spectra (UV-Vis DRS) were measured by a JASCO V-670 spectrometer equipped with an integrating sphere. Spectralon®, which was supplied by Labsphere Inc., was used as a standard reflection sample such as $BaSO_4$. SEM images were obtained with a KEYENCE VE-9800 scanning electron microscope (SEM). The structure and crystallinity of Zn-modified Ga_2O_3 samples were characterized by X-ray diffraction (XRD) using a Rigaku Multi Flex powder X-ray diffractometer. The Zn K-edge (9659 eV) and Ga K-edge (10367 eV) X-ray absorption fine structure (XAFS) measurements were made in the transmission mode at the BL01B1 beamline of the SPring-8 synchrotron radiation facility (Hyogo, Japan). The spectra were reduced with the Rigaku REX2000 program Ver. 2.5.9 (Rigaku Corp.). The XPS measurement was acquired using an X-ray photoelectron spectrometer (5500MT, ULVAC PHI, Kanagawa, JAPAN) equipped with a hemispherical energy analyzer. The Brunauer–Emmett–Teller (BET) surface area was measured by N_2 adsorption at 77 K using a volumetric gas adsorption apparatus (BELmini, Bel Japan, Inc.).

Results and Discussion

Figure 1 shows the formation rates of CO, H_2, and O_2 and selectivity toward CO evolution for the photocatalytic conversion of CO_2 by H_2O over Ag-loaded Zn-modified Ga_2O_3 with various amounts of Zn species. All photocatalysts tested could stoichiometrically produce CO, H_2, and O_2 under photoirradiation. These results indicate that H_2O acted as an electron donor and the number of photogenerated electrons used in the reduction of CO_2 and H^+ was similar to that of photogenerated holes consumed by the oxidation of H_2O. However, the selectivity of the generated electrons toward the reduction of CO_2 was quite different, and depended on the amount

of Zn species. The formation rate of H_2 over the Ag-loaded Ga_2O_3 without the Zn species was much higher than that of CO, hence the selectivity of the generated electrons toward the reduction of CO_2 was only 28.5%. When Ga_2O_3 was modified with 0.1 mol% of Zn species, the production of H_2 was suppressed. The formation rate of H_2 decreased proportionally with the increase in the amount of Zn species, and was negligible for Zn species concentrations higher than 3.0 mol%. In contrast, the formation rate of CO was not influenced by the amount of Zn species added. Eventually, the selectivity for CO evolution over Ag-loaded Zn-modified Ga_2O_3 gradually increased with elevated amounts of Zn species. When the Zn content was more than 3.0 mol%, the selectivity for CO evolution approached 100%, implying that only the reduction of CO_2 and oxidation of H_2O proceeded on the Ag-loaded Zn-modified Ga_2O_3.

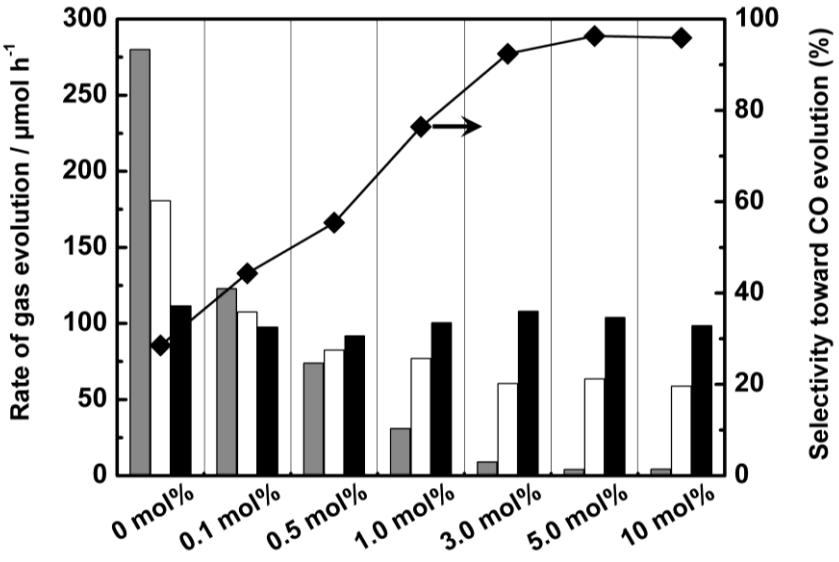

Figure 1 Rates of CO (black), O_2 (white), and H_2 (gray) evolution and selectivity toward CO evolution in the photocatalytic conversion of CO_2 by H_2O over Ag-loaded Zn-modified Ga_2O_3 with various amounts of Zn species. Reaction conditions: Amount of catalyst, 1.0 g; cocatalyst: 1.0 wt%; volume of water, 1.0 L; flow rate of CO_2, 30 mL min^{-1}; concentration of $NaHCO_3$, 0.1 mol L^{-1}; light source, high-pressure mercury lamp (400 W).

The UV-Vis diffuse reflectance spectra of bare Ga_2O_3 and Zn-modified Ga_2O_3 with various amounts of Zn species are shown in Figure 2. The bare Ga_2O_3 exhibited an absorption edge at 265 nm and the bandgap energy of Ga_2O_3 was estimated as 4.6 eV according to the Davis–Mott's equation.[19] Modification of Ga_2O_3 with different amounts of Zn species did not change the absorption edge of the spectra, thus

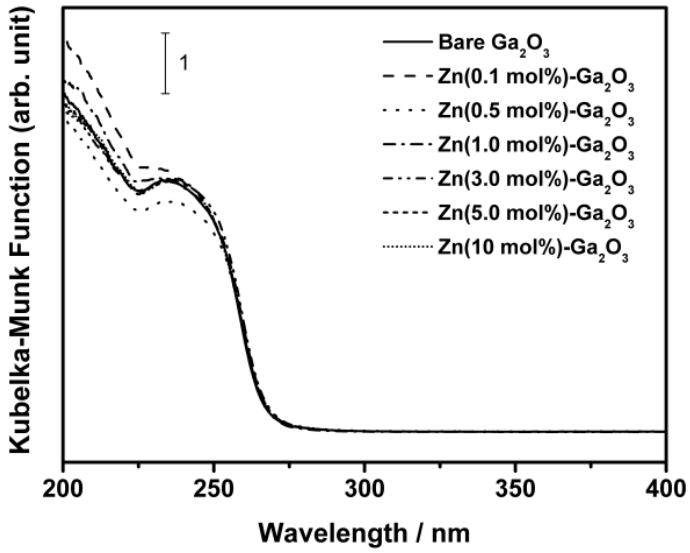

Figure 2 UV-Vis DRS of Zn-modified Ga_2O_3 with various Zn loading amount.

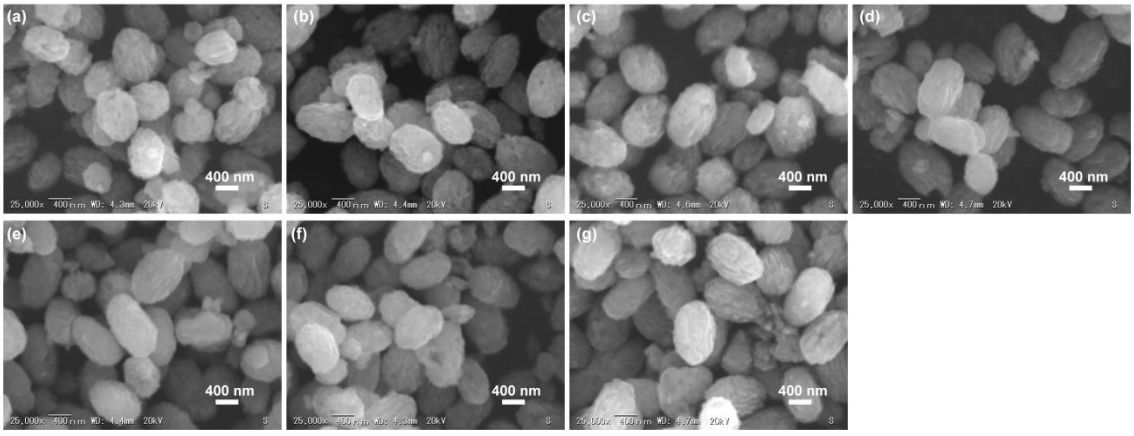

Figure 3 SEM images of bare Ga_2O_3 (a) and Zn-modified Ga_2O_3 with 0.1 mol% (b), 0.5 mol% (c), 1.0 mol% (d), 3.0 mol% (e), 5.0 mol% (f), and 10.0 mol% (g) of Zn species.

the addition of Zn species did not contribute to the band structure of Ga_2O_3. Figure 3 shows the SEM images of Ga_2O_3 with and without modification by Zn species. As shown, modification of Ga_2O_3 with various amounts of Zn species caused insignificant changes in the particle size compared to bare Ga_2O_3. Moreover, the morphology of each Zn-modified Ga_2O_3 with different amounts of Zn species was similar to that of bare Ga_2O_3. Since the light harvesting ability and surface morphology of Ga_2O_3 remained unchanged after modification with the Zn species, the altered selectivity toward CO evolution in the photocatalytic conversion of CO_2 must occur for a different reason than the addition of Zn species.

Zn-modified Ga_2O_3 was treated at high temperature after the impregnation of Ga_2O_3 with $Zn(NO_3)_2$, which means that the Zn ions should either form a new compound at the surface of Ga_2O_3 or be incorporated into the bulk structure of Ga_2O_3. Figure 4(A) shows the XRD patterns of bare Ga_2O_3 and Zn-modified Ga_2O_3 with various amounts of Zn species. Ga_2O_3 was calcined at 1273 K before the introduction of Zn species, thus all the samples exhibited the same monoclinic structure, β-Ga_2O_3, which is a thermally stable phase of the five polymorphic phases of Ga_2O_3. For the addition of Zn species from 0.1 mol% to 1.0 mol%, the XRD patterns of Zn-modified Ga_2O_3 were similar to that of bare Ga_2O_3. However, a diffraction peak representing the (311) facet of the $ZnGa_2O_4$ structure was observed in the XRD pattern of 3.0 mol% Zn-modified Ga_2O_3. This indicates that the Zn species react with Ga_2O_3 to generate $ZnGa_2O_4$, and the crystallinity of the $ZnGa_2O_4$ structure in Zn-modified Ga_2O_3 is promoted by adding higher amounts of Zn species. Furthermore, the diffraction peak of $ZnGa_2O_4$ became sharper and higher as the amount of Zn species was increased. When the amount of Zn species reached 10.0 mol%, the peaks for the (311), (400), (422), and

(440) facets of $ZnGa_2O_4$ were clearly observed. Therefore, based on the XRD results, the formation of highly crystalline $ZnGa_2O_4$ may be responsible for the highly selective photocatalytic conversion of CO_2 by H_2O, because the 3.0 mol%, 5.0 mol%, and 10.0 mol% Zn-modified Ga_2O_3 exhibited much higher selectivity toward CO evolution than the other samples.

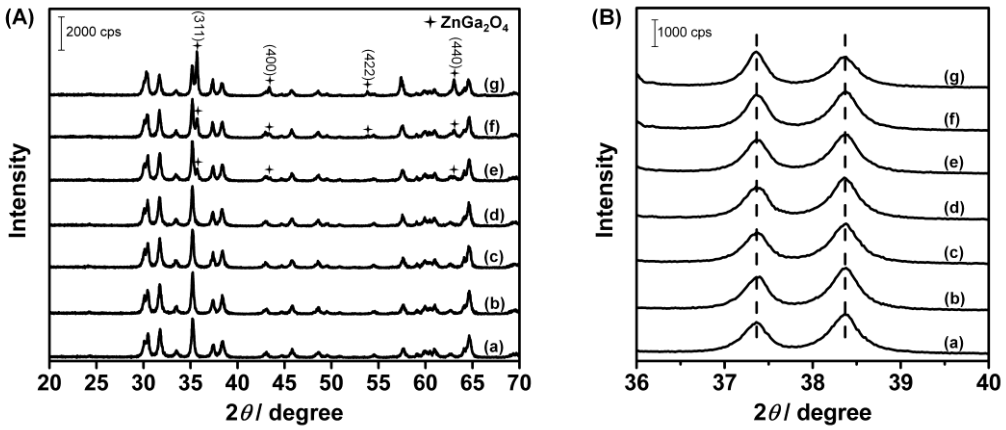

Figure 4 (A) XRD patterns of bare Ga_2O_3 (a) and Zn-modified Ga_2O_3 with 0.1 mol% (b), 0.5 mol% (c), 1.0 mol% (d), 3.0 mol% (e), 5.0 mol% (f), and 10.0 mol% (g) of Zn species; (B) The enlarged XRD patterns of all samples at 2θ ranged from 36.0° to 40.0°.

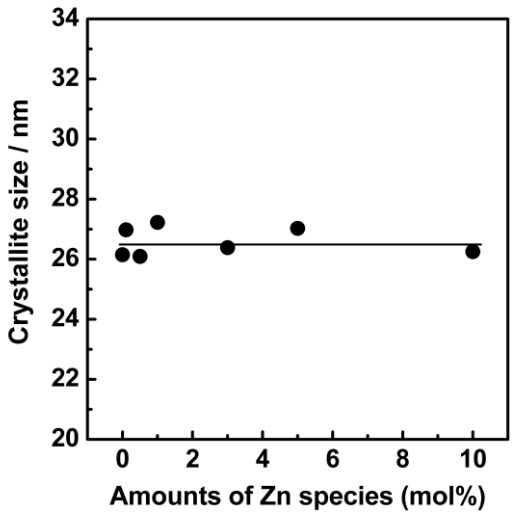

Figure 5 The change of Crystallite size in Zn-modified Ga_2O_3 with various amounts of Zn species.

When a foreign metal ion is inserted into a crystal structure, the substitution of

the original lattice ion or the residual stress from a new mixed compound usually results in the peak shift of the XRD pattern associated with the change in the interplanar distance.[20-22] Figure 4(B) shows the magnified XRD patterns of all samples in the 2θ range from 36.0° to 40.0°. The diffraction peaks of Zn-modified Ga_2O_3 with various amounts of Zn ions did not shift significantly in comparison to those of bare Ga_2O_3. The ionic radius of Zn^{2+} (0.074 nm) is larger than that of Ga^{3+} (0.062 nm);[20,21] however, the unaltered peak position in the XRD pattern implies that the Zn ion does not act as a dopant in the bulk Ga_2O_3 lattice. Furthermore, this result indicates that the formation of $ZnGa_2O_4$ in the Zn-modified Ga_2O_3 with larger amounts of Zn ions did not generate enough residual stress to distort the Ga_2O_3 structure.[22] The crystallite sizes of bare Ga_2O_3 and Zn-modified Ga_2O_3 derived from Scherrer's equation using the FWHM (Full Width of Half Maximum) of the XRD peaks are displayed in Figure 5. The crystallite size of bulk Ga_2O_3 remained in spite of the added amount of Zn ions, thus the crystallinity of Ga_2O_3 was stable during the process of modification with Zn species. Based on these results, we concluded that all of the Zn species are located on the surface of Ga_2O_3, and $ZnGa_2O_4$ is generated when a large amount of Zn species is added.

To examine the relationship between the selectivity toward CO evolution and the Zn modification, especially for the addition of a small amount of Zn species, the chemical state and local structure of the Zn species were analyzed by XAFS measurements. Figure 6 and 7 show the Zn K-edge XANES, EXAFS, and Fourier transforms (FT) of k^3-weighted EXAFS spectra of Zn-modified Ga_2O_3 with various amounts of Zn species. Zinc foil, ZnO, and $ZnGa_2O_4$ were used as references. The $ZnGa_2O_4$ reference was fabricated by calcining a mixture of ZnO and Ga_2O_3 at 1473 K for 20 h, and it showed the typical XRD pattern of spinel type $ZnGa_2O_4$. The absorption

edge of Zn-modified Ga_2O_3 samples in the Zn-K edge XANES spectra (Figure 6) are similar to those of the ZnO and $ZnGa_2O_4$ references, thus the chemical state of the Zn species is divalent. However, the spectrum of Zn-modified Ga_2O_3 samples with 0.1 mol% Zn species was quite different from those of ZnO and $ZnGa_2O_4$. Therefore, we speculate that the introduction of a tiny amount of Zn species by the impregnation method resulted in the isolated dispersion of Zn ions in the surface layer of Ga_2O_3 and a different local structure for the Zn species compared to that of $ZnGa_2O_4$. Moreover, as the amount of Zn increased, the XANES spectra became increasingly similar to that of $ZnGa_2O_4$, indicating that further addition of Zn ions could cause a gradual change in the local structure of the Zn species. For samples with more than 3.0 mol% of Zn species, the spectra were identical to that of $ZnGa_2O_4$. This result is in agreement with the XRD measurements. In the corresponding FT of the EXAFS spectra shown in Figure 7(B), the first coordination peaks are attributed to the Zn-O shell for both the ZnO and $ZnGa_2O_4$ references (*ca.* 1.98 Å). The position of the second coordination peak is assigned to the Zn-Ga shell for the $ZnGa_2O_4$ reference (*ca.* 3.46 Å), and is longer than that of the Zn-Zn shell peak for the ZnO reference (*ca.* 3.22 Å). All samples of Zn-modified Ga_2O_3 exhibited a Zn-O shell peak at the same characteristic position as the ZnO and $ZnGa_2O_4$ samples, and the intensity of the Zn-O shell peak increased with increasing Zn addition. A weak shell peak was observed in the spectrum of 0.1 mol% Zn-modified Ga_2O_3 at the same position as the Zn-Zn shell peak of the ZnO reference, implying that the highly dispersed Zn species mainly exist as ZnO on the surface of Ga_2O_3. However, the second shell peak of the 0.5 mol% sample appeared at the characteristic distance of the Zn-Ga shell, which indicates that the local structure of $ZnGa_2O_4$ was formed in Zn-modified Ga_2O_3 with 0.5 mol% Zn addition. The peak

corresponding to the Zn-Ga shell became higher and sharper with the addition of Zn up to 3.0 mol%, and then remained unchanged with further increases in the amount of Zn. The Zn-K edge XAFS results confirm that the introduction of a tiny amount of Zn species (>0.1 mol%) into Ga_2O_3 could result in the formation of the $ZnGa_2O_4$ structure, which was not detected by XRD measurements.

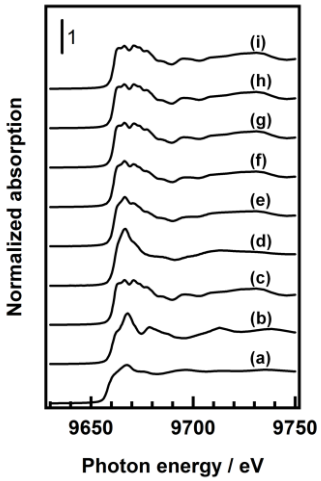

Figure 6 The Zn K-edge XANES spectra of Zn foil (a), ZnO (b), $ZnGa_2O_4$ (c) and Zn-modified Ga_2O_3 with different amount of Zn species: 0.1 mol% (d), 0.5 mol% (e), 1.0 mol% (f), 3.0 mol% (g), 5.0 mol% (h), and 10.0 mol% (i).

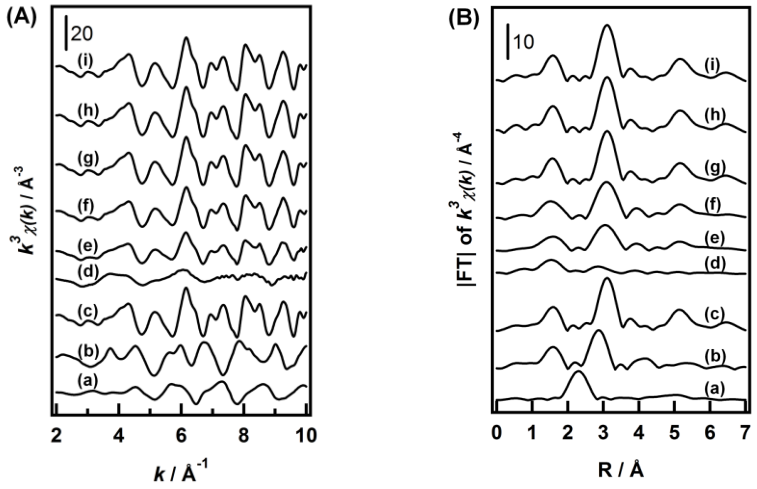

Figure 7 The Zn K-edge EXAFS (A) and Fourier transforms of EXAFS (B) spectra of Zn foil (a), ZnO (b), $ZnGa_2O_4$ (c) and Zn-modified Ga_2O_3 with different amount of Zn species: 0.1 mol% (d), 0.5 mol% (e), 1.0 mol% (f), 3.0 mol% (g), 5.0 mol% (h), and 10.0 mol% (i).

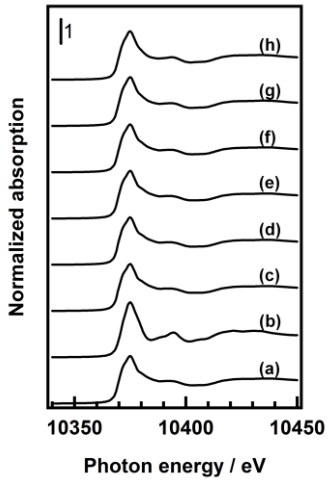

Figure 8 The Ga K-edge XANES spectra of Ga_2O_3 (a), $ZnGa_2O_4$ (b) and Zn-modified Ga_2O_3 with different amount of Zn species: 0.1 mol% (c), 0.5 mol% (d), 1.0 mol% (e), 3.0 mol% (f), 5.0 mol% (g), and 10.0 mol% (h).

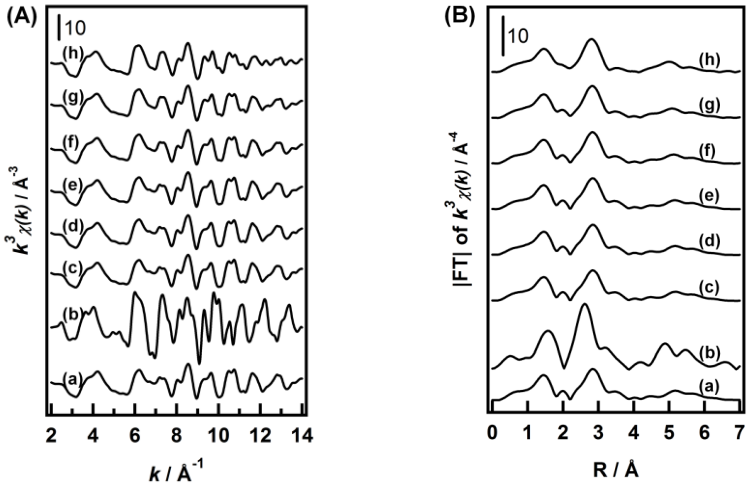

Figure 9 The Ga K-edge EXAFS (A) and Fourier transforms of EXAFS (B) spectra of Ga_2O_3 (a), $ZnGa_2O_4$ (b) and Zn-modified Ga_2O_3 with different amount of Zn species: 0.1 mol% (c), 0.5 mol% (d), 1.0 mol% (e), 3.0 mol% (f), 5.0 mol% (g), and 10.0 mol% (h).

On the other hand, Figure 8 and 9 exhibit the Ga K-edge XANES, EXAFS, and FT of the EXAFS spectra of Zn-modified Ga_2O_3 samples with Ga_2O_3 and $ZnGa_2O_4$ as the references. The XANES spectra of Zn-modified Ga_2O_3 with various amounts of Zn species were identical to that of bulk Ga_2O_3. For the FT of the EXAFS spectra, the

spectral shape of Zn-modified Ga_2O_3 was also consistent with that of bulk Ga_2O_3 and the intensity of the two coordination peaks were similar for each sample. These results suggest that the local structure of Ga ions in the Zn-modified Ga_2O_3 was not disturbed by the addition of Zn species.

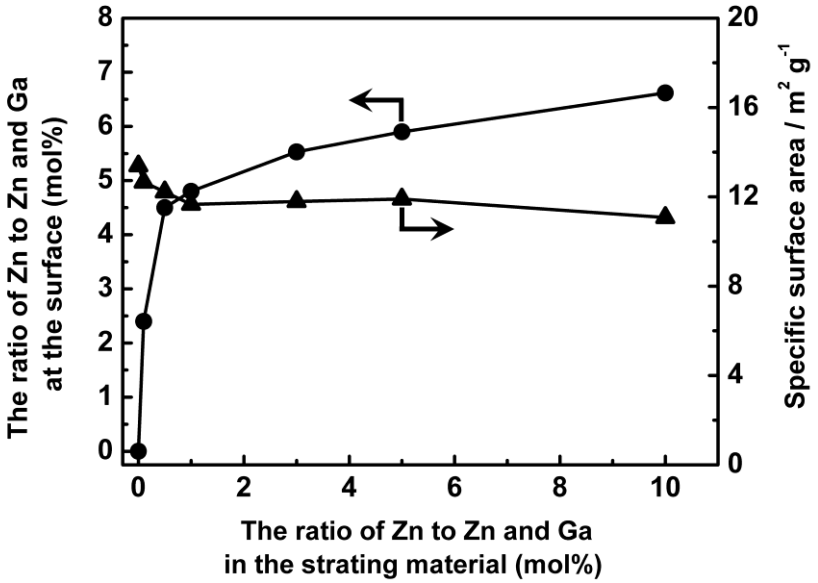

Figure 10 The surface ratios of Zn ions to total metal ions (Zn and Ga) and the specific surface area of Zn-modified Ga_2O_3 with various Zn contents.

Since the introduced Zn species could react with Ga_2O_3 to generate the $ZnGa_2O_4$ crystal structure with the bulk phase of Ga_2O_3 remaining unchanged, the surface of Ga_2O_3 is expected to be covered with a layer of $ZnGa_2O_4$. Figure 10 displays the dependence of the surface ratio of Zn atoms to total metal atoms (Zn and Ga), estimated by XPS measurements, on the ratio of the mixture in the starting material for Zn-modified Ga_2O_3. When the amount of Zn species added increased from 0.1 mol% to 1.0 mol%, the surface ratio of Zn atoms to total metal atoms sharply increased from 2.4 mol% to 4.8 mol%. Further increases in the amount of Zn species resulted in a continuous rise in the surface ratio of Zn atoms to total metal atoms. Therefore, the

high-temperature treatment of the $Zn(NO_3)_2$-impregnated Ga_2O_3 starting material promotes the surface reaction between $Zn(NO_3)_2$ and Ga_2O_3 to form the $ZnGa_2O_4$ layer. The coverage and thickness of the $ZnGa_2O_4$ layer on the surface of Ga_2O_3 would increase with greater loadings of $Zn(NO_3)_2$. In addition, the specific surface area of Zn-modified Ga_2O_3 measured by the BET method is also shown in Figure 10. The surface area of the modified Ga_2O_3 did not vary proportionally with the generation of the $ZnGa_2O_4$ layer on the surface of Ga_2O_3; thus, the thin $ZnGa_2O_4$ layer must grow evenly on the surface of Ga_2O_3.

Undoubtedly, the photocatalytic reaction on Zn-modified Ga_2O_3 is triggered by the absorption of photons, leading to the generation of electrons and holes in the conduction and valence bands, respectively. The photoexcited electrons in the conduction band subsequently migrate to the surface active sites to participate in the reduction of CO_2 and H^+, while the holes in the valence band oxidize H_2O into O_2. The electrochemical reduction of CO_2 into CO is known to efficiently and selectively occur on a Ag metal electrode in aqueous solution.[23] Therefore, the deposition of metallic Ag particles onto Ga_2O_3 and Zn-modified Ga_2O_3 created the preferable active sites to capture the photoexcited electrons for the reduction of CO_2. Thus, similar activity for the evolution of CO over the Ag-loaded Zn-modified Ga_2O_3 with different Zn contents is attributable to the same extraction efficiency of electrons from the conduction band of Ga_2O_3 by the Ag cocatalyst. Moreover, the crystallinity and surface area of Ga_2O_3 were almost unaltered after modification with the $ZnGa_2O_4$ layer, which maintained the formation rate of CO in the photocatalytic conversion of CO_2 by H_2O.

On the other hand, the reason for the suppression of H_2 production in the photocatalytic conversion of CO_2 by H_2O is due to the modification of Ga_2O_3 with Zn

species. The extremely high formation rate of H_2 over Ag-loaded Ga_2O_3 indicates that a large number of active sites exist for the reduction of H^+ on the surface of bare Ga_2O_3. The formation of the $ZnGa_2O_4$ layer by the introduction of Zn species, revealed by the XAFS and XPS measurements, can eliminate such active sites on the surface of Ga_2O_3 and prevent the H^+ approach to Ga_2O_3. Thus, growth of the $ZnGa_2O_4$ layer on the surface of Ga_2O_3 with the increase in Zn species addition resulted in the gradual decrease in H_2 evolution. Therefore, the selectivity toward the evolution of CO over H_2 is improved because of the generation of the $ZnGa_2O_4$ layer on the surface of Ga_2O_3.

Table 1 The formation rate of gas products and selectivity toward CO evolution in the photocatalytic conversion of CO_2 by H_2O over various photocatalysts[a]

Photocatalysts[b]	**Formation rate (μmol h^{-1})**			**Selectivity toward CO evolution (%)**
	H_2	**O_2**	**CO**	
Bare Ga_2O_3	280	181	111	28.4
Zn(3mol%)-modified Ga_2O_3	8.9	60.6	108	92.4
$ZnGa_2O_4$[c]	2.1	28.9	50.8	96.0
Ga_2O_3+$ZnGa_2O_4$[d]	233	165	109	31.9

[a] Reaction conditions: Amount of catalyst, 1.0 g; volume of water, 1.0 L; flow rate of CO_2, 30 mL min^{-1}; concentration of $NaHCO_3$, 0.1 mol L^{-1}; light source, high-pressure mercury lamp (400 W). [b] Ag cocatalyst was loaded by the photodeposition method and the loading amount was 1.0 wt%. [c] $ZnGa_2O_4$ was synthesized by the solid state reaction with calcination at 1223 K. [d] The physical mixture with the same composition as the Zn(3mol%)-modified Ga_2O_3 photocatalyst.

The function of the $ZnGa_2O_4$ layer on the surface of Ga_2O_3 was further confirmed by the reaction using pure $ZnGa_2O_4$ fabricated at the same temperature as the Zn-modified Ga_2O_3 and the physical mixture of Ga_2O_3 and $ZnGa_2O_4$. The evolution of CO, H_2, and O_2 in a stoichiometric ratio was obtained over the Ag-loaded $ZnGa_2O_4$ photocatalyst, and the selectivity for CO evolution over H_2 was consistent with that over

Ag-loaded Zn-modified Ga_2O_3 (Table 1). This result indicates that the $ZnGa_2O_4$ structure possesses suitable active sites for the conversion of CO_2 and oxidation of H_2O except for the reduction of H^+. When $ZnGa_2O_4$ was physically mixed with Ga_2O_3, the evolution of H_2 still dominated because the proton reduction sites on the surface of Ga_2O_3 are not covered by $ZnGa_2O_4$. Therefore, the $ZnGa_2O_4$ layer modified on the surface of Ga_2O_3 has a characteristic role to inhibit the production of H_2 and maintain the evolution of CO in the photocatalytic conversion of CO_2 by H_2O.

The mixture of CO and H_2, which is well known as synthesis gas, is one of the most crucial raw materials in the chemical industry. Especially, since it is very difficult to adjust the ratio of H_2 by CO (so-called, H_2/CO ratio) depending on products of the Fischer–Tropsch technology. In this study, we produced synthesis gas and controlled the ratio of H_2 to CO by the photocatalytic conversion of CO_2 with H_2O as an electron donor over Ag-loaded Zn-modified Ga_2O_3 photocatalysts.

Conclusions

Stoichiometric amounts of CO, H_2, and O_2 were evolved in the photocatalytic conversion of CO_2 by H_2O as an electron donor using an Ag-loaded Zn-modified Ga_2O_3 photocatalyst. The production of H_2 gradually decreased with increasing amounts of Zn species from 0.1 to 10.0 mol%, whereas the evolution of CO was almost unchanged. Consequently, the selectivity toward CO evolution increased to almost 100%. Characterization using UV-Vis DRS, SEM, XRD, XAFS, XPS, and BET measurements confirmed that a thin $ZnGa_2O_4$ layer was generated on the surface of Ga_2O_3 by the addition of Zn species, and the band structure, morphology, surface area, and crystallinity of Ga_2O_3 were not affected. The $ZnGa_2O_4$ layer has a special function to suppress the reduction of H^+ in the photocatalytic conversion of CO_2 by H_2O over

Ag-loaded Zn-modified Ga_2O_3 photocatalyst. Since the generation ratio of H_2 to CO can be finely tuned by using the Ag-loaded Zn-modified Ga_2O_3 photocatalyst, it is a promising way to produce synthesis gas through the photocatalytic conversion of CO_2 by H_2O.

References and Notes

[1] E. V. Kondratenko, G. Mul, J. Baltrusaitis, G. O. Larraz ábal, J. P érez-Ram írez, *Energy Environ. Sci.* **2013**, *6*, 3112.

[2] G. Centi, E. A. Quadrelli, S. Perathoner, *Energy Environ. Sci.* **2013**, *6*, 1711.

[3] W. Wang, S. Wang, X. Ma, J. Gong, *Chem. Soc. Rev.* **2011**, *40*, 3703.

[4] M. Fan, A. Abdullah, S. Bhatia, *ChemCatChem* **2009**, *1*, 192.

[5] A. Kubacka, M. Fern ández-Garc á, G. Col ón, *Chem. Rev.* **2012**, *112*, 1555.

[6] W. Tu , Y. Zhou, Z. Zou, *Adv. Mater.* **2014**, *26*, 4607.

[7] W. Fan, Q. Zhang, Y. Wang, *Phys. Chem. Chem. Phys.* **2013**, *15*, 2632.

[8] K. Li, A. Handoko, M. Khraisheh, J. Tang, *Nanoscale* **2014**, *6*, 9767.

[9] T. Inoue, A. Fujishima, S. Konishi, K. Honda, *Nature* **1979**, *277*, 637.

[10] I. H. Tseng, J. C. S. Wu, H. Y. Chou, *J. Catal.* **2004**, *221*, 432.

[11] Y. Liu, B. Huang, Y. Dai, X. Zhang, X. Qin, M. Jiang, M. H. Whangbo, *Catal. Commun.* **2009**, *11*, 210.

[12] S. C.Yan, S. X. Ouyang, J. Gao, M. Yang, J. Y. Feng, X. X. Fan, L. J. Wan, Z. S. Li, J. Ye, Y. Zhou, Z. G. Zou, *Angew. Chem., Int. Ed.* **2010**, *49*, 6400.

[13] Q. Liu, Y. Zhou, J. Kou, X. Chen, Z. Tian, J. Gao, S. Yan, Z. Zou, *J. Am. Chem. Soc.* **2010**, *132*, 14385.

[14] A. D. Klerk and E. Furimsky, in *Catalysis in the Refining of Fischer-Tropsch Syncrude*, Royal Society of Chemistry, London, 2010.

[15] K. Sayama, H. Arakawa, *J. Phys. Chem.* **1993**, *97*, 531.

[16] K. Iizuka, T. Wato, Y. Miseki, K. Saito, A. Kudo, *J. Am. Chem. Soc.* **2011**, *133*, 20863.

[17] T. Takayama, K. Tanabe, K. Saito, A. Iwase, A. Kudo, *Phys. Chem. Chem. Phys.*

2014, *16*, 24417.

[18] K. Teramura, Z. Wang, S. Hosokawa, Y. Sakata, T. Tanaka, *Chem. Eur. J.* **2014**, *20*, 9906.

[19] K. Teramura, S. Okuoka, H. Tsuneoka, T. Shishido, T. Tanaka, *Appl. Catal. B* **2010**, *96*, 565.

[20] Y. Sakata, Y. Matsuda, T. Yanagida, K. Hirata, H. Imamura, K. Teramura, *Catal. Lett.* **2008**, *125*, 22.

[21] X. Wang, S. Shen, S. Jin, J. Yang, M. Li, X. Wang, H. Han, C. Li, *Phys. Chem. Chem. Phys.* **2013**, *15*, 19380.

[22] W. Water, S. Chu, *Mater. Lett.* **2002**, *55*, 67.

[23] Y. Hori, K. Kikuchi, S. Suzuki, *Chem. Lett.* **1985**, *14*, 1695.

Chapter 3

Effect of additives on the photocatalytic conversion of CO_2 by H_2O over Ag-loaded Zn-modified Ga_2O_3

Abstract

The photocatalytic conversion of CO_2 with H_2O using Ag-loaded Zn-modified Ga_2O_3 in the presence of various additives was investigated. The activity for CO evolution was largely improved by the addition of Na_3PO_4, $NaHCO_3$, Na_2CO_3, and NaOH. The different alkaline chemicals in the reaction solutions also affected the formation of CO. The increase of $NaHCO_3$ content in the reaction solution dramatically enhanced the activity for the photocatalytic conversion of CO_2 with H_2O over Ag-loaded Zn-modified Ga_2O_3. Therefore, the highest formation rate of CO (171.0 μmol h^{-1}) was obtained in the $NaHCO_3$ solution with the concentration higher than 1.0 mol L^{-1}. According to equilibrium of carbon species (dissolved CO_2, HCO_3^-, and CO_3^{2-}), the major carbon species in the aqueous solutions of Na_3PO_4, $NaHCO_3$, Na_2CO_3, and NaOH was HCO_3^- during the photocatalytic reaction, which was related to the high activity for CO evolution. Moreover, the maintenance of the equilibrium between the dissolved CO_2 molecules and the HCO_3^- species was very important for the photocatalytic conversion of CO_2 with H_2O in the presence of weak acid salt and alkaline additives.

Introduction

As an artificial photosynthesis, photocatalytic conversion of CO_2 over a heterogeneous photocatalyst is a promising route to generate energy and useful chemicals by utilizing solar light and CO_2 as resources.[1,2] In order to achieve the conversion of CO_2 on a solid photocatalyst, it is important to capture CO_2 on the surface and make it into an active species because CO_2 is a stable and linear molecule. Typically, the activation of CO_2 can be enhanced by adsorption of CO_2 molecule on the base site. It was reported that the photocatalytic reduction of CO_2 in the presence of H_2 proceeded over many solid base oxides such as MgO[3], Ga_2O_3[4], and $ATaO_3$ (A = Li, Na, K)[5]. The adsorbed bicarbonate or carbonate species on the solid base oxides were clarified to be active for the reduction of CO_2.[3,4] As for the photocatalytic reduction of CO_2 with H_2O in the gas phase, it is also demonstrated that the modification of semiconductors with alkali[6] or solid base oxides[7,8] could facilitate the surface adsorption and fixation of CO_2, thus enhance the activity for the conversion of CO_2. However, in the case of the suspension system, it is difficult for the photocatalysts to capture CO_2 molecules because the property of base sites becomes very weak in water and large amount of H_2O molecules surrounded the catalyst powders block the adsorption of CO_2. Moreover, the solubility of gaseous CO_2 in the neutral water phase is quite limited at room temperature under the ambient pressure, which further decreases the probability of CO_2 molecule in contact with the photocatalyst surface. Thus, the photocatalytic activity for the conversion of CO_2 by H_2O in the suspension system is not so high.[9-12]

Due to the acidic property of CO_2 gas, it is straightforward to seize CO_2 molecule in the aqueous alkaline solution for the photocatalytic conversion of CO_2 with

H_2O. It has been reported that photocatalytic reduction of CO_2 in the $NaHCO_3$ solution proceeded over Cu-loaded ZrO_2 and $NaHCO_3$ functioned as the carbon source for the CO evolution.[13] Bubbling CO_2 gas into NaOH solution containing Na_2SO_3, Pd and RuO_2 coloaded TiO_2 could produce HCOOH as the reduction product under the UV light illumination.[14] CO_2 was photocatalytically reduced into CH_3OH in the CO_2-bubbled $KHCO_3$ solution over the CuO-impregnated TiO_2.[15] Moreover, CH_3OH was also evolved when the mesoporous g-C_3N_4 flakes were suspended in the CO_2-saturated NaOH solution under the visible light irradiation.[16] In Chapters 1 and 2, our group has found that CO together with stoichiometric amount of O_2 was generated over Ag-loaded Zn-modified Ga_2O_3 for the photocatalytic conversion of CO_2 with H_2O in the presence of $NaHCO_3$.[17] It can be demonstrated that the addition of alkaline species plays an essential role for the photocatalytic conversion of CO_2 in H_2O. However, the systematic study of the effect of additives in the reaction solution on the photocatalytic conversion of CO_2 has not been reported.

In this paper, the effect of various inorganic salts and alkalis on the activity for the photocatalytic conversion of CO_2 with H_2O was investigated using Ag-loaded Zn-modified Ga_2O_3 photocatalyst. The relationship between CO evolution and carbon species (dissolved CO_2, HCO_3^-, and CO_3^{2-}) was discussed.

Experimental section

Ga_2O_3 was fabricated by the precipitation method as reported in Chapters 1 and 2.[17] $Ga(NO_3)_3 \cdot xH_2O$ (12g, Kojundo, 99.999%) was first dissolved in the distilled water. Then the aqueous ammonia solution (28 wt%) was added by dropwise to the above gallium nitrate solution until the pH value reached to approximately 8.9. The white precipitation was centrifuged, washed extensively with distilled water, and dried

at 353 K in air to obtain a gallium hydroxide precursor. Ga_2O_3 was obtained by calcining the precursor at 1273 K for 6 h. Zn-modified Ga_2O_3 was synthesized by the impregnation method. The as-prepared Ga_2O_3 was dispersed in an aqueous solution containing various amount of $Zn(NO_3)_2$ by ultrasonication. After drying under vacuum at room temperature, the solid mixture of Ga_2O_3 and $Zn(NO_3)_2$ was calcined at 1223 K for 6 h. The amount of Zn species was 3.0 mol% against the total amount of metal species (Ga atoms and Zn atoms).

The Ag cocatalyst was loaded on Zn-modified Ga_2O_3 and Ga_2O_3 by the in-situ photodeposition method. The loading amount of Ag cocatalyst was 1 wt%. The prescribed amount of $AgNO_3$ was added in the reaction suspension. The deposition of Ag co-catalyst on the photocatalyst proceeded under photoirradiation. Photocatalytic conversion of CO_2 in water was carried out in a flow system using an inner-irradiation-type reaction vessel at room temperature and ambient pressure. The photocatalyst (1.0 g) was dispersed in ultra-pure water (1.0 L) containing various additives (such as $NaHCO_3$, Na_2CO_3, NaOH, NaCl, Na_2SO_4, Na_3PO_4, Li_2CO_3, LiOH, K_2CO_3, KOH, Cs_2CO_3, and CsOH), and CO_2 (99.999%) was bubbled into the solution at a flow rate of 30 mL min^{-1}. The suspension was irradiated under a 400 W high-pressure mercury lamp with a quartz filter connected to a cooling water system. Generated gaseous products such as H_2, O_2, and CO were analyzed by thermal conductivity detector-gas chromatography (TCD-GC) using a GC-8A chromatograph (Shimadzu Corp.) equipped with a Molecular Sieve 5A column, (carrier gas: Ar) and by flame ionization detector-gas chromatography (FID-GC) using a methanizer and a Shincarbon ST column (carrier gas: N_2).

Results and Discussion

Figure 1 represents the formation rates of H_2, O_2, and CO in the photocatalytic conversion of CO_2 by H_2O over Ag-loaded Zn-modified Ga_2O_3 photocatalyst from various aqueous solutions. As compared with the tiny amount of evolved CO, H_2 was formed as the main reduction product during the photocatalytic conversion of CO_2 in the pure water. The stoichiometric amount of O_2 was produced together with H_2 and CO, which proved that the oxidation of H_2O proceeded on the Ag-loaded Zn-modified Ga_2O_3 to consume the photogenerated holes. The selectivity toward CO evolution ($CO/(H_2+CO)\times100$) was only 36.0%. The activity for H_2, O_2, and CO evolution in the aqueous Na_2SO_4 solution slightly decreased and the selectivity toward CO evolution also declined, which means that the Na_2SO_4 additive has a negative effect on the photocatalytic conversion of CO_2 by H_2O over Ag-loaded Zn-modified Ga_2O_3. The addition of NaCl in the reaction solution could enhance the activity for CO formation to a certain extent. Thus the selectivity toward CO evolution increased by 67.4%. The time course for the photocatalytic conversion of CO_2 by H_2O in the NaCl solution in Figure 2(a) shows that the amount of evolved CO, H_2, and O_2 did not increased in the stoichiometric ratio. The low rate of O_2 evolution and the high rate of CO evolution in the initial stage indicate that H_2O did not acted as an electron donor for the reduction of CO_2. Our group has found that the Cl^- ions could promote the photocatalytic conversion of CO_2 to CO in the aqueous solution by functioning as the hole scavengers.[18] It is expected that the simple 2-electron redox process in the photooxidation of Cl^- to Cl_2 proceeds more smoothly than the 4-electron redox process in the photooxidation of H_2O to O_2.[19] With the gradual consumption of Cl^- ions under the photoirradiation, the formation rate of O_2 from the photooxidation of H_2O increased and the rate of CO

evolution decreased.

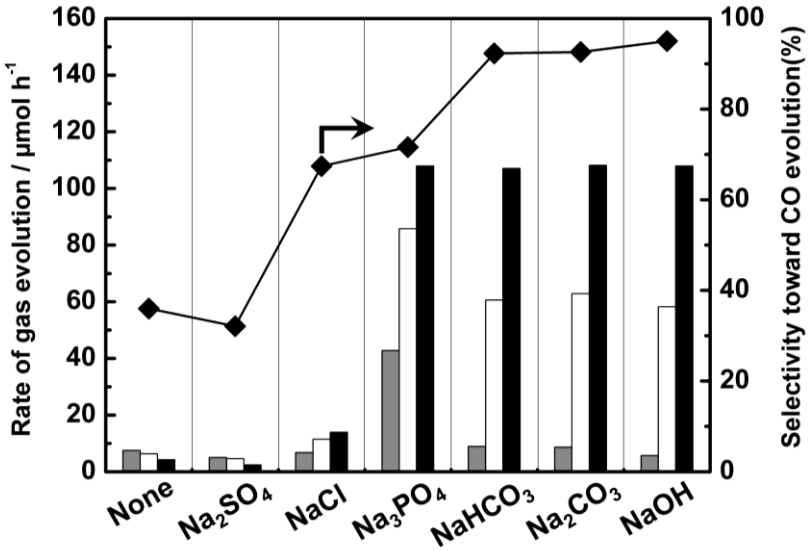

Figure 1 The rates of CO (black), O_2 (white), and H_2 (gray) evolution and selectivity toward CO for the photocatalytic conversion of CO_2 by H_2O over Ag-loaded Zn-modified Ga_2O_3 photocatalyst in various aqueous solutions. Reaction conditions: Amount of catalyst, 1.0 g; cocatalyst: 1.0 wt%; volume of water, 1.0 L; flow rate of CO_2, 30 mL min^{-1}; concentration of Na^+ ions , 0.1 mol L^{-1}; light source, high-pressure mercury lamp (400 W).

The activity for the photocatalytic conversion of CO_2 by H_2O was drastically improved in the Na_3PO_4 solution (Figure 1). The formation rates of CO and H_2 were achieved to 108 μmol $h^{-1}$and 42.7 μmol h^{-1}. Due to the increase of H_2 evolution, the selectivity toward CO evolution in the Na_3PO_4 solution was just 71.6%. Similarly, the evolution of CO in the photocatalytic conversion of CO_2 by H_2O was much enhanced in the presence of $NaHCO_3$ additive, while the evolution of H_2 was obviously restrained. It is interesting that the addition of Na_2CO_3 and NaOH could result in the same activity for the evolutions of CO and H_2 as that of $NaHCO_3$. The selectivity toward CO evolution over H_2 in the aqueous solution of $NaHCO_3$, Na_2CO_3 and NaOH dramatically reached

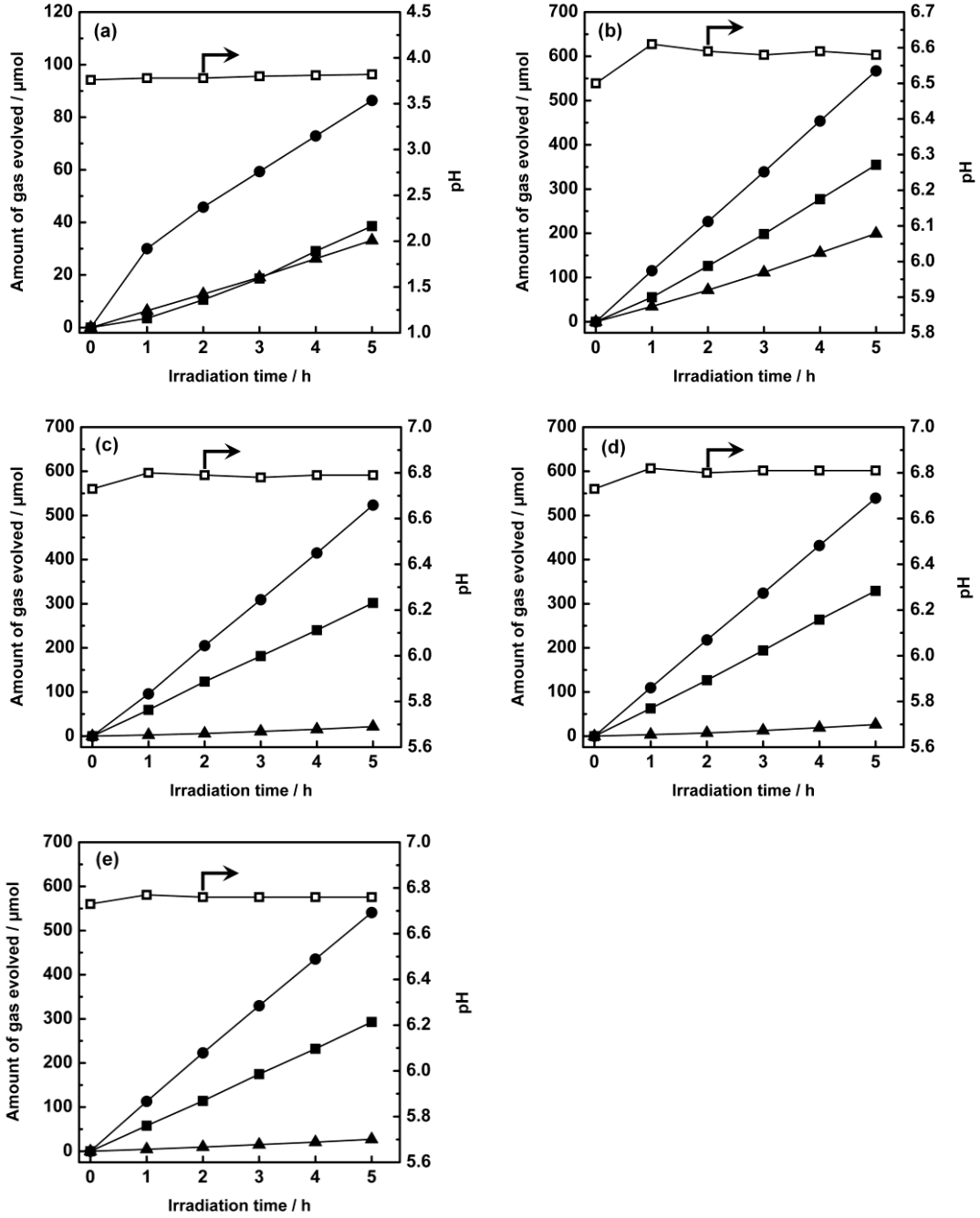

Figure 2 Time courses of CO (circle), O_2 (square), and H_2 (triangle) evolutions for the photocatalytic conversion of CO_2 by H_2O over Ag-loaded Zn-modified Ga_2O_3 photocatalyst in the aqueous solutions of NaCl (a), Na_3PO_4 (b), $NaHCO_3$ (c), Na_2CO_3 (d), and NaOH (e). Amount of catalyst, 1.0 g; cocatalyst: 1.0 wt%; volume of water, 1.0 L; flow rate of CO_2, 30 mL min^{-1}; concentration of Na^+ ions , 0.1 mol L^{-1}; light source, high-pressure mercury lamp (400 W).

more than 92.0%. Moreover, O_2 was generated stoichiometrically during the photocatalytic conversion of CO_2 from Na_3PO_4, $NaHCO_3$, Na_2CO_3 and NaOH solutions, indicating that H_2O worked as electron donors for the reduction of CO_2. Therefore, the evolutions of CO, H_2, and O_2 in the aqueous solutions of Na_3PO_4, $NaHCO_3$, Na_2CO_3 and NaOH linearly increased under the UV light irradiation as shown in Figure 2(b)-(e). The pH values of the reaction solution in the presence of Na_3PO_4, $NaHCO_3$, Na_2CO_3 and NaOH were steadily kept between 6.5 and 6.8 and remained unchanged during the photocatalytic conversion of CO_2, it is because CO_2 gas was continuously supplied into the solution to maintain the equilibrium of carbon species (dissolved CO_2, HCO_3^-, and CO_3^{2-}). Conversely, the pH of the NaCl solution was stabilized at about 3.8 during the photocatalytic reaction in Figure 2(a).

It is known that gaseous CO_2 is soluble in H_2O, the dissolved CO_2 either exchanges with gaseous CO_2, or reacts with H_2O to form H_2CO_3 (carbonic acid), which is a weak acid because of its incomplete ionization in H_2O:

$$CO_2\,(g) + H_2O \rightleftarrows CO_2\,(aq) + H_2O \quad (1)$$

$$CO_2\,(aq) + H_2O \rightleftarrows H_2CO_3 \quad (2)$$

The solubility of CO_2 gas in H_2O is directly proportional to the partial pressure of CO_2 gas above water phase (Henry's law)[20]:

$$k_{cp} = \frac{[CO_2(aq)]}{P_{CO_2}} \quad (3)$$

In addition, H_2CO_3 can dissociate into HCO_3^- and CO_3^{2-} according to:

$$H_2CO_3 \rightleftarrows HCO_3^- + H^+ \quad (4)$$

$$HCO_3^- \rightleftarrows CO_3^{2-} + H^+ \quad (5)$$

When the equilibrium conditions are achieved, the true dissociation constants are

defined as:

$$K_1 = \frac{[HCO_3^-][H^+]}{[H_2CO_3]} \quad (6)$$

$$K_2 = \frac{[CO_3^{2-}][H^+]}{[HCO_3^-]} \quad (7)$$

Since the concentration of dissolved CO_2 far exceeds that of H_2CO_3 (in the order of 10^3), the often-quoted first dissociation constant is an apparent constant including all dissolved CO_2[21]:

$$K_1^* = \frac{[HCO_3^-][H^+]}{[CO_2(aq)]} \quad (8)$$

According to the above equilibriums, the concentration of dissolved CO_2 in the reaction solution is dominated by the gaseous pressure of CO_2 in the reaction system, whereas the concentrations of HCO_3^- and CO_3^{2-} are affected by the pH value of the reaction solution. Furthermore, the fractions of carbon species (dissolved CO_2, HCO_3^-, and CO_3^{2-}) at the equilibrium are often assumed to be given by Bjerrum plot equations [22]:

$$\frac{[CO_2(aq)]}{[CO_2(aq)]+[HCO_3^-]+[CO_3^{2-}]} = \frac{[H^+]^2}{[H^+]^2 + K_1^*[H^+] + K_1^*K_2} \quad (9)$$

$$\frac{[HCO_3^-]}{[CO_2(aq)]+[HCO_3^-]+[CO_3^{2-}]} = \frac{K_1^*[H^+]}{[H^+]^2 + K_1^*[H^+] + K_1^*K_2} \quad (10)$$

$$\frac{[CO_3^{2-}]}{[CO_2(aq)]+[HCO_3^-]+[CO_3^{2-}]} = \frac{K_1^*K_2}{[H^+]^2 + K_1^*[H^+] + K_1^*K_2} \quad (11)$$

Table 1 displays the pH values of the solutions with different additives before CO_2 bubbling and during the reaction and the fraction of carbon species (dissolved CO2, HCO_3^-, and CO_3^{2-}) during the photocatalytic conversion of CO_2 in H_2O. Flowing CO_2 gas into the reaction solution saturated water with dissolved CO_2 molecules, which was

almost constant under the reaction conditions in spite of the addition of various salts and alkalis. The decrease in the pH value of the aqueous solution was resulted from the formation and dissociation of H_2CO_3 after the continuous introduction of CO_2 gas. The equilibrium of carbon species (dissolved CO_2, HCO_3^-, and CO_3^{2-}) was achieved and maintained during the photocatalytic reaction. Therefore, the major fraction of carbon species in the pure H_2O was dissolved CO_2 molecules. The addition of Na_2SO_4 and NaCl did not change the pH of the solution, the dissolved CO_2 molecules still existed as the main carbon species. When Na_3PO_4, $NaHCO_3$, Na_2CO_3 and NaOH were used as the additives, the pH of the reaction solution significantly increased owing to alkaline properties of the Na_3PO_4, $NaHCO_3$, Na_2CO_3 and NaOH solutions. Hence, the majority of carbon species in the Na_3PO_4, $NaHCO_3$, Na_2CO_3 and NaOH solutions turned into HCO_3^- species, which may be responsible for the high activity for CO evolution in the photocatalytic conversion of CO_2 with H_2O.

Table 1 The pH value of various solutions and the fraction of dissolved CO_2, HCO_3^-, and CO_3^{2-} in various solution at the equilibrium during the reaction. Reaction temperature, 303 K; pressure of CO_2 gas above the solution, 1 atm; k_{cp}, 0.0298 mol L^{-1} atm^{-1}; K_1*, 4.71×10^{-7} mol L^{-1}; K_2: 5.13×10^{-11} in mol L^{-1}.

Additives	pH before CO_2 flowing	pH during the reaction	Fraction of carbon species in the reaction solution (%)		
			CO_2(aq.)	HCO_3^-	CO_3^{2-}
None	7.33	3.89	99.6	0.36	1.45×10^{-7}
Na_2SO_4	7.35	4.15	99.3	0.66	4.79×10^{-7}
NaCl	7.29	3.82	99.6	0.31	1.05×10^{-7}
Na_3PO_4	11.9	6.58	35.8	64.1	0.01
$NaHCO_3$	8.16	6.79	25.6	74.3	0.02
Na_2CO_3	11.0	6.81	24.7	75.2	0.03
NaOH	12.8	6.76	26.9	73.0	0.02

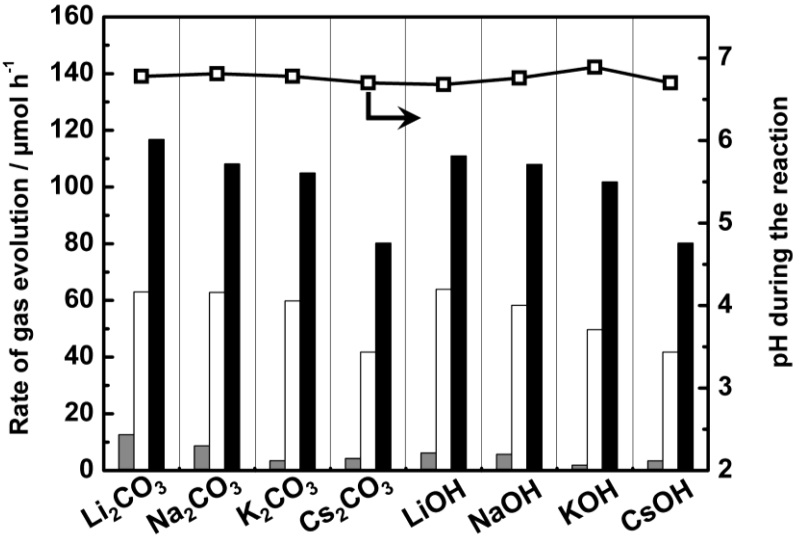

Figure 3 The rates of CO (black), O_2 (white), and H_2 (gray) evolution for the photocatalytic conversion of CO_2 by H_2O over Ag-loaded Zn-modified Ga_2O_3 photocatalyst in various carbonate and alkaline solutions. Reaction conditions: Amount of catalyst, 1.0 g; cocatalyst: 1.0 wt%; volume of water, 1.0 L; flow rate of CO_2, 30 mL min^{-1}; concentration of alkaline metal ions , 0.1 mol L^{-1}; light source, high-pressure mercury lamp (400 W).

Figure 3 exhibits the activity for the photocatalytic conversion of CO_2 by H_2O in the presence of various carbonate salts and alkalis. The stoichiometric amounts of CO, H_2, and O_2 were evolved in the aqueous solutions of various carbonates and alkalis. The formation rate of CO in the carbonate solutions slightly declined in the order: Li_2CO_3, Na_2CO_3, and K_2CO_3, while the rate of CO evolution in the Cs_2CO_3 solution reduced obviously. The addition of LiOH, NaOH, KOH, and CsOH has the same effect on the CO evolution. Moreover, pH values of these solutions during the photocatalytic reaction were similar to those of Na_2CO_3 and NaOH, indicating HCO_3^- species still existed as the main carbon species in the aqueous solutions of various carbonates and alkalis.

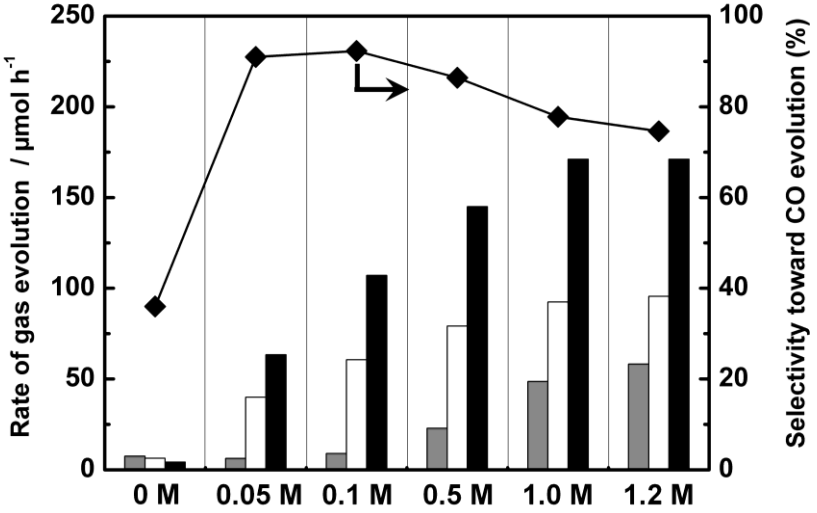

Figure 4 The rates of CO (black), O_2 (white), and H_2 (gray) evolution and selectivity toward CO for the photocatalytic conversion of CO_2 by H_2O over Ag-loaded Zn-modified Ga_2O_3 photocatalyst in different concentration of $NaHCO_3$ solutions. Reaction conditions: Amount of catalyst, 1.0 g; cocatalyst: 1.0 wt%; volume of water, 1.0 L; flow rate of CO_2, 30 mL min^{-1}; concentration of Na^+ ions , 0.1 mol L^{-1}; light source, high-pressure mercury lamp (400 W).

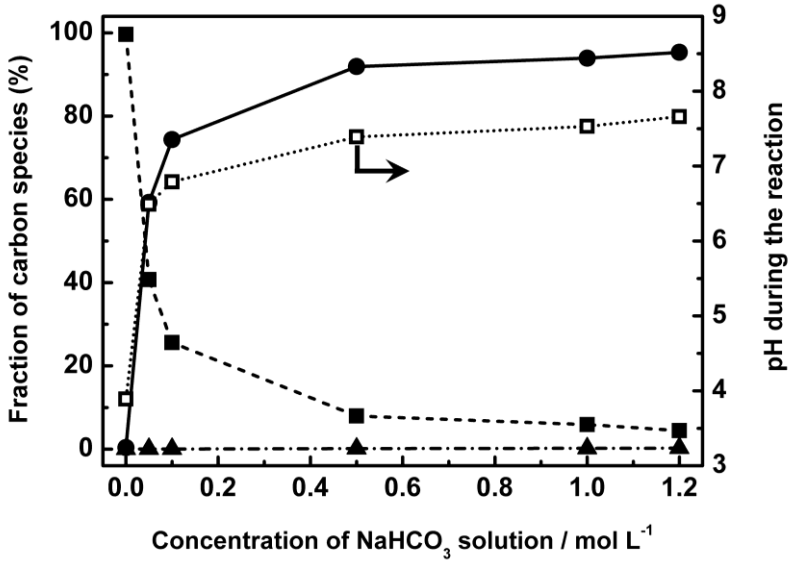

Figure 5 The fraction of dissolved CO_2 (square), HCO_3^- (circle), and CO_3^{2-} (triangle) and pH value of $NaHCO_3$ solution with different concentrations at the equilibrium of carbon species during the reaction. Reaction temperature, 303 K; pressure of CO_2 gas above the solution, 1 atm; k_{cp}, 0.0298 mol L^{-1} atm^{-1}; K_1*, 4.710×10^{-7} mol L^{-1}; K_2: 5.129×10^{-11} in mol L^{-1}.

The activity for the photocatalytic conversion of CO_2 in different concentration of $NaHCO_3$ solutions is shown in Figure 4. It is clearly observed that the rates of CO, H_2, and O_2 evolution were improved with changing the concentration of $NaHCO_3$ solution from 0 to 1.0 mol L^{-1}. The increase of the $NaHCO_3$ content did not affect the stoichiometric ratio of CO and H_2 to O_2, indicating that H_2O could function as the reductant for the photocatalytic conversion of CO_2 in the different concentrations of $NaHCO_3$ solutions. When the concentration of $NaHCO_3$ solution increased to 1.2 mol L^{-1}, which is the saturated $NaHCO_3$ solution, the activity for the CO, H_2, and O_2 evolution kept steadily. The highest formation rate of CO reached 171.0 μmol h^{-1}, in the aqueous solution of $NaHCO_3$ with the concentration higher than 1.0 mol L^{-1}. Moreover, the selectivity toward CO evolution climbed up then declined step by step with the increase of the $NaHCO_3$ addition, it is due to the increase of H_2 production in the photocatalytic reaction. Figure 5 represents the distribution of carbon species (dissolved CO_2, HCO_3^-, and CO_3^{2-}) in the $NaHCO_3$ solution with different concentrations, which was calculated from the equilibrium of carbon species during the reaction. The fraction of dissolved CO_2 species in the reaction solution without $NaHCO_3$ was estimated to be approximately 99.6% under the equilibrium conditions, whereas the fraction of HCO_3^- species was only 0.3%. With the increase of $NaHCO_3$ content from 0 to 0.1 mol L^{-1}, the dramatic drop in the fraction of dissolved CO_2 species during the equilibrium accompanied with the obvious ascent of the fraction of HCO_3^- species. Then the portion of HCO_3^- species rose smoothly and reached 95.3% with the further increase of $NaHCO_3$ additive. In contrast, the portion of dissolved CO_2 species decreased gradually. The concentration of CO_3^{2-} species in the $NaHCO_3$ solution at the equilibrium was negligible. In addition, the pH value of the $NaHCO_3$ solution during the reaction did not

change obviously. It can be understood that the enhancement of the photocatalytic activity for CO evolution was related to the incremental concentration of HCO_3^- species in the reaction solution.

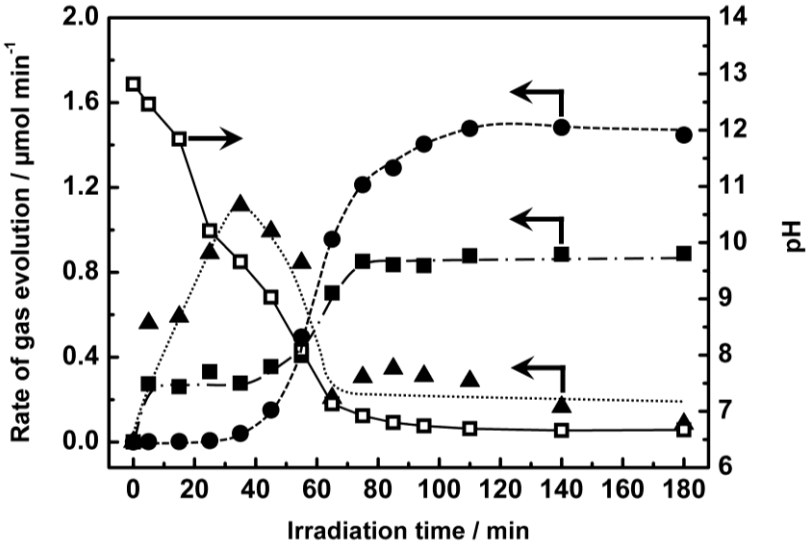

Figure 6 Time dependence of the rates of CO (circle), O_2 (square), and H_2 (triangle) evolution and pH value in the photocatalytic conversion of CO_2 by H_2O over Ag-loaded Zn-modified Ga_2O_3 photocatalyst in NaOH solution. Reaction conditions: Amount of catalyst, 1.0 g; cocatalyst: 1.0 wt%; volume of water, 1.0 L; flow rate of CO_2, 30 mL min^{-1}; concentration of NaOH , 0.1 mol L^{-1}; light source, high-pressure mercury lamp (400 W).

In chapter 1, we have reported that the evolution of CO over Ag-loaded Zn-modified Ga_2O_3 in the absence of either CO_2 gas or $NaHCO_3$ additive was much lower than that in the presence of both CO_2 molecules and $NaHCO_3$ additive.[17] This means the coexistence of dissolved CO_2 molecules and HCO_3^- species played an important role in the photocatalytic conversion of CO_2 with H_2O over Ag-loaded Zn-modified Ga_2O_3. Figure 6 shows the activity for the photocatalytic conversion of CO_2 with H_2O in the NaOH solution before the equilibrium was achieved. The flowing of CO_2 gas and photoirradiation started simultaneously. The amount of CO_2 molecules

dissolved in H_2O was constant because the volume and the temperature of the solution during the photoirradiation were unchanged and the CO_2 gas was continuously supplied into the solution. The dissolved CO_2 molecules could react with OH^- to form CO_3^{2-} and HCO_3^- species. The decrease of pH value represented the decrease of the concentration of OH^- species and the increase of the concentration of CO_3^{2-} and HCO_3^- species. When the pH was located between 12.82 and 10.21, CO_3^{2-} should be the main carbon species and only water splitting occurred in the photocatalytic reaction. As the pH declined from 10.21 to 8.08, HCO_3^- became the main species and the activity for CO evolution was obviously improved. Further introduction of CO_2 resulted in the continuous decrease of pH and the drastic increase of the activity for CO evolution. After 110 min, the pH of the reaction solution became stable at 6.69, indicating that the dynamic equilibrium of dissolved CO_2 and HCO_3^- was obtained. The formation rate of CO at this stage reached the maximum and remained steadily. Although it is difficult to speculate whether CO_2 molecule or HCO_3^- was the reducible species for the photocatalytic conversion of CO_2 with H_2O in the presence of alkaline additives, it is necessary to maintain the HCO_3^- as the major carbon species by making the balance between the dissolved CO_2 molecules and the HCO_3^- species in the reaction solution.

Conclusions

The photocatalytic conversion of CO_2 with H_2O over Ag-loaded Zn-modified Ga_2O_3 in the presence of various additives was examined. The addition of weak acid salts and alkalis (Na_3PO_4, $NaHCO_3$, Na_2CO_3, and NaOH) largely enhanced the activity for the evolution of CO as compared to the addition of NaCl and Na_2SO_4. The alkaline chemicals also affected the formation of CO for the photocatalytic conversion of CO_2 by H_2O in the presence of the carbonates and alkalis. The activity for the photocatalytic

conversion of CO_2 with H_2O over Ag-loaded Zn-modified Ga_2O_3 was promoted dramatically with the increase of the concentration of $NaHCO_3$ solution. The highest rate of CO evolution over Ag-loaded Zn-modified Ga_2O_3 reached 171.0 μmol h^{-1}, when the concentration of $NaHCO_3$ solution was higher than 1.0 mol L^{-1}. Based on the Bjerrum plot equations, it is known that the main carbon species in the aqueous solutions of weak acid salts and alkalis (Na_3PO_4, $NaHCO_3$, Na_2CO_3, and NaOH) was HCO_3^- species during the photocatalytic reaction. The equilibrium between the dissolved CO_2 molecules and the HCO_3^- species was essential for the photocatalytic conversion of CO_2 with H_2O in the aqueous solutions of weak acid salts and alkalis.

List of symbols

CO_2 (g): The gaseous CO_2;

CO_2 (aq): The dissolved CO_2;

[CO_2 (aq)]: The concentration of the dissolved CO_2, in mol L^{-1};

k_{cp}: The constant of Henry's law, in mol L^{-1} atm^{-1};

P_{CO_2} : Partial pressure of CO_2 above the solution, in atm;

[H_2CO_3]: The concentration of H_2CO_3 species, in mol L^{-1};

[HCO_3^-]: The concentration of HCO_3^- species, in mol L^{-1};

[CO_3^{2-}]: The concentration of CO_3^{2-} species, in mol L^{-1};

[H^+]: The concentration of H^+, in mol L^{-1};

K_1: The true first acid dissociation constant, in mol L^{-1};

K_1*: The apparent first acid dissociation constant, in mol L^{-1};

K_2: The second acid dissociation constant, in mol L^{-1}.

References and Notes

[1] E. V. Kondratenko, G. Mul, J. Baltrusaitis, G. O. Larrazábal, J. Pérez-Ramírez, *Energy Environ. Sci.* **2013**, *6*, 3112.

[2] A. Kubacka, M. Fernández-García, G. Colón, *Chem. Rev.* **2012**, *112*, 1555.

[3] K. Teramura, T. Tanaka, H. Ishikawa, Y. Kohno, T. Funabiki, *J. Phys. Chem. B* **2004**, *108*, 346.

[4] H. Tsuneoka, K. Teramura, T. Shishido, T. Tanaka, *J. Phys. Chem. C* **2010**, *114*, 8892.

[5] K. Teramura, S. Okuoka, H. Tsuneoka, T. Shishido, T. Tanaka, *Appl. Catal. B* **2010**, *96*, 565.

[6] X. Meng, S. Ouyang, T. Kako, P. Li, Q. Yu, T. Wang, J. Ye, *Chem. Commun.* **2014**, *50*, 11517.

[7] S. Xie, Y. Wang, Q. Zhang, W. Fan, W. Deng, Y. Wang, *Chem. Commun.* **2013**, *49*, 2451.

[8] L. Liu, C. Zhao, D. Pitts, H. Zhao, Y. Li, *Catal. Sci. Technol.* **2014**, *4*, 1539.

[9] K. Iizuka, T. Wato, Y. Miseki, K. Saito, A. Kudo, *J. Am. Chem. Soc.* **2011**, *133*, 20863.

[10] K. Teramura, S. Iguchi, Y. Mizuno, T. Shishido, T. Tanaka, *Angew. Chem. Int. Ed.* **2012**, *51*, 8008.

[11] T. Takayama, K. Tanabe, K. Saito, A. Iwasea, A. Kudo, *Phys. Chem. Chem. Phys.* **2014**, *16*, 24417.

[12] Z. Wang, K. Teramura, S. Hosokawa, T. Tanaka, *Appl. Catal. B* **2015**, *163*,241.

[13] K. Sayama, H. Arakawa, *J. Phys. Chem.* **1993**, *97*, 531.

[14] T. Xie , D. Wang, L. Zhu, T. Li, Y. Xu, *Mater. Chem. Phys.* **2001**, *70*, 103.

[15] Slamet, H. Nasution, E. Purnama, S. Kosela, J. Gunlazuardi, *Catal. Commun.* **2005**, *6*, 313.

[16] J. Mao, T. Peng, X. Zhang, K. Li, L. Ye, L. Zan, *Catal. Sci. Technol.* **2013**, *3*, 1253.

[17] K. Teramura, Z. Wang, S. Hosokawa, Y. Sakata, T. Tanaka, *Chem. Eur. J.* **2014**, *20*, 9906.

[18] S. Iguchi, K. Teramura, S. Hosokawa, T. Tanaka, *Catal. Today* **2014**, Ahead of Print 10.1016/j.cattod.2014.09.005.

[19] K. Maeda, H. Masuda, K. Domen, *Catal. Today* **2009**, *147*, 173.

[20] R. Sander, *Atmos. Chem. Phys. Discuss.* **2014**, *14*, 29615.

[21] Jolly, L. William, *Modern Inorganic Chemistry (McGraw-Hill* **1984***)*, p.196.

[22] M. Hofmann, H. Schellnhuber, *Energy Environ. Sci.* **2010**, *3*, 1883.

Chapter 4

Highly efficient photocatalytic conversion of CO_2 into CO using H_2O as a reductant over Ag-modified $ZnGa_2O_4$

Abstract

Highly crystalline spinel phase $ZnGa_2O_4$ modified with a Ag cocatalyst exhibited high activity and selectivity toward CO evolution in the photocatalytic conversion of CO_2 using H_2O as a reductant under UV light irradiation. The stoichiometric evolution of CO, H_2, and O_2 clearly indicated that H_2O worked as an electron donor for the photoreduction of CO_2. The catalyst fabrication conditions, such as calcination temperature and duration, had a significant effect on the degree of crystallinity in the $ZnGa_2O_4$ at the expense of surface area, and the photocatalytic activity of the catalyst was maximized by optimizing the balance of these properties. Furthermore, the formation of metallic Ag particles with different sizes and dispersions on the surface of $ZnGa_2O_4$ influenced the evolution of CO. When Ag nanoparticles were loaded onto the $ZnGa_2O_4$ calcined at 1123 K for 40 h using the chemical reduction method, the highest formation rates of CO, H_2, and O_2 (155.0, 8.5, and 74.3 μmol h^{-1}, respectively) were obtained, and the selectivity toward CO evolution reached 95.0%. An isotope-labeling experiment using $^{13}CO_2$ confirmed that the origin of the evolved CO was not from organic contamination but from the CO_2 gas introduced during the reaction process.

Introduction

Owing to the large global consumption of fossil fuels, the emission of greenhouse gases, such as CO_2, has resulted in an increase in their atmospheric concentration and an accelerated rise of global temperatures.[1-3] Growing concern about environmental problems has driven researchers to seek control of the atmospheric level of CO_2 through capture and storage.[2,3] From the viewpoint of the global carbon cycle, the catalytic conversion of CO_2 to liquid fuels and chemicals, utilizing CO_2 as a natural resource, is an attractive technology.[3,4] The recycling of CO_2 into fuels usually requires an extremely high energy input and a large supply of reductant, such as H_2 or CH_4.[3,4] Using solar light as an energy source and H_2O as a reductant, both of which are highly abundant, the photocatalytic conversion of CO_2 into useful chemical products such as CO, HCOOH, HCHO, CH_3OH, and CH_4 under ambient temperature and pressure would be a renewable and environmentally beneficial process.[3,5-7]

The photocatalytic conversion of CO_2 by H_2O, which can be regarded as artificial photosynthesis, is an uphill reaction making use of electrons generated by light energy.[5,7] The generation of H_2 from the reduction of protons usually competes for the photo-excited electrons and takes precedence over the reduction of CO_2, because the redox potential of H^+/H_2 (−0.41 V *vs.* NHE, at pH 7) is more positive than that of CO/CO_2 (−0.51 V *vs.* NHE, at pH 7).[8] In order to achieve the conversion of CO_2 rather than the production of H_2 by H_2O over heterogeneous photocatalysts, it is extremely important to improve the selectivity of generated electrons toward the reduction of CO_2.[9] Moreover, a stoichiometric amount of O_2 should be evolved if H_2O functions efficiently as an electron donor.[9] Although various metal oxide photocatalysts have been reported for CO_2 reduction in H_2O, only a few materials, i.e.,

$ALa_4Ti_4O_{15}$ (where A = Ca, Sr and Ba),[10] Zn-doped Ga_2O_3,[9] and $La_2Ti_2O_7$,[11] showed higher selectivity for CO_2 reduction and simultaneously produced O_2 stoichiometrically. Therefore, the development of more active photocatalysts for the conversion of CO_2 using H_2O as a reductant is imperative.

It is known that the spinel type oxide $ZnGa_2O_4$, with a wide band gap of 4.4-5.0 eV, can efficiently decompose H_2O into H_2 and O_2, without any sacrificial reagents, under UV irradiation.[12] Since the reduction of CO_2 requires a reduction potential higher than that of H^+, the wide band gap of $ZnGa_2O_4$, which is capable of generating photoelectrons with a high reduction potential, should result in the efficient reduction of CO_2. Indeed, $ZnGa_2O_4$ possessing various morphologies, such as mesoporous,[13] nanocube,[14] and ultrathin nanosheet,[15] has been studied in the photocatalytic reduction of CO_2 with H_2O. However, the conversion efficiency of CO_2 in these studies was still low, and a stoichiometric amount of O_2 was not generated in the reactions. In addition, high crystallinity in a photocatalyst has a positive effect on its activity due to the elimination of defects, which usually act as recombination centers for photogenerated pairs.[16] In this study, we investigated the fabrication conditions for highly crystalline $ZnGa_2O_4$, prepared by the typical solid state reaction method, for the photocatalytic conversion of CO_2 using H_2O as an electron donor, and examined the relationship between the crystallinity of the $ZnGa_2O_4$ and its photocatalytic activity. Furthermore, we studied the effect of a Ag cocatalyst on the selectivity toward CO evolution.

Experimental section

$ZnGa_2O_4$ was fabricated by a conventional solid state reaction method. A stoichiometric mixture of Ga_2O_3 (99.0%, Kojundo) and ZnO (99.0%, Wako) was ground

in the presence of small amount of water as a dispersant. The slurry was mixed thoroughly for 1 h and then dried at 353 K for 1 h. The resulting mixture was calcined from 973 K to 1473 K for 5–90 h in static air. The Ag cocatalyst was introduced to the $ZnGa_2O_4$ by photodeposition, impregnation, and chemical reduction methods. The photodeposition method was employed *in situ* during the photocatalytic conversion of CO_2. For the impregnation method, photocatalyst (1.5 g) were dispersed in an aqueous $AgNO_3$ solution homogeneously, followed by evaporation, drying, and calcination at 723 K for 2 h in a stream of dry air. For the chemical reduction method, an aqueous $NaPH_2O_2$ solution (0.4 μmol L^{-1}) was added to 50 mL of a suspension of the photocatalyst (1.5 g) containing a given amount of $AgNO_3$. After stirring at 353 K for 1.5 h, the modified photocatalyst was filtered and dried *in vacuo* at room temperature.

The structure and crystallinity of $ZnGa_2O_4$ samples were characterized by X-ray diffraction (XRD) using a Rigaku Multi Flex powder X-ray diffractometer. The Brunauer–Emmett–Teller (BET) surface area was measured by N_2 adsorption at 77 K using a volumetric gas adsorption apparatus (BELmini, Bel Japan, Inc.). The Ag K-edge (25.5 keV) X-ray absorption fine structure (XAFS) measurements were made in fluorescence mode at the BL01B1 beamline of the SPring-8 synchrotron radiation facility (Hyogo, Japan). The spectra were reduced by a Rigaku REX2000 program Ver. 2.5.9 (Rigaku Corp.). The UV-Vis diffuse reflectance spectra (UV-Vis DRS) were measured by a JASCO Corporation V-670 spectrometer equipped with an integrating sphere. Spectralon like $BaSO_4$, supplied by Labsphere Inc. was used as a reflection standard. TEM images were obtained with a JEOL JEM-1400 transmission electron microscope (TEM) operating at an accelerating voltage of 120 kV.

The photocatalytic reaction was carried out in a flow system using an inner-irradiation-type reaction vessel at room temperature and ambient pressure. The photocatalyst (1.0 g) was dispersed in ultra-pure water (1.0 L) containing 0.1 mol of $NaHCO_3$, and CO_2 gas (99.999%) was bubbled into the solution at a flow rate of 30 mL min^{-1}. The suspension was irradiated under a 400 W high-pressure mercury lamp with a quartz filter connected to a water cooling system. Generated gaseous products such as H_2, O_2, and CO were analyzed by thermal conductivity detector-gas chromatography (TCD-GC) using a GC-8A chromatograph (Shimadzu Corp.) equipped with a Molecular Sieve 5A column with Ar as the carrier gas, and by flame ionization detector-gas chromatography (FID-GC) using a methanizer and a ShinCarbon ST column with N_2 as the carrier gas. In the isotope-labeling experiment, $^{12}CO_2$ gas was replaced by $^{13}CO_2$. The formation of ^{13}CO and ^{12}CO under photoirradiation was analyzed by a quadrupole-type mass spectrometer (BEL Japan, Inc., BEL Mass) combined with the TCD-GC using Ar as the carrier gas.

Results and Discussion

The synthesis of highly crystalline $ZnGa_2O_4$ by the solid state reaction method requires thermal treatment at a high calcination temperature for a long duration. Figures 1(A) and (B) show the XRD patterns of $ZnGa_2O_4$ under different thermal treatment conditions. All samples calcined from 973 K to 1473 K exhibited the typical spinel structure of $ZnGa_2O_4$ (Figure 1(A)), but there was some impurity assigned to ZnO in the case of $ZnGa_2O_4$ calcined at 973 K. This indicates that calcination above 973 K after the physical mixing procedure employed here successfully causes crystallization of $ZnGa_2O_4$. Moreover, all the peaks in the XRD patterns of $ZnGa_2O_4$ became sharper and more intense when the calcination temperature increased from 973 K to 1473 K,

implying that the crystallinity of bulk $ZnGa_2O_4$ increases with an increase in the calcination temperature.

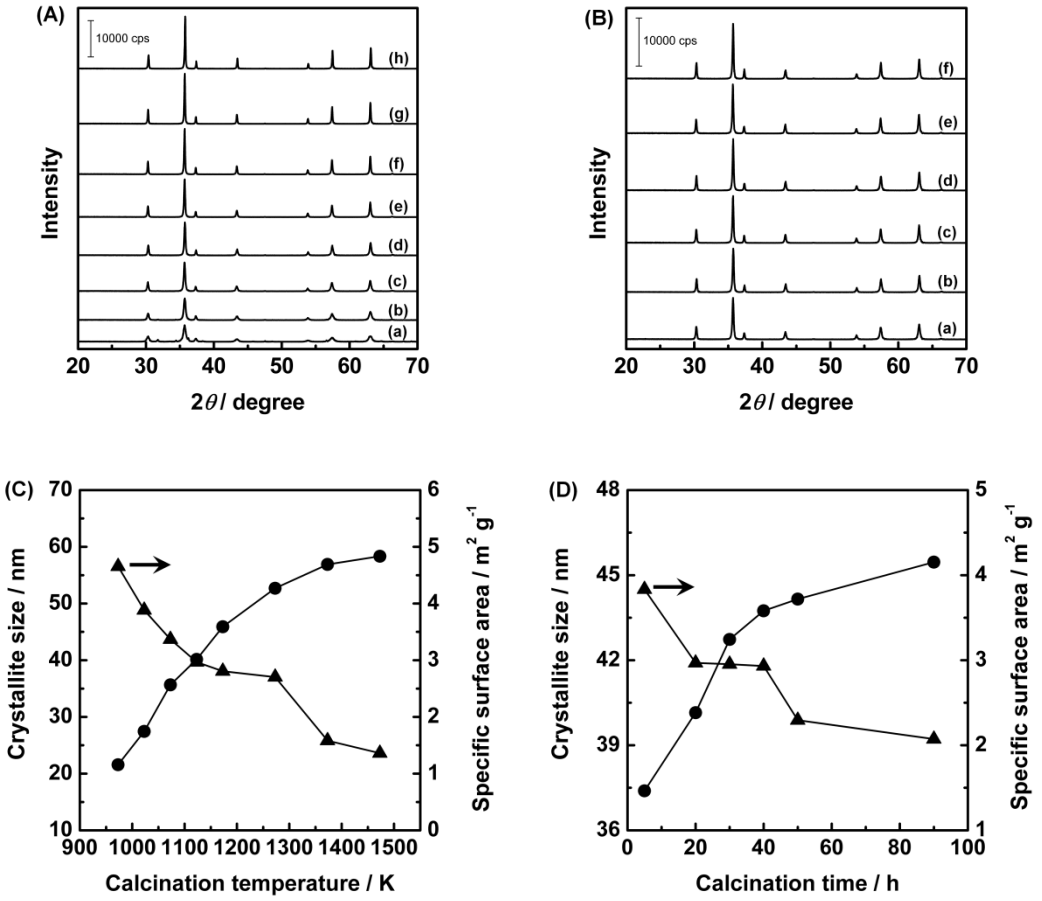

Figure 1 (A) XRD patterns of $ZnGa_2O_4$ calcined at 973 K (a), 1023 K (b), 1073 K (c), 1123 K (d), 1173 K (e), 1273 K (f), 1373 K (g), and 1473 K (h) for 20 h; (B) XRD patterns of $ZnGa_2O_4$ calcined at 1123 K for 5 h (a), 20 h (b), 30 h (c), 40 h (d), 50 h (e), and 90 h (f); (C) Crystallite size and specific surface area of $ZnGa_2O_4$ calcined at various temperatures for 20 h; (D) Crystallite size and specific surface area of $ZnGa_2O_4$ calcined at 1123 K for different time.

The calcination time also promoted the crystallinity of $ZnGa_2O_4$. As shown in Figure 1(B), the XRD patterns for $ZnGa_2O_4$ samples that were calcined at 1123 K for 5 h to 90 h show a slight increase in peak intensity. In addition, the increased crystallinity of $ZnGa_2O_4$ is indicated by the larger crystallite size. The crystallite size of $ZnGa_2O_4$

can be obtained using FWHM (Full Width of Half Maximum) for the XRD peaks, based on Scherrer's equation. Figure 1(C) shows that the crystallite size of $ZnGa_2O_4$ calcined at temperatures ranging from 973 K to 1473 K increased gradually from 21.5 nm to 58.3 nm. Conversely, the specific surface area of $ZnGa_2O_4$ samples, which was measured by the BET method, decreases as the calcination temperature is elevated. Similarly, a small increase in the crystallite size and a small reduction in the BET surface area with longer calcination time are observed in Figure 1(D). These results show that calcination at various temperatures for different times affects not only the crystallite size, but also their specific surface area.

It is known that the photocatalytic activity is highly influenced by the crystallinity and specific surface area of the photocatalyst. This is because the photocatalytic reaction occurs mainly on the surface of the photocatalyst, and high crystallinity in the photocatalyst provides smooth charge separation. However, calcination temperature and time promote the crystallization of the photocatalyst and simultaneously diminish the surface area. The balance between crystallization and specific surface area must be finely tuned to obtain the maximum photocatalytic activity. Thus, the activities for the photocatalytic conversion of CO_2 by H_2O under UV irradiation of $ZnGa_2O_4$ catalysts prepared under different conditions were compared. Figure 2(A) shows the formation rates of CO, O_2 and H_2 and the selectivity toward CO evolution with $ZnGa_2O_4$ calcined at various temperatures for 20 h. The surfaces of all the samples were modified with Ag by the photodeposition method. All the $Ag/ZnGa_2O_4$ photocatalysts produced CO as a main reduction product and significantly suppressed the production of H_2, except for the sample sintered at 973 K. According to the XRD patterns, the impurity in this particular $ZnGa_2O_4$ structure may be responsible for the

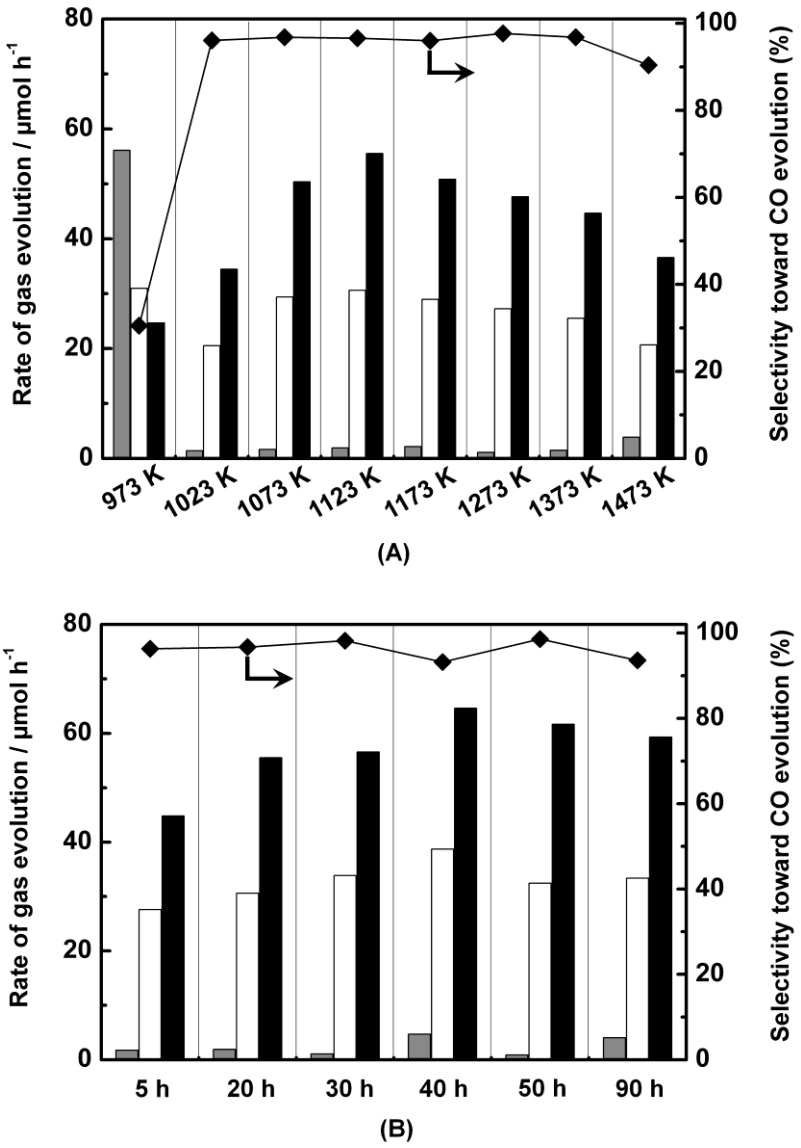

Figure 2 (A) The rate of CO (black), O_2 (white), and H_2 (gray) evolution and selectivity toward CO evolution over $ZnGa_2O_4$ calcined at various temperatures for 20 h; (B) The rate of CO (black), O_2 (white), and H_2 (gray) evolution and selectivity toward CO evolution over $ZnGa_2O_4$ at 1123 K for different time. Ag cocatalyst was modified by the photodeposition method and the loading amount was 1.0 wt%. Amount of catalyst under photoirradiation using a 400 W high-pressure mercury lamp: 1.0 g, volume of water: 1.0 L, CO_2 flow rate: 30 mL min^{-1}, additve: $NaHCO_3$ (0.1 mol L^{-1}).

much higher yield of H_2. Thus, the selectivity toward CO evolution over H_2 evolution on $ZnGa_2O_4$ with a pure spinel phase was stable above 90%. The simultaneous

stoichiometric evolution of O_2 confirmed that H_2O functions as an electron donor and consumes the photo-holes generated during the photocatalytic conversion of CO_2. The evolution of CO over Ag-modified $ZnGa_2O_4$ was improved with an increase in the calcination temperature from 973 K to 1123 K, which can be attributed to the increased crystallinity of the $ZnGa_2O_4$, despite the decrease in its specific surface area. The highest formation rate of CO was obtained over $ZnGa_2O_4$ calcined at 1123 K. However, the formation rate of CO declined with an increase in the calcination temperatures beyond 1123 K due to the diminishing surface area of the $ZnGa_2O_4$ catalyst. As with the calcination temperature, the increase of calcination time from 5 h to 90 h also influenced the activity of the $ZnGa_2O_4$ (Figure 2(B)). The incremental crystallite size of $ZnGa_2O_4$ heated at 1123 K from 5 h to 40 h resulted in the promotion of CO evolution. Further increase in the calcination time led to a slight increase in crystallite size and a slight decrease in surface area, thus the formation rate of CO did not drop significantly. It is noteworthy that $ZnGa_2O_4$ calcined at 1123 K for 40 h had the optimized balance of crystallite size and specific surface area, and exhibited the highest activity for the photocatalytic conversion of CO_2 with H_2O.

Ag metal has been employed as an effective electrode in the electrochemical reduction of CO_2 for CO production.[17] The modification of the surface of $ZnGa_2O_4$ with a Ag cocatalyst also has a significant effect on the photocatalytic conversion of CO_2 with H_2O. Figure 3 and Figure 4 show the Ag K-edge XANES, EXAFS, and Fourier transforms (FT) of EXAFS spectra of Ag-modified $ZnGa_2O_4$ prepared by the photodeposition, impregnation and chemical reduction methods. The XANES spectral shape of the three samples was similar to that of Ag foil (Figure 3), indicating that all

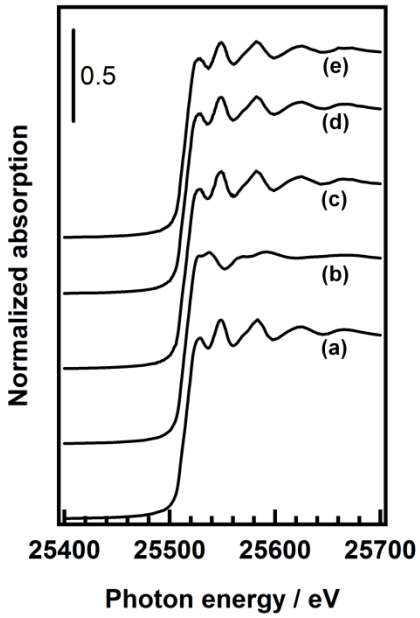

Figure 3 Ag K-edge XANES spectra of Ag foil (a), Ag_2O (b), and the Ag-modified $ZnGa_2O_4$ prepared by the photodeposition method (c), impregnation method (d), and chemical reduction method (e). $ZnGa_2O_4$ was calcined at 1123 K for 40 h and the loading amount of Ag was 1.0 wt%.

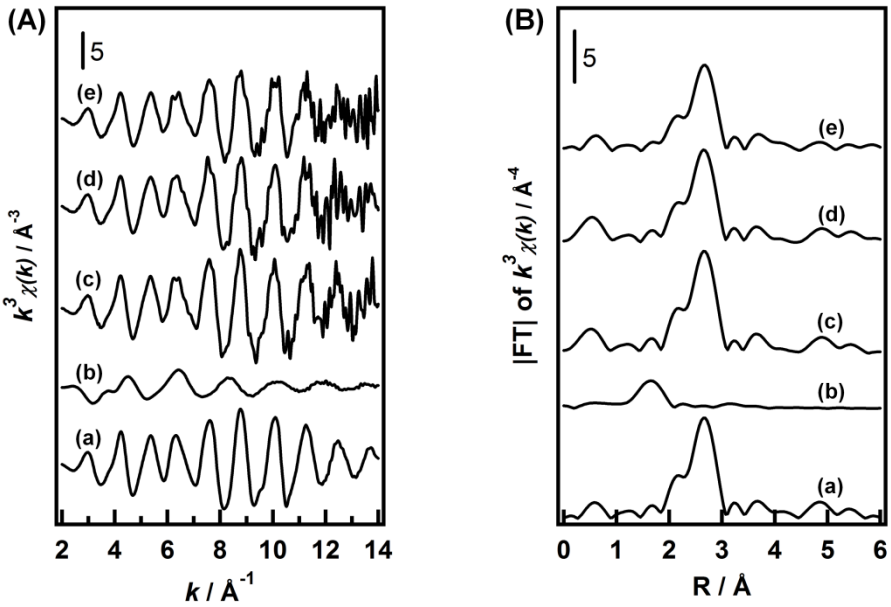

Figure 4 Ag K-edge EXAFS (A), and Fourier transforms (FT) of EXAFS (B) spectra of Ag foil (a), Ag_2O (b), and the Ag-modified $ZnGa_2O_4$ prepared by the photodeposition method (c), impregnation method (d), and chemical reduction method (e). $ZnGa_2O_4$ was calcined at 1123 K for 40 h and the loading amount of Ag was 1.0 wt%.

Ag species loaded by the three methods are metallic Ag. Moreover, the same characteristic distance of Ag-Ag shell peaks for the three photocatalysts and Ag foil in the FT of EXAFS spectra (Figure 4) confirm that Ag metal is present on the $ZnGa_2O_4$. However, the height of the Ag-Ag shell peak of $ZnGa_2O_4$ Ag-modified by the chemical reduction method was lower than those of the samples synthesized by the photodeposition and impregnation methods, indicating that the particle size of the Ag cocatalyst in the chemical reduction sample is the smallest among the three samples.

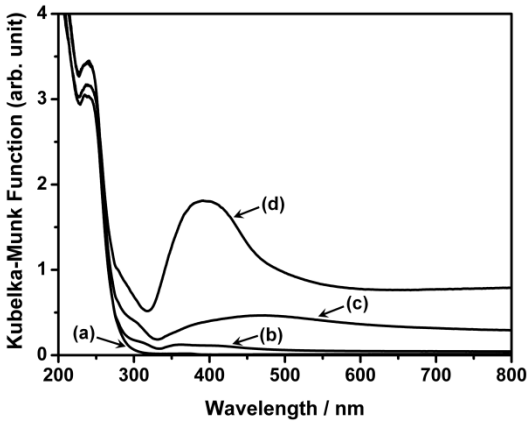

Figure 5 UV-Vis DRS of bare $ZnGa_2O_4$ (a), and the Ag-modified $ZnGa_2O_4$ prepared by the photodeposition method (b), impregnation method (c), and chemical reduction method (d). $ZnGa_2O_4$ was calcined at 1123 K for 40 h and the loading amount of Ag was 1.0 wt%.

The UV-Vis DRS of bare $ZnGa_2O_4$ and Ag-modified $ZnGa_2O_4$ loaded by the three methods are shown in Figure 5. The absorption edge of bare $ZnGa_2O_4$ was located at 270 nm and the band gap energy of $ZnGa_2O_4$ was estimated to be 4.67 eV by Davis–Mott's equation.[18] All the Ag-modified $ZnGa_2O_4$ samples exhibited the same intrinsic absorption as bare $ZnGa_2O_4$. A strong surface plasmon absorption at around 400 nm and a wide absorption in the visible and near-infrared region were observed for the Ag-modified $ZnGa_2O_4$ prepared by the chemical reduction method, indicating that

the Ag particles with small size were densely dispersed on the surface of the $ZnGa_2O_4$.[19] For Ag-modified $ZnGa_2O_4$ fabricated by the photodeposition and impregnation methods, weak surface plasmon absorptions could be attributed to the aggregation and poor dispersion of Ag particles. Figure 6 shows the TEM images of Ag-modified $ZnGa_2O_4$ prepared by the three methods. Clearly, the chemical reduction method formed highly dispersed Ag particles with a narrow particle size distribution in comparison with the photodeposition and wet impregnation methods, which is consistent with the results of the XAFS and UV-Vis DRS experiments.

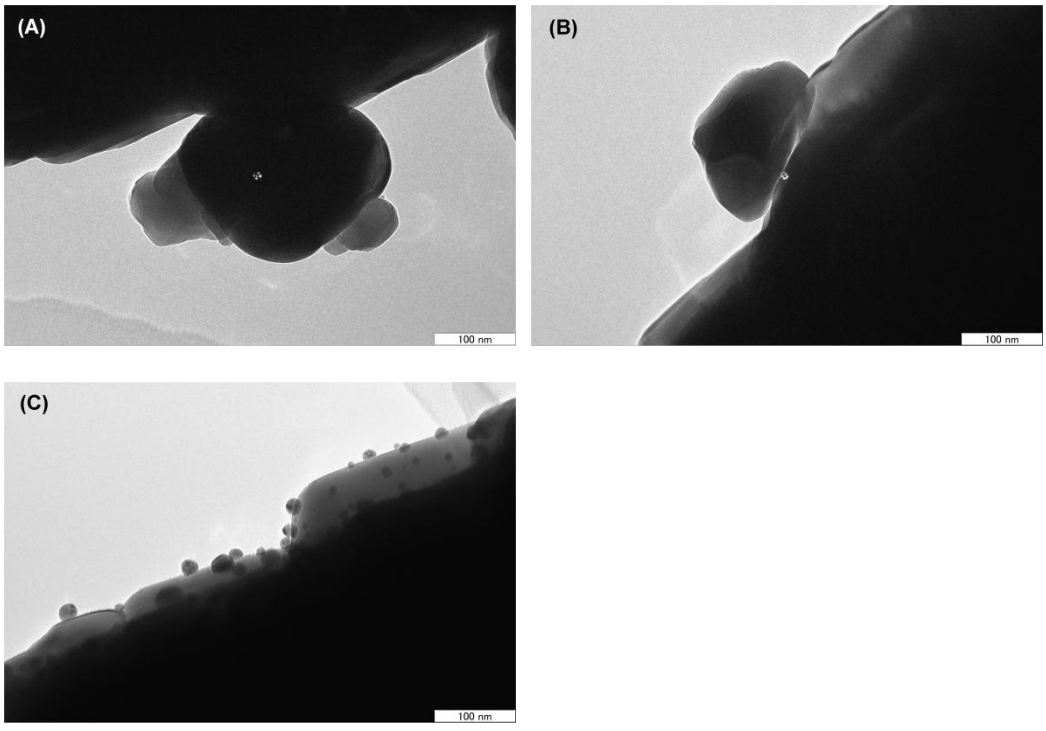

Figure 6 TEM images of Ag-modified $ZnGa_2O_4$ prepared by photodeposition method (A), impregnation method (B), and chemical reduction method (C). $ZnGa_2O_4$ was calcined at 1123 K for 40 h and the loading amount of Ag was 1.0 wt%.

Figure 7 shows the dependence of the activity for the photocatalytic conversion of CO_2 by H_2O on the Ag-modification method. It can be seen that CO, H_2, and O_2 are evolved in stoichiometric amounts over the Ag-modified $ZnGa_2O_4$ prepared by the three

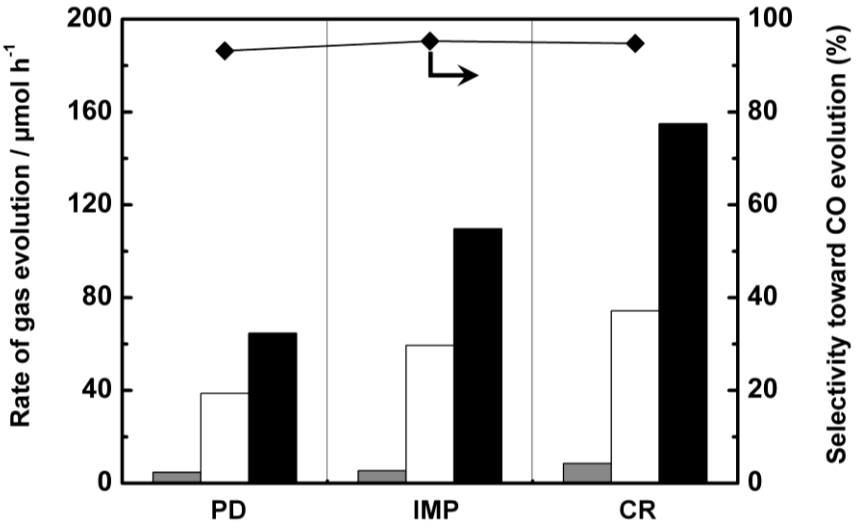

Figure 7 The rates of CO (black), O_2 (white), and H_2 (gray) evolution and selectivity toward CO evolution over Ag-modified $ZnGa_2O_4$ prepared by PD (photodeposition method), IMP (impregnation method), and CR (chemical reduction method). $ZnGa_2O_4$ was calcined at 1123 K for 40 h and the loading amount of Ag was 1.0 wt%. Amount of catalyst under photoirradiation using a 400 W high-pressure mercury lamp: 1.0 g, volume of water: 1.0 L, CO_2 flow rate: 30 mL min^{-1}, additve: $NaHCO_3$ (0.1 mol L^{-1}).

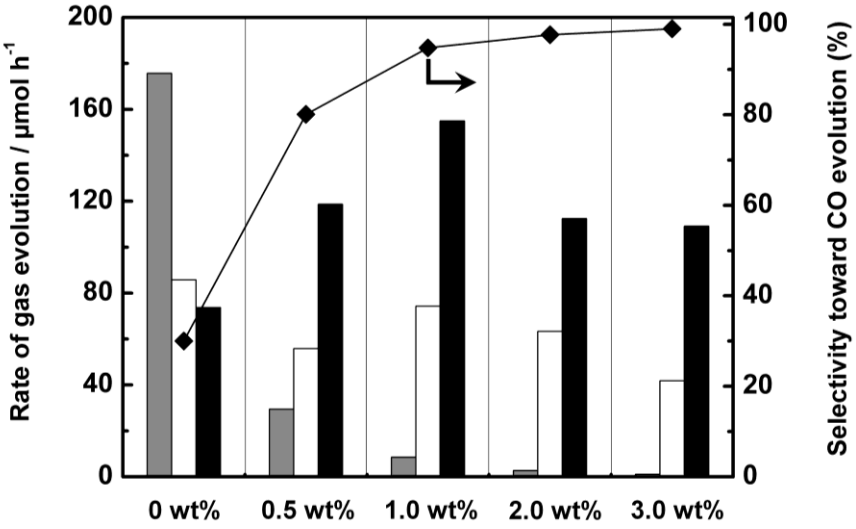

Figure 8 The rate of CO (black), O_2 (white), and H_2 (gray) evolution and selectivity toward CO evolution over Ag-modified $ZnGa_2O_4$ with different Ag contents. $ZnGa_2O_4$ was calcined at 1123 K for 40 h. Ag cocatalyst was modified by chemical reduction method. Amount of catalyst under photoirradiation using a 400 W high-pressure mercury lamp: 1.0 g, volume of water: 1.0 L, CO_2 flow rate: 30 mL min^{-1}, additve: $NaHCO_3$ (0.1 mol L^{-1}).

methods, and that the selectivity toward CO evolution was similar in each case. Due to the formation of metallic Ag nanoparticles with small size and good dispersion on the $ZnGa_2O_4$, the Ag-modified $ZnGa_2O_4$ by the chemical reduction method exhibited significantly enhanced photocatalytic activity for the conversion of CO_2 to CO. The effect of loading amount of Ag cocatalyst on the evolution of CO is shown in Figure 8. Conversion of CO_2 to CO can take place on bare $ZnGa_2O_4$, but in that case the rate of H_2 evolution (175.7 μmol h^{-1}) was higher than that of CO evolution (73.7 μmol h^{-1}). The total photocatalytic activity of the bare $ZnGa_2O_4$ was high, whereas the selectivity toward CO evolution was quite low. This is because the number of suitable reaction sites for the reduction of CO_2 is insufficient on the surface of the highly crystalline $ZnGa_2O_4$, and the water-splitting reaction competed with the reduction of CO_2 for these reaction sites. The modification of $ZnGa_2O_4$ with a Ag cocatalyst caused a dramatic increase in the photocatalytic activity for the evolution of CO. While the formation rate of CO increased with the addition of larger amounts of Ag from 0 to 1.0 wt%, the rate declined with further loading of Ag. The maximum activity was obtained with $ZnGa_2O_4$ loaded with 1 wt% of the Ag cocatalyst. Conversely, the production of H_2 steadily decreased with an increase of Ag loading, thus the selectivity for CO over H_2 increased and reached 99.0%. It is clear that the surface modification of the photocatalyst efficiently changes the selectivity toward CO evolution. The introduction of an Ag cocatalyst provides enough catalytic sites for the reduction of CO_2 on the surface of $ZnGa_2O_4$, therefore the conversion of CO_2 to CO took precedence over the production of H_2 at such sites.

The time course of CO, H_2, and O_2 evolved during the photocatalytic conversion of CO_2 by H_2O over Ag-modified $ZnGa_2O_4$ under optimized conditions is

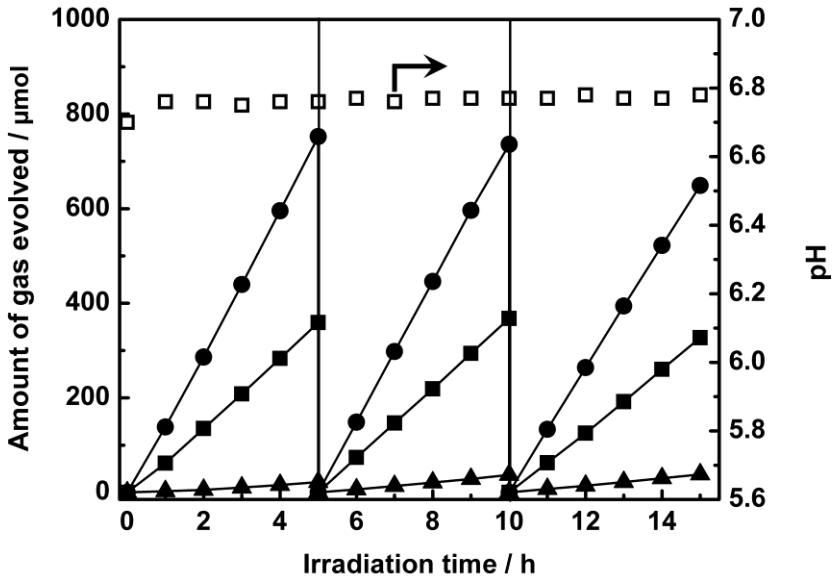

Figure 9 Time courses of CO (circle), O_2 (square), and H_2 (triangle) evolutions for the photocatalytic conversion of CO_2 by H2O over Ag-modified $ZnGa_2O_4$. $ZnGa_2O_4$ was calcined at 1123 K for 40 h. Ag cocatalyst was modified by chemical reduction method and the loading amount was 1.0 wt%. Amount of catalyst under photoirradiation using a 400 W high-pressure mercury lamp: 1.0 g, volume of water: 1.0 L, CO_2 flow rate: 30 mL min^{-1}, additve: $NaHCO_3$ (0.1 mol L^{-1}).

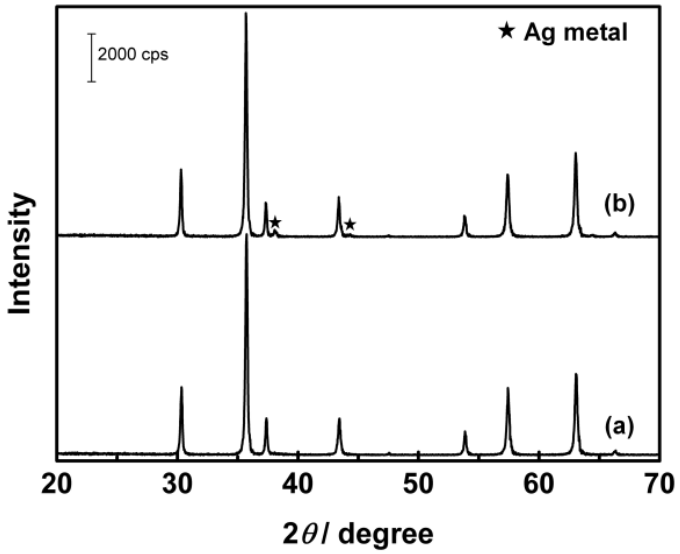

Figure 10 XRD patterns of Ag-modified $ZnGa_2O_4$ before (a) and after (b) the 15h reaction. $ZnGa_2O_4$ was calcined at 1123 K for 40 h. Ag cocatalyst was modified by chemical reduction method and the loading amount was 1.0 wt%.

shown in Figure 9. CO was evolved as a main reduction product, and only a very small amount of H_2 was generated. Simultaneously, the evolution of O_2 linearly increased during the reaction. The formation rates of CO, H_2, and O_2 (155.0, 8.5 and 74.3 μmol h^{-1}, respectively) were in an approximately stoichiometric ratio, indicating that the number of photogenerated electrons used in the reduction of CO_2 and protons was equivalent to that of holes consumed by the oxidation of H_2O. After 5 h of photoirradiation, we obtained 752 μmol of CO, 21.7 μmol of H_2, and 359 μmol of O_2. The reaction was repeated three times, and the evolution of CO slightly decreased on the third run. The XRD patterns of Ag-modified $ZnGa_2O_4$ before and after the photocatalytic reaction in Figure 10 indicate that the crystalline structure of $ZnGa_2O_4$ is very stable under UV light irradiation and in aqueous medium. A diffraction peak assigned to the metallic Ag appeared in the case of Ag-modified $ZnGa_2O_4$ after the reaction, indicating that the Ag particles undergo aggregation under photoirradiation. Moreover, the coalesced Ag particles after the reaction are distinct in the TEM images, as shown in Figure 11. It is believed that the change in the particle size of the Ag cocatalyst, which is caused by the redeposition and aggregation of Ag species on the $ZnGa_2O_4$ during photoirradiation, is responsible for the decrease in evolution of CO in the long-duration reaction. It is important to maintain the small particle size and uniform dispersion of the metallic Ag cocatalyst during the conversion of CO_2 in H_2O, and investigation of this phenomenon is currently underway in our group in order to improve the activity and stability of the Ag-modified photocatalysts.

In the photocatalytic conversion of CO_2, any organic contamination could result in the misestimating of carbon-containing products. Although the residual carbon species on the $ZnGa_2O_4$ surface could be eliminated through the high-temperature

fabrication process, it is important to confirm the carbon source of the gas products,

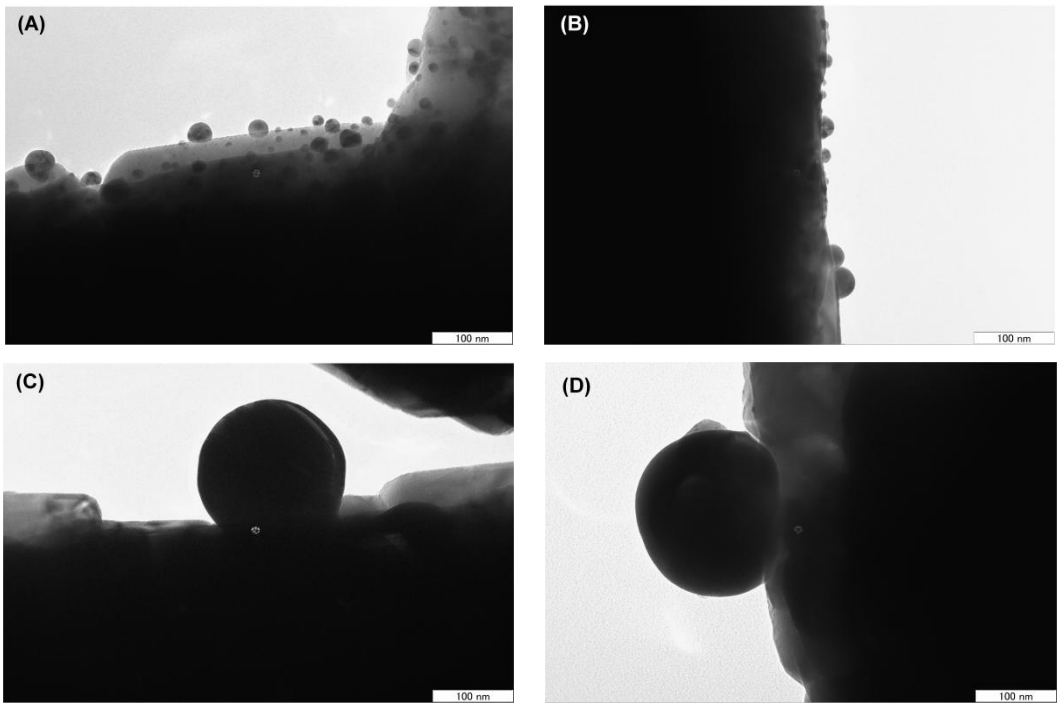

Figure 11 TEM images of Ag-modified $ZnGa_2O_4$ prepared by chemical reduction method before (A, B) and after (C, D) the photocatalytic conversion of CO_2. $ZnGa_2O_4$ was calcined at 1123 K for 40 h. The loading amount of Ag cocatalyst was 1.0 wt%.

which we have done through an isotope-labeling experiment using $^{13}CO_2$. Figure 12 shows the mass spectra (*m*/*z* 28 and 29) during the photocatalytic conversion of $^{13}CO_2$ by H_2O over $ZnGa_2O_4$ modified with Ag by the chemical reduction method. Sampled gases were introduced to a mass spectrometer after separation by gas chromatography. The peak in the spectrum of *m*/*z* = 29, which is attributed to the ^{13}CO gas, appears at the same retention time as that monitored by GC. This result shows that the CO evolved over Ag-modified $ZnGa_2O_4$ originates from the introduced CO_2 gas.

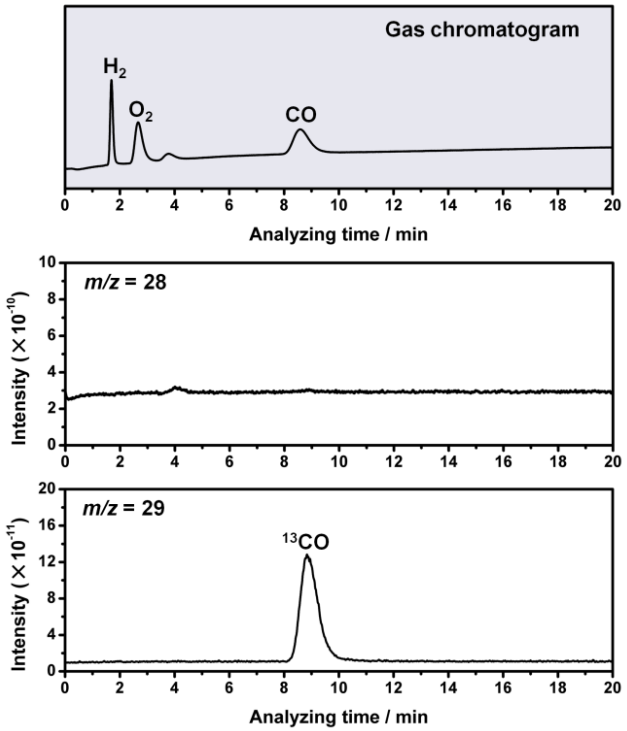

Figure 12 Gas chromatogram and mass spectra (*m/z* 28 and 29) in the photocatalytic conversion of $^{13}CO_2$ by H_2O over Ag-modified $ZnGa_2O_4$. $ZnGa_2O_4$ was calcined at 1123 K for 40 h. Ag cocatalyst was modified by chemical reduction method and the loading amount was 1.0 wt%. Amount of catalyst under photoirradiation using a 400 W high-pressure mercury lamp: 1.0 g, volume of water: 1.0 L, CO_2 flow rate: 30 mL min^{-1}, additve: $NaHCO_3$ (0.1 mol L^{-1}).

Conclusion

Ag-modified $ZnGa_2O_4$ exhibited high activity and selectivity toward CO production in the photocatalytic conversion of CO_2 by H_2O. The stoichiometric evolution of O_2 proves that H_2O can function efficiently as an electron donor during the photocatalytic conversion of CO_2. The crystallinity of the $ZnGa_2O_4$ catalyst increased, and the surface area decreased, with increasing calcination temperature and time. The maximum amount of CO was produced over $ZnGa_2O_4$ calcined at 1123 K for 40 h. Modification of the catalyst with an Ag cocatalyst by the chemical reduction method

also improved the photocatalytic activity of $ZnGa_2O_4$. Thus, 155.0 μmol h^{-1} of CO, 8.5 μmol h^{-1} of H_2, and 74.3 μmol h^{-1} of O_2 were obtained using Ag-modified $ZnGa_2O_4$ under optimized conditions. An isotope-labeling reaction using $^{13}CO_2$ provided evidence that the carbon source of evolved CO is not residual carbon species on the photocatalyst surface, but is the CO_2 introduced in the gas phase.

References and Notes

[1] J. Hansen, L. Nazarenko, R. Ruedy, M. Sato, J. Willis, A. Del Genio, D. Koch, A. Lacis, K. Lo, S. Menon, T. Novakov, J. Perlwitz, G. Russell, G. A. Schmidt, N. Tausnev, *Science* **2005**, *308*, 1431.

[2] M. Mikkelsen, M. Jorgensen, F. C. Krebs, *Energy Environ. Sci.* **2010**, *3*, 43.

[3] E. V. Kondratenko, G. Mul, J. Baltrusaitis, G. O. Larraz ábal, J. P érez-Ram írez, *Energy Environ. Sci.* **2013**, *6*, 3112.

[4] G. Centi, E. A. Quadrelli, S. Perathoner, *Energy Environ. Sci.* **2013**, *6*, 1711.

[5] A. Kubacka, M. Fern ández-Garc á, G. Col ón, *Chem. Rev.* **2012**, *112*, 1555.

[6] J. Mao, K. Li, T. Peng, *Catal. Sci. Technol.* **2013**, *3*, 2481.

[7] W. Fan, Q. Zhang, Y. Wang, *Phys. Chem. Chem. Phys.* **2013**,*15*, 2632.

[8] K. Li, A. D. Handoko, M. Khraisheh, J. Tang, *Nanoscale* **2014**, *6*, 9767.

[9] K. Teramura, Z. Wang, S. Hosokawa, Y. Sakata, T. Tanaka, *Chem. Eur. J.* **2014**, *20*, 9906.

[10] K. Iizuka, T. Wato, Y. Miseki, K. Saito, A. Kudo, *J. Am. Chem. Soc.* **2011**, *133*, 20863.

[11] Z. Wang, K. Teramura, S. Hosokawa, T. Tanaka, *Appl. Catal. B* **2015**, *163*,241.

[12] K. Ikarashi, J. Sato, H. Kobayashi, N. Saito, H. Nishiyama, Y. Inoue, *J. Phys. Chem.*

B **2002**, *106*, 9048.

[13] S. C.Yan, S. X. Ouyang, J. Gao, M. Yang, J. Y. Feng, X. X. Fan, L. J. Wan, Z. S. Li, J. Ye, Y. Zhou, Z. Zou, *Angew. Chem., Int. Ed.* **2010**, *49*, 6400.

[14] S. Yan, J. Wang, H. Gao, N. Wang, H. Yu, Z. Li, Y. Zhou, Z. Zou, *Adv. Funct. Mater.* **2013**, *23*, 758.

[15] Q. Liu, D. Wu, Y. Zhou, H. Su, R. Wang, C. Zhang, S. Yan, M. Xiao, Z. Zou, *ACS Appl. Mater. Interfaces* **2014**, *6*, 2356.

[16] K. Maeda, K. Domen, *J. Phys. Chem. C* **2007**, *111*, 7851.

[17] Y. Hori, K. Kikuchi, S. Suzuki, *Chem. Lett.* **1985**, *14*, 1695.

[18] K. Teramura, S. Okuoka, H. Tsuneoka, T. Shishido, T. Tanaka, *Appl. Catal. B* **2010**, *96*, 565.

[19] K. Chen, Y. Pu, K. Chang, Y. Liang, C. Liu, J. Yeh, H. Shih, Y. Hsu, *J. Phys. Chem. C* **2012**, *116*, 19039.

Chapter 5

Photocatalytic conversion of CO_2 in water over Ag-modified $La_2Ti_2O_7$

Abstract

We have found that Ag-modified $La_2Ti_2O_7$ with a layered perovskite structure exhibits activity for the photocatalytic conversion of CO_2 to CO in pure water. The evolution of O_2 proves that H_2O works as an electron donor for the photocatalytic conversion of CO_2. CO was generated as the main product, and CO, H_2, and O_2 were produced in stoichiometric amounts. The crystallite size of $La_2Ti_2O_7$ increased and the surface area decreased with increasing calcination temperature and time. Maximization of the photocatalytic activity of $La_2Ti_2O_7$ was accomplished by making a trade-off between the crystallite size and surface area. In addition, the loading amount and modification method of the Ag cocatalyst also influenced the amount of CO evolved. An isotope labeling experiment using $^{13}CO_2$ confirmed that the origin of evolved CO was not the residual carbon species on the $La_2Ti_2O_7$ surface, but was rather the CO_2 gas that was introduced during the experimental process.

Introduction

Due to the increased rates of deforestation and combustion of fossil fuels, CO_2 greenhouse gas emissions in the atmosphere is increasingly becoming an environmental hazard due to an accelerated rise in global temperatures [1,2]. Therefore, it is essential to not only control the level of CO_2 emissions, but to devise strategies to effectively remove CO_2 from the atmosphere. Among the various strategies for reducing the concentration of CO_2, the catalytic conversion of CO_2 to liquid fuels and chemicals is appealing due to the utilization of CO_2 as a natural derivative for production [3,4]. However, elevated temperature-pressure processes require a significant input of energy. Using solar light as an ideal and abundant energy source, it is possible to devise a promising route for the photocatalytic conversion of CO_2 into useful chemical products such as CO, HCOOH, HCHO, CH_3OH, and CH_4 under ambient temperature and pressure conditions [5,6].

The photocatalytic conversion of CO_2, an example of artificial photosynthesis, is a thermodynamically uphill reaction that utilizes photo-generated electrons as a source of energy [7]. It is difficult to achieve the reduction of CO_2 by H_2O over heterogeneous photocatalysts due to the competing generation of H_2 gas from the overall splitting of water [8]. Moreover, a stoichiometric amount of evolved O_2 should also be obtained if H_2O functions as an electron donor during the photocatalytic conversion of CO_2. Although various photocatalysts such as TiO_2 [9,10], CdS [11], $BiVO_4$ [12], and $ZnGa_2O_4$ [13] have been reported for the reduction of CO_2 in H_2O, the evolution of O_2 was not observed in the reaction, implying that the consumption of photogenerated holes is ambiguous. Until recently, Kudo et al. have discovered the photocatalytic conversion of CO_2 by H_2O over Ag modified $ALa_4Ti_4O_{15}$ (A=Ca, Sr, and

Ba), where the amount of evolved CO was higher than the amount of evolved H_2, and a stoichiometric amount of O_2 was also simultaneously observed [14].

It is known that La-Ti based oxide materials with a layered perovskite structure can efficiently decompose H_2O into H_2 and O_2 without any sacrificial reagents under UV light irradiation [15-18]. Among La-Ti oxides, $La_2Ti_2O_7$, which possesses a (110) plane-type perovskite structure, was reported to show good photocatalytic activity for overall water splitting [15,16,18]. Since the reduction of CO_2 requires a reduction potential higher than that for H^+, the wide bandgap of $La_2Ti_2O_7$, which is capable of generating photoelectrons with a high reduction potential, should result in the efficient reduction of CO_2. In order to obtain a high crystallinity and surface area at low calcination temperature, we used a polymerized complex method over the typical solid state reaction method to prepare $La_2Ti_2O_7$ [15,18]. In this study, $La_2Ti_2O_7$ was fabricated using the polymerized complex method, and the photocatalytic conversion of CO_2 by H_2O over Ag-modified $La_2Ti_2O_7$ was investigated.

Experimental section

$La_2Ti_2O_7$ was fabricated using a polymerized complex method, where a defined amount of titanium tetraisopropoxide ($Ti[OCH(CH_3)_2]_4$, 95.0%, Wako) was dissolved in 0.2 mol of ethylene glycol ($C_2H_6O_2$, 99.5%, Wako) at room temperature. 0.3 mol of anhydrous citric acid ($C_6H_8O_7$, 98.0%, Wako) was then added and the mixture was heated with continuous stirring at 333 K. After the complete dissolution of citric acid, an appropriate amount of lanthanum nitrate ($La(NO_3)_3$ $6H_2O$, 99.9%, Wako) and 20 mL of methanol were added into the above solution. The additive ratio between $La(NO_3)_3$ and $Ti[OCH(CH_3)_2]_4$ was 1:1. The mixture was heated at 403 K for 3 h to obtain a transparent gel without any precipitated solid. The viscous gel was pyrolyzed at 623 K

to remove all carbon-containing compounds, and the resulting powder precursor was calcined from 1173 to 1423K for 1–8 h in static air. The Ag cocatalyst was chemically modified on $La_2Ti_2O_7$ through a series of chemical reduction, impregnation, and photodeposition methods. In the chemical reduction method, an aqueous $NaPH_2O_2$ solution was added into 100 mL of a suspension of photocatalysts (2.0 g) containing $AgNO_3$. After stirring at 333 K for 2 h, the modified photocatalyst was washed with deionized water three times and dried under vacuum at room temperature. In the impregnation method, photocatalysts were homogeneously dispersed in an aqueous $AgNO_3$ solution. The solution was then evaporated, dried, and calcinated at 723 K in a stream of dry air for 2 h. The photodeposition method was employed in situ during the photocatalytic conversion of CO_2.

The structure and crystallinity of $La_2Ti_2O_7$ samples were characterized by X-ray diffraction (XRD) using a Rigaku Multi Flex powder X-ray diffractometer. The UV-Vis diffused reflectance spectra (UV-Vis DRS) were measured by a JASCO Corporation V-670 spectrometer equipped with an integrating sphere. Spectralon®, supplied by Labsphere Inc., was used as a standard reflection sample. The Brunauer–Emmett–Teller (BET) surface area was measured by N_2 adsorption at 77 K using a volumetric gas adsorption apparatus (BELmini, Bel Japan, Inc.). The Ag K-edge (25.5 keV) X-ray absorption fine structure (XAFS) measurements were made in the fluorescence mode at the BL01B1 beamline of the SPring-8 synchrotron radiation facility (Hyogo, Japan). The spectra were reduced by a Rigaku REX2000 program Ver. 2.5.9 (Rigaku Corp.). TEM images were obtained with a JEOL JEM-1400 transmission electron microscope (TEM) operating at an accelerating voltage of 120 kV.

The photocatalytic reaction was carried out in a flow system using an

inner-irradiation-type reaction vessel at room temperature and ambient pressure. The photocatalyst (1.0 g) was dispersed in ultra-pure water (1.0 L), and CO_2 (99.999%) was bubbled into the water at a flow rate of 30 mL min^{-1}. The suspension was irradiated under a 400 W high-pressure mercury lamp with a quartz filter connected to a cooling water system. Generated gaseous products such as H_2, O_2, and CO were analyzed by thermal conductivity detector-gas chromatography (TCD-GC) using a GC-8A chromatograph (Shimadzu Corp.) equipped with a Molecular Sieve 5A column, (carrier gas: Ar) and by flame ionization detector-gas chromatography (FID-GC) using a methanizer and a Shincarbon ST column (carrier gas: N_2). In the isotope labeling reaction using $^{13}CO_2$, an inner-irradiation-type reaction vessel was connected to a closed circulating system with a vacuum line. The prepared Ag-modified $La_2Ti_2O_7$ sample (500 mg) was dispersed in ultrapure water (350 mL). $^{13}CO_2$ (2000 mmol), which was purified by vacuum distillation at liquid-N_2 temperature, was introduced into the reactor, and the suspension was irradiated by a 400 W high-pressure mercury lamp through a quartz filter connected to a cooling water system. The formation of either ^{13}CO or ^{12}CO after 5.5 h was analyzed by a quadrupole-type mass spectrometer (BEL Japan, Inc., BEL Mass) combined with a TCD-GC (Carrier gas: Ar).

Results and Discussion

Figure 1 shows the XRD patterns of $La_2Ti_2O_7$, which was prepared using the polymerized complex method with subsequent calcination at 1373 K for 4 h. In accordance with the standard pattern (ICSD#1950), $La_2Ti_2O_7$ exhibits a layered perovskite structure, which consists of perovskite-like slabs with a thickness equivalent to four corner-linked (TiO_6) octahedra. The edge of the TiO_6 octahedra is exposed to the interlayers of $La_2Ti_2O_7$, which run parallel to the (110) plane of the bulk perovskite slabs

to give a (110) plane-type perovskite structure [18]. Figure 2 shows the UV–Vis DRS of $La_2Ti_2O_7$ after conversion of the reflection coefficient, R, to the absorption coefficient, $F(R_\infty)$, through the Kubelka–Munk function, $F(R_\infty)=(1-R^2)/2R$. The bandgap energy was derived from Davis–Mott's equation, $\alpha h\nu=(h\nu-E_g)^n$, where α is the absorption coefficient; $h\nu$ is the energy of the irradiated light; and E_g is the bandgap energy. n is an experimental value, where the values for indirect allowed, indirect forbidden, direct allowed, and direct forbidden transitions are 2, 3, 1/2, and 3/2, respectively [19]. As shown in the inset of Figure 2, this equation (n = 1/2, direct allowed transition), gives an estimated value of 4.05 eV for the bandgap energy of $La_2Ti_2O_7$.

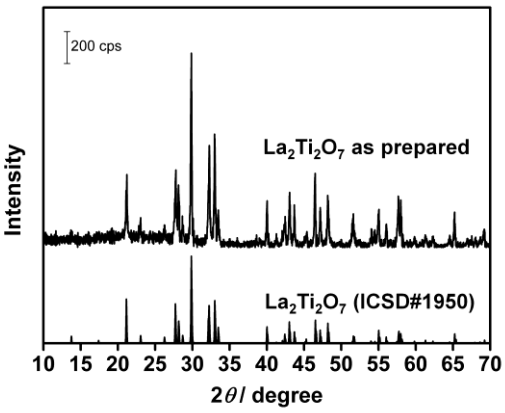

Figure 1 XRD patterns of $La_2Ti_2O_7$ fabricated by polymerized complex method with calcination at 1373 K for 4 h.

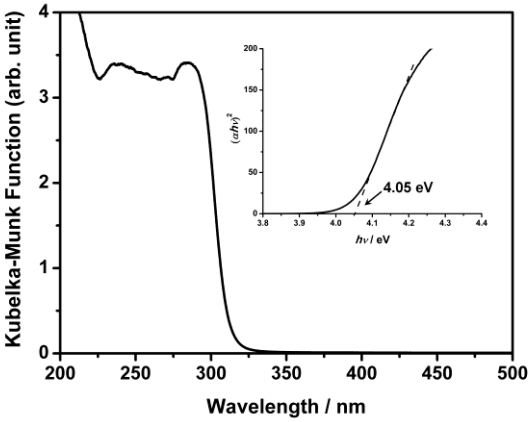

Figure 2 UV-vis DRS of $La_2Ti_2O_7$ prepared by polymerized complex method with calcination at 1373 K for 4 h. Inset: The plots of $(\alpha h\nu)^2$ versus the energy of light ($h\nu$) afford the band gap energy for $La_2Ti_2O_7$.

Figure 3(a) shows XRD patterns of a sample of $La_2Ti_2O_7$ that was treated at temperatures ranging from 1173 K to 1423 K. All samples exhibited the layered perovskite structure of $La_2Ti_2O_7$ without any impurity phases, which indicates that calcination above 1173 K following the polymerized complex procedure successfully

caused crystallization of $La_2Ti_2O_7$. It has already been reported that crystalline $La_2Ti_2O_7$ was obtained by calcination above 1173 K, and that the photocatalytic activity of $La_2Ti_2O_7$ calcined below 1173 K was almost negligible [18]. In addition, all the peaks in the XRD patterns of $La_2Ti_2O_7$ became sharper and higher with an increase in the calcination temperature. The crystallite size of $La_2Ti_2O_7$ could be obtained using the FWHM (Full Width of Half Maximum) of XRD peaks, based on Scherrer's equation. As shown in Figure 3(b), the crystallite size of $La_2Ti_2O_7$ calcined at temperatures ranging from 1173 k to 1423 K increased linearly from 34.0 nm to 50.8 nm. On the other hand, the specific surface area of $La_2Ti_2O_7$, measured by the BET method, decreased when the calcination temperature was elevated (Figure 3(b)). These results mean that calcination at various high temperatures affects not only the crystallite size, but also the specific surface area of $La_2Ti_2O_7$. Since photocatalytic activity is dependent on the crystallinity and surface area of the photocatalyst, the activities of $La_2Ti_2O_7$ calcined at various temperatures were monitored to compare the photocatalytic conversion of CO_2 by H_2O under UV irradiation. All the samples were modified with Ag using the chemical reduction method. Figure 3(c) shows the amount of CO, O_2, and H_2 evolved in 7 h. CO was evolved as the main reduction product, and a significantly smaller yield of evolved H_2 was observed. The simultaneous evolution of O_2 indicated that H_2O worked as an electron donor to consume the holes generated during the photocatalytic conversion of CO_2. Increasing the calcination temperature of $La_2Ti_2O_7$ from 1173 K to 1373 K caused an increase in the activity for the photocatalytic conversion of CO_2. This can be attributed to the high crystallinity of $La_2Ti_2O_7$ in spite of the decrease in the specific surface area. The maximum amount of CO evolved was observed over $La_2Ti_2O_7$ calcined at 1373 K. However, the activity of $La_2Ti_2O_7$ declined

upon calcination at temperatures higher than 1373 K.

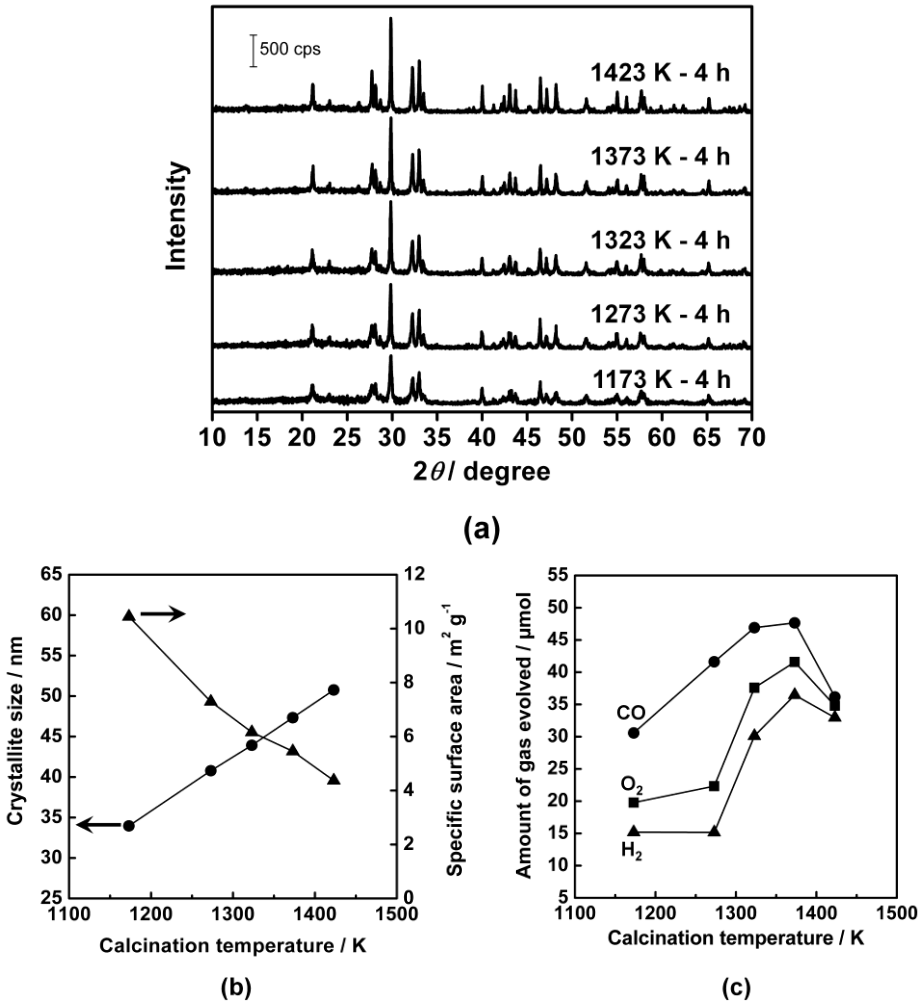

Figure 3 (a) XRD patterns of $La_2Ti_2O_7$ at various calcination temperature; (b) Crystallite size and specific surface area of $La_2Ti_2O_7$ at various calcination temperature; (c) Evolution of CO (circle), O_2 (square), and H_2 (triangle) in 7 h over $La_2Ti_2O_7$ calcined at various temperature for 4 h. Ag cocatalyst was modified by chemical reduction method and the loading amount was 1 wt%.

The calcination time also influences the crystallinity and surface area of $La_2Ti_2O_7$. As shown in Figure 4(a), $La_2Ti_2O_7$ samples that were calcined at 1373 K for 1 to 8 h experienced an increase in peak intensities in the XRD pattern for each sample. The crystallinity of $La_2Ti_2O_7$ grew with longer calcination times, whereas the BET

surface area was reduced (Figure 4(b)). As seen with varied calcination temperature, changes in calcination time from 1 h to 8 h also influence the activity of $La_2Ti_2O_7$.

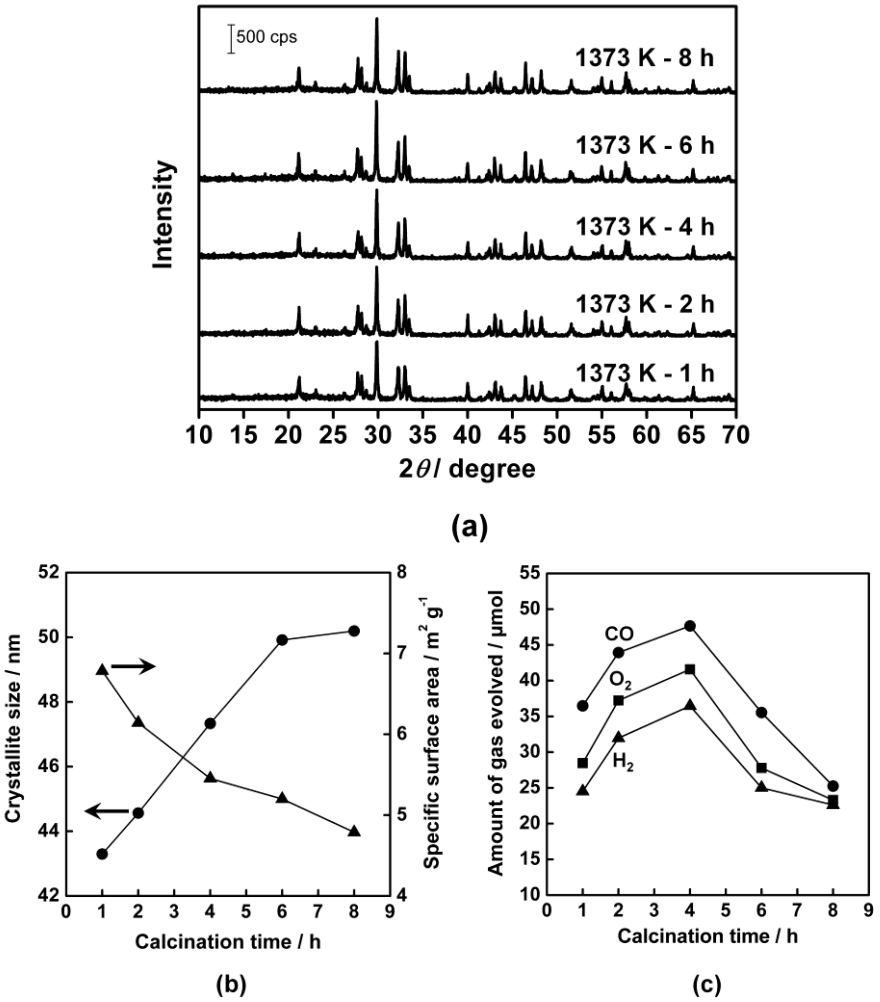

Figure 4 (a) XRD patterns of $La_2Ti_2O_7$ calcined at 1373 K for different time; (b) Crystallite size and specific surface area of $La_2Ti_2O_7$ calcined at 1373 K for different time; (c) Evolution of CO (circle), O_2 (square), and H_2 (triangle) in 7 h over $La_2Ti_2O_7$ calcined at 1373 K for different time. Ag cocatalyst was modified by chemical reduction method and the loading amount was 1 wt%.

$La_2Ti_2O_7$ that was calcined at 1373 K for 4 h possessed a crystallite size of 47.3 nm and a specific surface area of 5.5 $m^2 g^{-1}$ to afford the highest activity for the photocatalytic conversion of CO_2 by H_2O. Generally, a high specific surface area and crystallinity are

essential for an efficient heterogeneous photocatalyst. This is because the photocatalytic reaction occurs mostly on the surface of the photocatalyst, and the high crystallinity of the photocatalyst allows a smooth charge separation. Unfortunately, fabrication conditions such as calcination temperature and time can only promote high crystallization of the photocatalyst at the expense of a diminished surface area. This inverse relationship needs to be fine-tuned in order to maximize photocatalytic activity.

In the electrochemical reduction of CO_2, it has been proven that metallic Ag functions as an effective electrode for the conversion of CO_2 to CO [20]. In the case of the photocatalytic conversion of CO_2 by H_2O, the introduction of an Ag cocatalyst plays an important role in generating CO. In comparison with impregnation and in-situ photo deposition methods, Figure 5 shows that Ag species prepared by the chemical reduction method significantly enhanced the photocatalytic activity for the conversion of CO_2 to CO. This result indicates that the structure of the Ag cocatalyst on the surface of $La_2Ti_2O_7$ is highly dependent on the modification method. The UV–Vis DRS of Ag-modified $La_2Ti_2O_7$ loaded by various methods (Figure 6) showed the same intrinsic absorption as that of bare $La_2Ti_2O_7$. Different surface plasmon absorption in the visible and near-infrared region could be observed for the three samples due to the different particle size and dispersion of Ag cocatalysts. [14,21] The Ag-K edge XANES and Fourier-transforms of Ag K-edge EXAFS spectra of Ag-modified $La_2Ti_2O_7$ prepared by the three methods are shown in Figure 7, of which Ag foil and Ag_2O were used as references. The similar XANES spectra of the three samples and Ag foil clearly proves that Ag species modified by the three methods are metallic Ag. This means the photocatalytic activity is not affected by the chemical state of Ag cocatalyst. Otherwise the Ag-Ag shell intensity of Ag species prepared by the chemical reduction method is

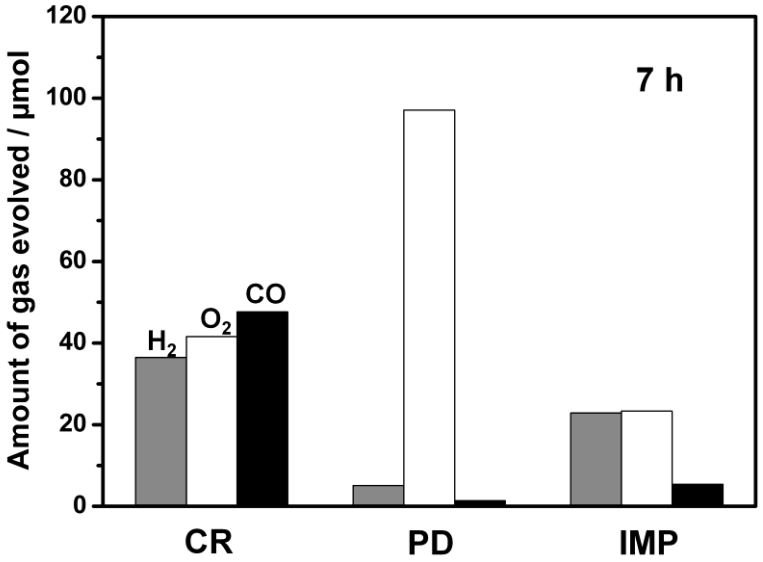

Figure 5 Amount of evolved gases for the photocatalytic reduction of CO_2 in 7 h over Ag-modified $La_2Ti_2O_7$ prepared by CR (chemical reduction method), PD (photodeposition method), and IMP (impregnation method). $La_2Ti_2O_7$ was calcined at 1373 K for 4 h and the loading amount of Ag was 1 wt%.

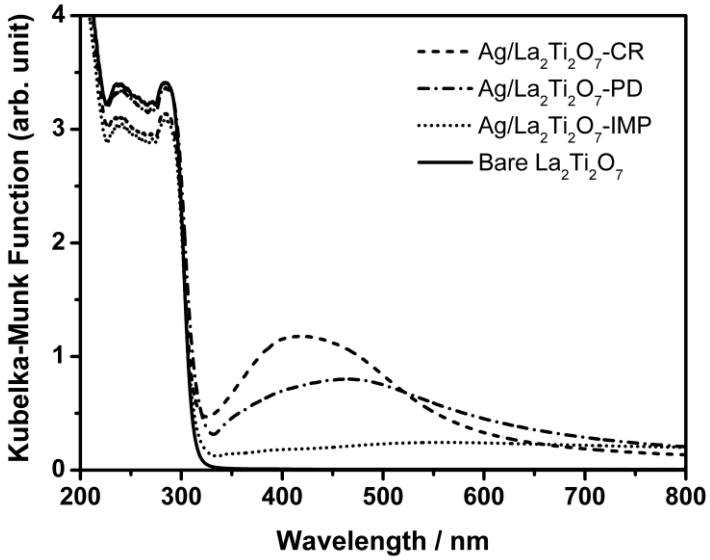

Figure 6 UV-vis DRS of $Ag/La_2Ti_2O_7$-CR (chemical reduction method), $Ag/La_2Ti_2O_7$-PD (photodeposition method), and $Ag/La_2Ti_2O_7$-IMP (impregnation method). $La_2Ti_2O_7$ was calcined at 1373 K for 4 h and the loading amount of Ag was 1 wt%.

much lower than those of Ag species fabricated by the impregnation and photodeposition methods in the FT of EXAFS spectra, which indicates the particle size of Ag cocatalysts in the chemical reduction sample is the smallest among the three samples. Figure 8 represents TEM images of Ag-modified $La_2Ti_2O_7$ loaded by the three methods. Actually, Ag nanoparticles prepared by the chemical reduction method are highly dispersed on the surface of $La_2Ti_2O_7$ with the particle size between 2 and 10 nm. In contrast, the wet impregnation and photodeposition methods result in the aggregation of Ag particles and poor Ag dispersion on $La_2Ti_2O_7$. It is noted that the formation of metallic Ag nanoparticles with the small size and uniform distribution by the chemical reduction method caused the enhancement for the photocatalytic conversion of CO_2 in water.

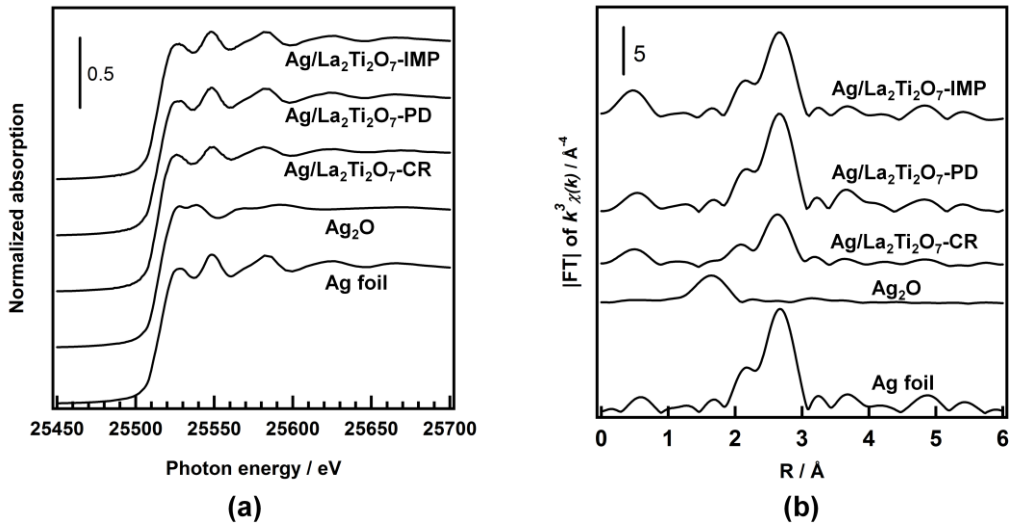

Figure 7 Ag K-edge XANES (a) and Fourier transforms of EXAFS (b) spectra of the Ag-modified $La_2Ti_2O_7$ prepared by chemical reduction method, photodeposition method, impregnation method. Ag foil and Ag_2O were references. $La_2Ti_2O_7$ was calcined at 1373 K for 4 h and the loading amount of Ag was 1 wt%.

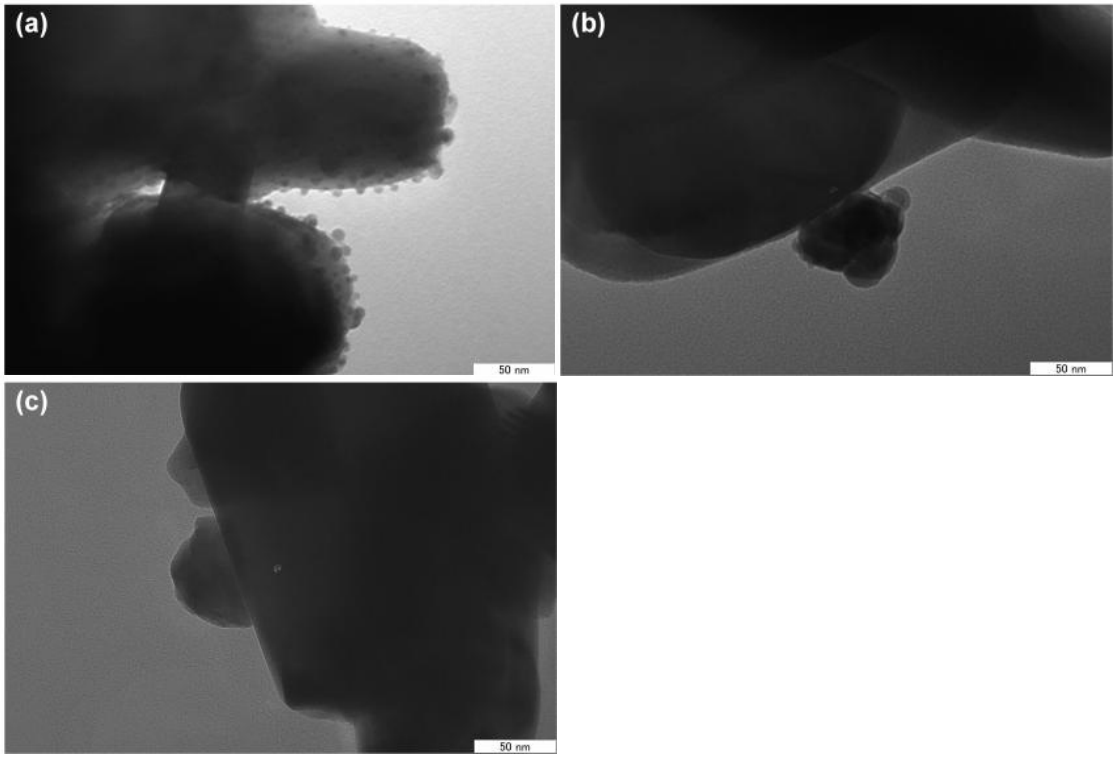

Figure 8 TEM images of Ag-modified $La_2Ti_2O_7$ prepared by chemical reduction (a), photodeposition (b), and impregnation (c) methods. $La_2Ti_2O_7$ was calcined at 1373 K for 4 h and the loading amount of Ag was 1 wt%.

Table 1 Effect of Ag content on the photocatalytic conversion of CO_2. $La_2Ti_2O_7$ was calcined at 1373 K for 4 h. Ag cocatalyst was modified by chemical reduction method.

Loading amount	**Activity / μmol h^{-1}**			**Reacted electrons / μmol h^{-1}**	**Reacted holes / μmol h^{-1}**
	H_2	**O_2**	**CO**		
0 wt%	2.7	2.3	0.8	7.0	9.2
0.5 wt%	4.9	5.2	4.6	19	21
1.0 wt%	4.9	5.3	5.2	20	21
1.5 wt%	4.3	4.8	4.3	17	19
2.0 wt%	3.9	4.4	4.1	16	18

Table 1 shows the photocatalytic activity of Ag-modified $La_2Ti_2O_7$ prepared by the chemical reduction method with various loading amounts of Ag. While conversion

of CO_2 could occur on bare $La_2Ti_2O_7$, the formation rate of H_2 (2.7 μmol h^{-1}) was higher than that of CO (0.8 μmol h^{-1}). This is because conversion of CO_2 competes with the splitting of water at an insufficient number of suitable reaction sites on bare $La_2Ti_2O_7$. Modification of $La_2Ti_2O_7$ with an Ag cocatalyst caused a dramatic increase in the photocatalytic activity for CO evolution. While the formation rate of CO increased with the addition of larger amounts of Ag ranging from 0 to 1.0 wt%, the rate declined with higher amounts of Ag. The maximum activity was obtained for $La_2Ti_2O_7$ with 1 wt% of the Ag cocatalyst. It is clear that the modification by the Ag cocatalyst provided enough catalytic sites for the reduction of CO_2 on the surface of $La_2Ti_2O_7$, and the conversion of CO_2 to CO took precedence over H_2 production at such sites. In addition, the evolution of H_2 was also improved through the introduction of the Ag cocatalyst, possibly owing to the promotion of electron-hole separation. The Ag cocatalyst efficiently captures the photogenerated electrons and supplies them for the reductions of both CO_2 and H^+. Any remaining photogenerated holes are consumed by the oxidation of H_2O to produce a stoichiometric amount of O_2. The equivalence between the reacted electrons and holes confirms that a perfect redox reaction occurred on the surface of Ag-modified $La_2Ti_2O_7$.

Figure 9 shows the time course of CO, H_2, and O_2 evolution during the photocatalytic conversion of CO_2 by H_2O over Ag-modified $La_2Ti_2O_7$ under optimized conditions. The formation rates of CO, H_2, and O_2 at the steady state (5.2, 4.9 and 5.3 μmol h^{-1}, respectively) are in a stoichiometric ratio, indicating that CO_2 is efficiently reduced by H_2O over the Ag-modified $La_2Ti_2O_7$ photocatalyst, and that H_2O is simultaneously oxidized by the generated holes. In addition, CO was produced in priority to H_2. After 7 h, the amount of evolved CO was 47.7 μmol, which was higher than the amount of evolved H_2 (36.4 μmol). It can be observed that the formation rate of

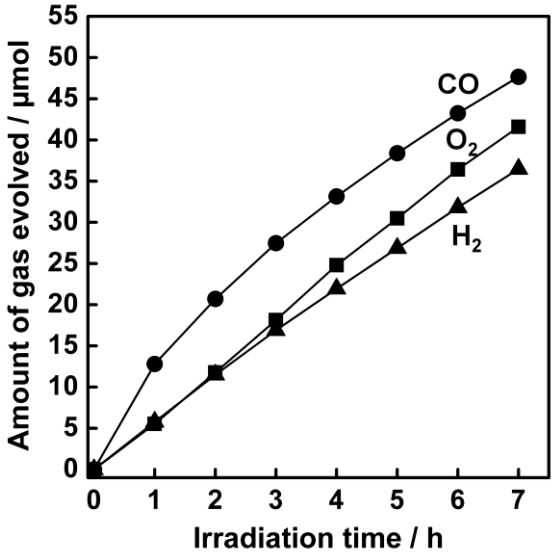

Figure 9 Time courses of CO (circle), O_2 (square), and H_2 (triangle) evolved for the photocatalytic conversion of CO_2 in water over Ag-modified $La_2Ti_2O_7$. $La_2Ti_2O_7$ was calcined at 1373 K for 4 h. Ag cocatalyst was modified by chemical reduction method and the loading amount was 1 wt%.

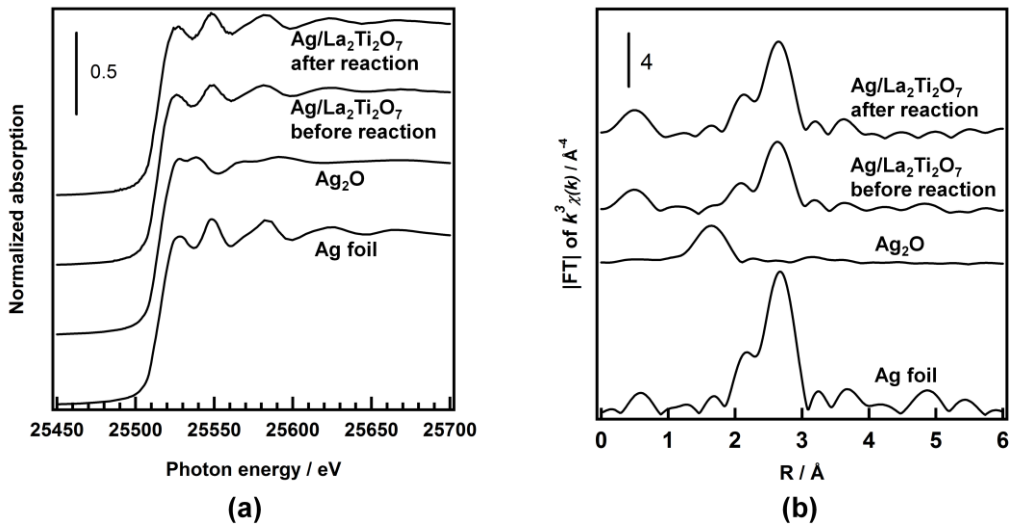

Figure 10 Ag K-edge XANES (a) and Fourier transforms of EXAFS (b) spectra of the optimized Ag-modified $La_2Ti_2O_7$ before and after the photocatalytic conversion of CO_2. Ag foil and Ag_2O were references. $La_2Ti_2O_7$ was calcined at 1373 K for 4 h. Ag cocatalyst was modified by chemical reduction method and the loading amount was 1 wt%.

CO declined gradually at the initial stage of the reaction. Figure 10 shows the Ag K-edge XANES and Fourier-transforms of Ag K-edge EXAFS spectra of Ag-modified $La_2Ti_2O_7$ before and after the photocatalytic reaction using Ag foil and Ag_2O as references. The XANES spectra of the Ag-modified $La_2Ti_2O_7$ before and after the reactions were similar to that of Ag foil, implying that the Ag species remained as metallic Ag after the photocatalytic reaction. In the corresponding EXAFS spectra, the height of the Ag-Ag shell peak increased after the photocatalytic reaction, indicating that the particle size of the Ag cocatalyst on the surface of $La_2Ti_2O_7$ became larger after the reaction. Moreover, the grown Ag particles after the reaction can be distinctly observed in TEM images as shown in Figure 11. The change in the Ag particle size is attributed to the redeposition and aggregation of Ag species on the photocatalyst during photoirradiation [14]. This decreased the rate of formation of CO during the initial stage. After 3 h of photoirradiation, the rate became constant. On the other hand, the amount of evolved H_2 and O_2 increased linearly over 7 h of photoirradiation. This means that Ag-modified $La_2Ti_2O_7$ is a very stable photocatalyst for the photocatalytic conversion of CO_2 by H_2O, and is not affected by the oxidation and reduction of the generated hole and electron. The XRD patterns of fresh and recycled Ag-modified $La_2Ti_2O_7$ (Figure 12) clarified that the crystalline structure of $La_2Ti_2O_7$ after the photocatalytic reaction was almost the same as that before the photocatalytic reaction. The $La_2Ti_2O_7$ photocatalyst prepared by the polymerized complex method is very stable under UV light irradiation and in aqueous medium.

The $La_2Ti_2O_7$ photocatalyst was calcined at high temperatures in air during the fabrication process; this high-temperature treatment eliminates any carbon residues on the photocatalyst surface. However, it is necessary to confirm the carbon source of the

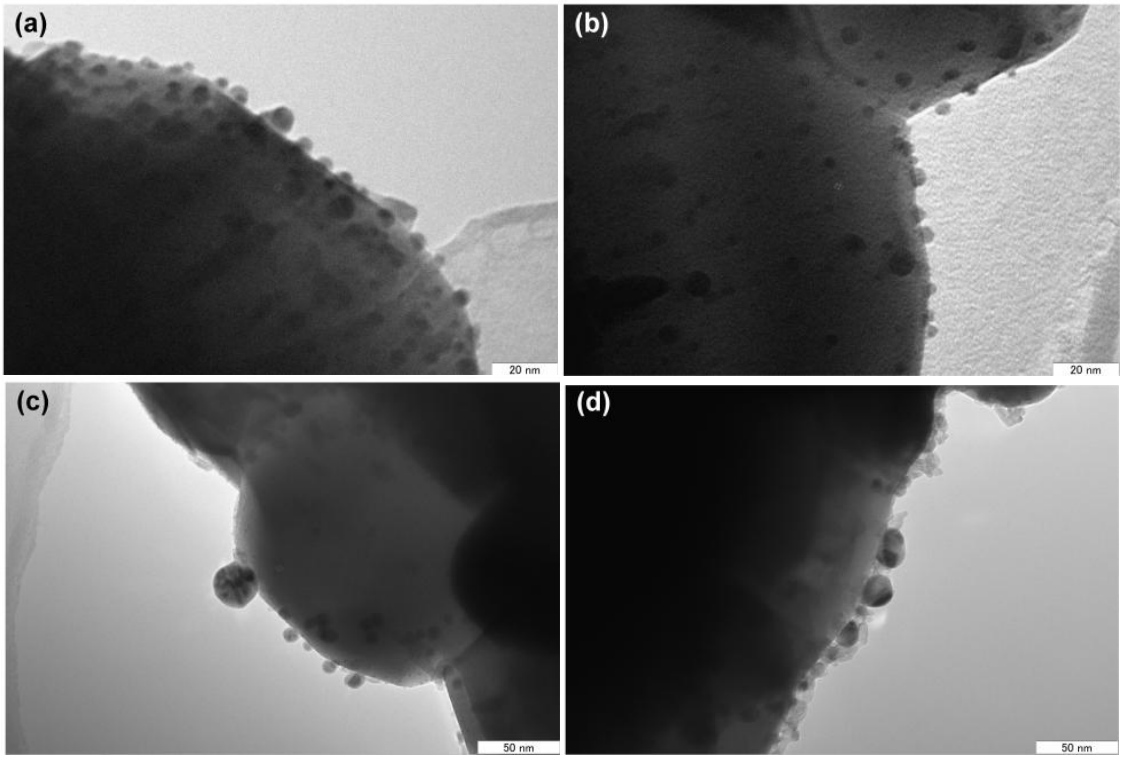

Figure 11 TEM images of Ag-modified $La_2Ti_2O_7$ prepared by chemical reduction method before (a, b) and after (c, d) the photocatalytic conversion of CO_2 in water. $La_2Ti_2O_7$ was calcined at 1373 K for 4 h and the loading amount of Ag was 1 wt%.

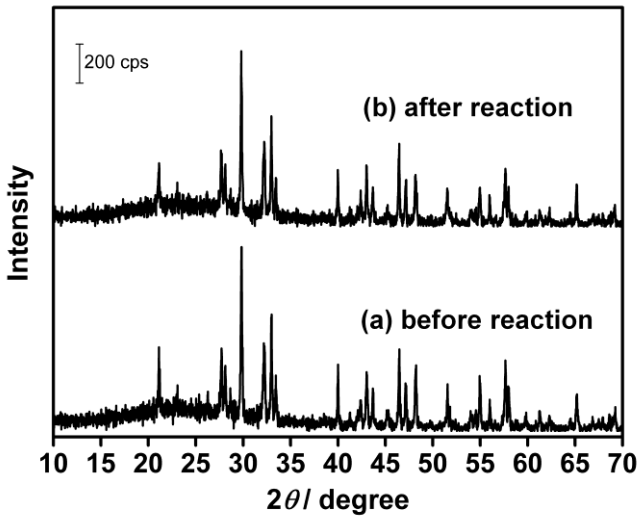

Figure 12 XRD patterns of $La_2Ti_2O_7$ (a) before and (b) after the reaction. $La_2Ti_2O_7$ was synthesized by polymerized complex method and calcined at 1373 K for 4 h. Ag cocatalyst was modified by chemical reduction method and the loading amount was 1 wt%.

gaseous products such as CO through an isotope-labeling reaction using ^{13}CO to avoid any misestimations in the photocatalytic conversion of CO_2. Figure 13 displays the mass spectra (m/z 28 and 29) during the photocatalytic conversion of $^{13}CO_2$ by H_2O over Ag-modified $La_2Ti_2O_7$ under optimized conditions. Sampling gas was introduced into the mass spectrometer after it was segregated by a gas chromatograph. The peak in the spectrum at m/z = 29, which appeared at the same retention time as that observed by GC, can be directly attributed to ^{13}CO gas. The amount of ^{13}CO estimated by mass spectrometry was almost consistent with the amount of CO determined by TCD-GC. This result revealed that the evolution of CO was not from the contamination of $La_2Ti_2O_7$, but from the introduced CO_2 gas.

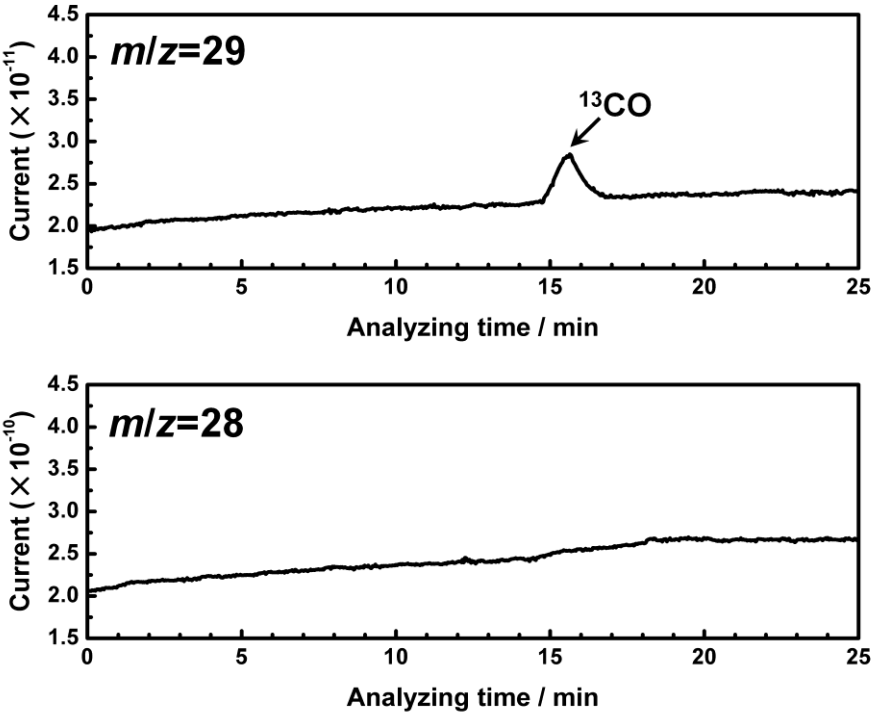

Figure 13 Mass spectra (m/z 28 and 29) after 5.5 h of photoirradiation in the photocatalytic conversion of $^{13}CO_2$ in water over Ag-modified $La_2Ti_2O_7$. $La_2Ti_2O_7$ was calcined at 1373 K for 4 h. Ag cocatalyst was modified by chemical reduction method and the loading amount was 1 wt%.

Conclusions

Ag-modified $La_2Ti_2O_7$ exhibited activity for the photocatalytic conversion of CO_2 to CO together with the oxidization of H_2O to O_2. H_2O functions as an efficient electron donor for the reduction of CO_2, and the stoichiometric amounts of evolved CO, H_2, and O_2 indicate that the number of electrons used for the evolution of CO and H_2 is equal to the number of holes consumed for the evolution of O_2. The photocatalytic activity depends on the crystallinity and surface area of $La_2Ti_2O_7$, which are influenced by the calcination temperature and time. Thus, the maximum amount of CO was produced over $La_2Ti_2O_7$ that was synthesized using the polymerized complex method and calcined at 1373 K for 4 h. The isotope labeling reaction using $^{13}CO_2$ provided evidence that the evolved CO did not originate from carbon contamination of $La_2Ti_2O_7$, but from experimentally introduced CO_2 gas.

References and Notes

[1] J. Hansen, L. Nazarenko, R. Ruedy, M. Sato, J. Willis, A. Del Genio, D. Koch, A. Lacis, K. Lo, S. Menon, T. Novakov, J. Perlwitz, G. Russell, G. A. Schmidt, N. Tausnev, *Science* **2005**, *308*, 1431.

[2] M. Mikkelsen, M. Jorgensen, F. C. Krebs, *Energy Environ. Sci.* **2010**, *3*, 43.

[3] T. Sakakura, J. C. Choi, H. Yasuda, *Chem. Rev.* **2007**, *107*, 2365.

[4] W. Wang, S. Wang, X. Ma, J. Gong, *Chem. Soc. Rev.* **2011**, *40*, 3703.

[5] E. V. Kondratenko, G. Mul, J. Baltrusaitis, G. O. Larraz ábal, J. P érez-Ram írez, *Energy Environ. Sci.* **2013**, *6*, 3112.

[6] J. Mao, K. Li, T. Peng, *Catal. Sci. Technol.* **2013**, *3*, 2481.

[7] A. Kubacka, M. Fern ández-Garc á, G. Col ón, *Chem. Rev.* **2012**, *112*, 1555.

[8] K. Teramura, H. Tsuneoka, T. Shishido, T. Tanaka, *Chem. Phys. Lett.* **2008**, *467*, 191.

[9] T. Inoue, A. Fujishima, S. Konishi, K. Honda, *Nature* **1979**, *277*, 637.

[10] I. H. Tseng, J. C. S. Wu, H. Y. Chou, *J. Catal.* **2004**, *221*, 432.

[11] H. Fujiwara, H. Hosokawa, K. Murakoshi, Y. Wada, S. Yanagida, T. Okada, H. Kobayashi, *J. Phys. Chem. B* **1997**, *101*, 8270.

[12] Y. Liu, B. Huang, Y. Dai, X. Zhang, X. Qin, M. Jiang, M. H. Whangbo, *Catal. Commun.* **2009**, *11*, 210.

[13] S. C.Yan, S. X. Ouyang, J. Gao, M. Yang, J. Y. Feng, X. X. Fan, L. J. Wan, Z. S. Li, J. Ye, Y. Zhou, Z. G. Zou, *Angew. Chem., Int. Ed.* **2010**, *49*, 6400.

[14] K. Iizuka, T. Wato, Y. Miseki, K. Saito, A. Kudo, *J. Am. Chem. Soc.* **2011**, *133*, 20863.

[15] R. Abe, M. Higashi, K. Sayama, Y. Abe, H. Sugihara, *J. Phys. Chem. B* **2006**, *110*, 2219.

[16] J. Kim, D. W. Hwang, H. G. Kim, S. W. Bae, J. S. Lee, W. Li, S. H. Oh, *Top. Catal.* **2005**, *35*, 295.

[17] Y. Miseki, H. Kato, A. Kudo, *Energy Environ. Sci.* **2009**, *2*, 306.

[18] H. G. Kim, D. W. Hwang, S. W. Bae, J. H. Jung, J. S. Lee, *Catal. Lett.* **2003**, *91*, 193.

[19] K. Teramura, S. Okuoka, H. Tsuneoka, T. Shishido, T. Tanaka, *Appl. Catal. B* **2010**, *96*, 565.

[20] Y. Hori, K. Kikuchi, S. Suzuki, *Chem. Lett.* **1985**, *14*, 1695.

[21] K. H. Chen, Y. C. Pu, K. D. Chang, Y. F. Liang, C. M. Liu, J. W. Yeh, H. C. Shih, Y. J. Hsu, *J. Phys. Chem. C* **2012**, *116*, 19039.

Chapter 6

Photocatalytic Conversion of CO_2 by H_2O over Ag-loaded SrO-modified Ta_2O_5

Abstract

We found that incorporation of alkaline earth metal oxides into Ag-loaded Ta_2O_5 (Ag/Ta_2O_5) suppresses the H_2 production from overall water splitting for the photocatalytic conversion of CO_2 by using H_2O as an electron donor. Four different combinations of the photocatalysts ($Ag/MO/Ta_2O_5$ (M = Mg, Ca, Sr, or Ba)) were utilized; of these, the highest amount of CO was generated over Ag-loaded SrO-modified Ta_2O_5 ($Ag/SrO/Ta_2O_5$) with the evolution of a stoichiometric amount of O_2. It was demonstrated that the presence of low quantities of SrO considerably enhanced the selectivity toward CO evolution. We also confirmed that a Ag cocatalyst increased the selectivity toward CO evolution and relatively small Ag nanoparticles maximized the selectivity toward CO evolution. It was therefore concluded that the particle size of the Ag cocatalysts should be controlled, and alkaline earth metal oxides should be introduced into Ag/Ta_2O_5 in order to achieve high conversion of CO_2 and good selectivity toward O_2 evolution.

Introduction

The reduction in human-induced emissions of CO_2 from automobiles, factories, power stations etc., over the next 15 years is currently one of the most important issues facing the planet. The Intergovernmental Panel on Climate Change (ICPP) warned that temperature change has to be controlled lower than 2 degrees Celsius relative to average temperature before the Industrial Revolution by the end of century.[1] It has also warned that if no action is taken to deal with the rate of CO_2 emissions, this will result in grave consequences for the planet, leading to sea surface elevation and desertification. In recent years, a potential solution that has been considered is to preserve CO_2 in geological formations (e.g. carbon capture and storage (CCS)).[2-4] However, this is not a perfect approach to solving the problem because of low levels of accumulation, high costs, and the significant energy requirements needed for the process. We should therefore attempt to develop industrial processes using CO_2 as a feedstock in order to build a sustainable society in the near future.

We previously reported that the use of ZrO_2[5,6], MgO[7,8], $ATaO_3$ (A = Li, Na, and K)[9], and Ga_2O_3[10] results in the production of CO as the main product from the photocatalytic conversion of CO_2 in the presence of H_2 and CH_4. In addition, it was found that many solid bases show activity for the reduction of CO_2 under photoirradiation. Linear CO_2 molecules adsorbed on the surface of the solid bases are converted into unique structures, such as bicarbonate and carbonate species possessing lattice oxygen atoms. We believe that the process involves the capture and distortion of CO_2 upon adsorption on a solid base through activation by photoirradiation. Unstable CO_2 species adsorbed onto the surface can then be reduced by electrons with protons derived from H_2O ($CO_2 + 2e^- + 2H^+ \rightarrow CO + H_2O$). It is well-known that the catalytic

sites are easily poisoned by H_2O. In order to prevent the catalyst poisoning, we previously developed several layered double hydroxides as water-resistant photocatalysts for the reduction of CO_2 in H_2O.[11,12]

More recently, our approach has been recognized by a number of scientists and engineers. Wang *et al.*, quoting inspiration from our work[7,8], recently reported an improvement in the activity of the Pt-TiO_2 catalyst by the addition of MgO.[13] The quantity of CH_4 evolved over Pt-MgO/TiO_2 was twice that evolved over Pt-TiO_2 alone. When the reduction of CO_2 is performed in H_2O, the reduction of CO_2 competes with the reduction of H^+ to H_2 (so-called water splitting). With the addition of MgO, Wang *et al.* also controlled the selectivity of the generated electrons toward the reduction of CO_2 into CO and CH_4 in the presence of H_2O vapor.[14] Li *et al.*[15,16] also reported that MgO-modified TiO_2 exhibits a higher CO production rate during the photocatalytic conversion of CO_2 with H_2O vapor compared to TiO_2 alone. In 2014, Yang *et al.*[17] observed that in the presence of a Pt cocatalyst, CO was generated as the major product. They demonstrated the enhancement of CH_4 evolution by the addition of Pt into the MgO/TiO_2 film, although when utilizing MgO/TiO_2 film alone, the amount of CH_4 evolved was higher than that of CO. From these studies, it could be concluded that the combination of a CO_2 absorbent with a photocatalyst has the possibility to function as an effective photocatalyst for the reduction of CO_2 using H_2O as an electron donor.

Unfortunately, the above publications did not mention the monitoring of O_2 evolution, despite the fact that O_2 must be produced simultaneously with CO evolution. Each CO_2 molecule is reduced to a CO molecule by 2 electrons and a H_2O molecule is oxidized to a O_2 molecule by 4 holes. Half as much amount of O_2 evolved as that of CO evolved should be observed simultaneously if CO_2 is reduced by 2 electrons into CO. In

the case of the photocatalytic conversion of CO_2, monitoring the stoichiometries of the CO_2 reduction products, including O_2 evolution is extremely important, to the extent that the origin of the carbon atom of reduction products such as CO has been confirmed using $^{13}CO_2$ as starting material. The first report of the production of stoichiometric amounts of CO and O_2 from the photocatalytic conversion of CO_2 by H_2O was by Kudo *et al.*[18,19] Indeed we also reported on the stoichiometric production of CO and O_2 over a number of photocatalysts.[20,21] The studies discussed inspired us to return to the development of composites consisting of absorbents and photocatalysts to produce stoichiometric amounts of CO and O_2. However, as the conduction band level of TiO_2 is not suitable for the reduction of CO_2, we envisioned that Ta_2O_5 is preferable for the photocatalytic conversion of CO_2 by H_2O, as it has a suitable conduction band level to reduce CO_2 to CO.

Experimental

Ag/MO/Ta_2O_5 (M = Mg, Ca, Sr, or Ba) was prepared by a typical impregnation method. Ta_2O_5 (99.9%, High Purity Chemical) was introduced to 25 mL of a 0.5 mol% aqueous solution of MNO_3 (M = Mg, Ca, Sr, or Ba). The suspension was stirred at 353 K for 1 h, and then gradually evaporated to dryness at 353 K. The sample was dried at room temperature, followed by calcination at 1023 K for 2 h under a constant flow of air. Four different modification methods of Ag cocatalysts were applied: an impregnation method (IMP); a chemical reduction method (CR); an electroless plating method (EP); and a photodeposition method (PD). Ag/SrO/Ta_2O_5 (*via* IMP) was prepared by impregnating pre-prepared SrO/Ta_2O_5 with an aqueous solution of $AgNO_3$ (0.1 M) at 353 K for 1 h, followed by evaporation at 353 K for 1 h, drying at 353 K, and calcination at 723 K for 2 h. $AgNO_3$ was reduced by an aqueous $NaPH_2O_2$ solution

(0.4 M) at 333 K for 2 h in an aqueous solution to obtain Ag/SrO/Ta_2O_5 (*via* CR). The filtrate was washed by Milli-Q® water and dried under vacuum at room temperature. Ag/SrO/Ta_2O_5 (*via* EP) was obtained *via* the method described as follows. An aqueous solution of NH_3 (4 wt%) was added dropwise to a mixture of $AgNO_3$ and KOH until a transparent solution was obtained. This solution was added to the suspension of as-prepared SrO/Ta_2O_5 (60 mL), followed by plating using an aqueous solution of glucose (1%, 50 mL). The filtrate was then washed by Milli-Q® water, stirred for 20 min, and dried at 353 K. A photodeposition process to draw up Ag/SrO/Ta_2O_5 (*via* PD) was carried out *in situ* in an aqueous solution of $AgNO_3$ (286.7 μmol L^{-1}) under photoirradiation with a 400 W high-pressure lamp for 20 h after degassing the solution.

The photocatalytic conversion of CO_2 by H_2O was carried out using a quartz inner-irradiation reaction vessel (1.0 L) in a quasi-flowing batch system. The synthesized photocatalysts (1.0 g) were dispersed in an aqueous solution of $NaHCO_3$ (0.1 M). CO_2 gas (99.999%) was bubbled into the water at a flow rate of 30 mL min^{-1}. The suspension was irradiated using a 400 W high-pressure mercury lamp through a quartz filter equipped with a cooling water system (thickness: 10 mm). The quantities of CO, H_2, and O_2 evolved from the reaction were analyzed by thermal conductivity detector-gas chromatography (TCD-GC) using a GC-8A chromatograph (Shimadzu) equipped with a Molecular Sieve 5A column (carrier gas: Ar), and also by flame ionization detector-gas chromatography (FID-GC) using a GC-8A chromatograph (Shimadzu) with a methanizer and a Shincarbon ST column (carrier gas: N_2).

The X-ray diffraction (XRD) patterns of Ag/MO/Ta_2O_5 (M = Mg, Ca, Sr, or Ba) were recorded using a Rigaku Ultima IV powder diffractometer. The UV–Vis diffuse reflectance spectra (UV–vis DRS) were measured by a JASCO Corporation

V-670 spectrometer equipped with an integrating sphere. Spectralon®, which was supplied by Labsphere Inc., was used as a standard reflection sample such as $BaSO_4$. TEM images were obtained on a JEOL JEM-1400 transmission electron microscope (TEM) operating at an accelerating voltage of 120 kV. TEM samples were prepared by depositing drops of a suspension of the powders in MeOH onto a carbon-coated copper grid (Okenshoji Co. Ltd.) and allowing the MeOH to evaporate under atmospheric conditions. Ag K-edge (25.5 keV) X-ray absorption fine structure (XAFS) measurements were obtained under fluorescence mode at the BL01B1 beamline of the SPring-8 synchrotron radiation facility (Hyogo pref., Japan). The ring energy used was 8 GeV, and the stored current was 99.5 mA. A Si (311) two crystal monochromator was used to obtain the monochromatic X-ray beam. The photon energy of the X-ray was calibrated using Ag foil as a reference. Data reduction was performed using the REX2000 program Ver. 2.5.9 (Rigaku Corp.). Fourier transform of the extended X-ray absorption fine structure (EXAFS) spectra was performed in the 3.0−12.0 $Å^{-1}$ regions.

Results and Discussion

Figure 1 shows the XRD patterns of 3.0 wt% Ag-loaded (*via* IMP) and 0.5 mol% alkaline earth metal-modified Ta_2O_5 ($Ag/MO/Ta_2O_5$ (M = Mg, Ca, Sr, or Ba)) with Ta_2O_5 as a reference. All XRD patterns were comparable to that of Ta_2O_5 alone, although the loading amount of alkaline earth metal oxides was 0.5 mol%, indicating that the amorphous alkaline earth metal oxides spread on the surface of Ta_2O_5. In addition, we also observed that Ag nanoparticles are also highly dispersed on the surface of both MO (M = Mg, Ca, Sr, or Ba) and Ta_2O_5 due to the fact that there is no signal corresponding to Ag metal in any of the XRD patterns. As shown in Figure 2, the band gap energy did not change when the alkaline earth metals were modified on the

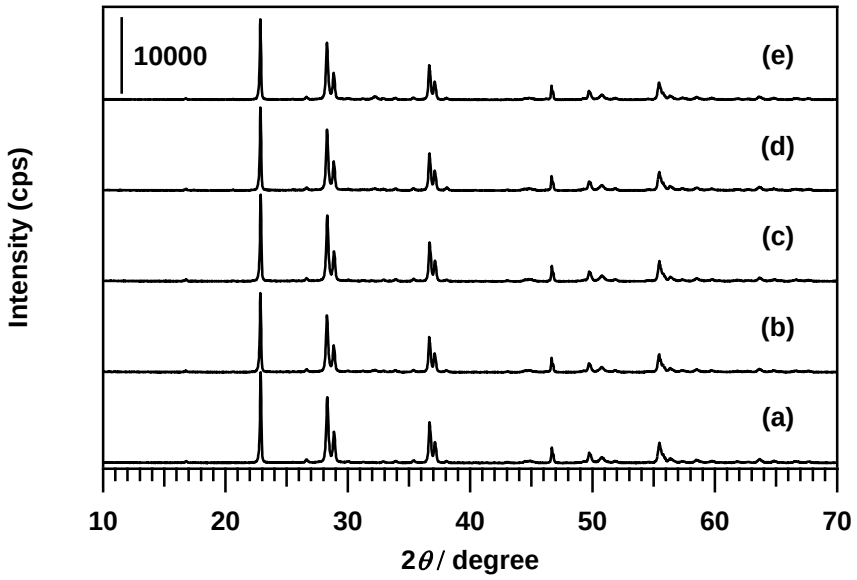

Figure 1 XRD patterns of Ag(3.0wt%)-loaded (a) Ta_2O_5, (b) MgO/Ta_2O_5, (c) CaO/Ta_2O_5, (d) SrO/Ta_2O_5, and (e) BaO/Ta_2O_5 (*via* IMP). Loading amount of alkaline earth metal oxides is 0.5 mol%.

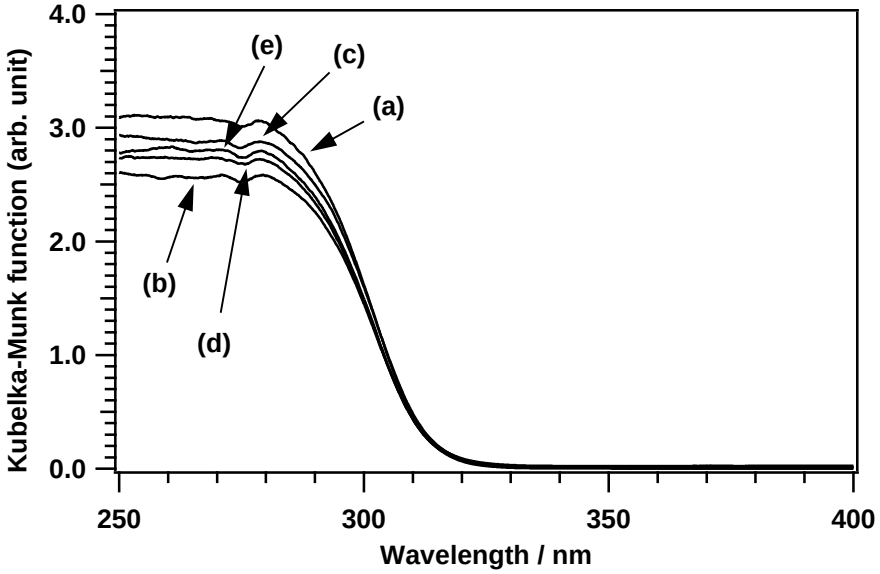

Figure 2 UV-Vis. Diffuse Reflectance spectra of (a) Ta_2O_5, (b) MgO/Ta_2O_5, (c) CaO/Ta_2O_5, (d) SrO/Ta_2O_5, and (e) BaO/Ta_2O_5. Loading amount of alkaline earth metal oxides is 0.5 mol%.

surface of Ta_2O_5. The UV-Vis spectra obtained were also comparable, and the diffuse reflectance spectra of MO/Ta_2O_5 (M = Mg, Ca, Sr, and Ba) were comparable to that of

Ta_2O_5. From these data, it could therefore be concluded that the modification with the alkaline earth metal did not influence the physical properties of Ta_2O_5. On the other hand, chemical properties such as photocatalytic activity were dramatically altered after the modification. Figure 3 shows the amount of H_2, O_2, and CO evolved for the photocatalytic conversion of CO_2 by H_2O over Ag(3.0 wt%)/MO(0.5 mol%)/Ta_2O_5 (M = Mg, Ca, Sr, or Ba) (*via* IMP) after 5 h of photoirradiation. Electrons generated by charge transfer in a photocatalyst can reduce not only CO_2 into CO but also H^+ into H_2, and therefore, the reduction of CO_2 to CO completes the production of H_2 from H_2O (overall water splitting). Generated holes then oxidize H_2O into O_2. Over a Ag/Ta_2O_5 catalyst, H_2 was evolved preferentially, indicating that overall water splitting was successful and that CO_2 was hardly reduced over Ag/Ta_2O_5. In this study, the selectivity toward CO evolution is defined (by %) in terms of the amount of CO evolved, divided by the total amount of H_2 and CO evolved ($CO/(CO+H_2)\times100$). It therefore gives an indication of the efficiency of the generated electrons for the photocatalytic conversion of CO_2 by H_2O. In the case of Ag/Ta_2O_5, the observed selectivity was very low (17.7%). Surprisingly, the modification with the alkaline earth metal oxides dramatically enhanced the selectivity toward CO evolution, depending on the alkaline earth metal oxide utilized in the process. Ag/SrO/Ta_2O_5 showed the best selectivity toward CO evolution (64.7%) among the 4 variations of alkaline earth metal oxides studied. Figure 4 shows the amount of CO, H_2, and O_2 evolved over time during the photocatalytic conversion of CO_2 by H_2O over Ag(3.0 wt%)/SrO(0.5 mol%)/Ta_2O_5 (*via* IMP). As expected, the incorporation of SrO into Ag/Ta_2O_5 improved the reduction of CO_2 and suppressed the production H_2 from H_2O, and after 7 h of photoirradiation, 47.4 μmol of CO was generated. It is well-known that a layered $Sr_2Ta_2O_7$ perovskite functions as an

active photocatalyst.[22] In this study, $Sr_2Ta_2O_7$ was prepared *via* a polymerized complex (PC) method and calcined at 1173 K for 20 h. In our case, however, no signal corresponding to $Sr_2Ta_2O_7$ was observed in the XRD pattern of $Ag/SrO/Ta_2O_5$. In addition, H_2 was preferentially generated over $Ag(3.0\ wt\%)/Sr_2Ta_2O_7$ (*via* IMP) as shown in Figure 5. It is therefore imperative that amorphous SrO should be incorporated onto the surface of Ta_2O_5 so as to achieve the successful photocatalytic conversion of CO_2 by H_2O. Therefore, the potential exists for a stoichiometric amount of O_2 to be generated over all of the $Ag/MO/Ta_2O_5$ (M = Mg, Ca, Sr, or Ba) photocatalysts used in this study, indicating that in this system, H_2O functions as an electron donor for the photocatalytic conversion of CO_2. Accordingly, we achieved an effective artificial photosynthetic system using our Ag-loaded SrO-modified Ta_2O_5 photocatalyst.

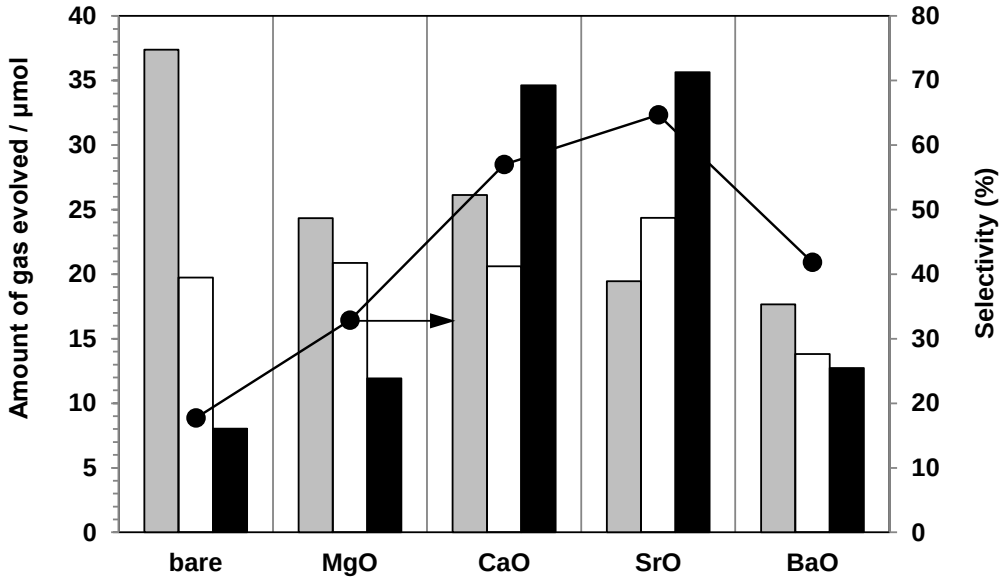

Figure 3 Amount of H_2 (gray), O_2 (white) and CO (black) evolved for the photocatalytic conversion of CO_2 by H_2O over $Ag(3.0wt\%)/Ta_2O_5$ (*via* IMP) and $Ag(3.0wt\%)/MO(0.5mol\%)/Ta_2O_5$ (*via* IMP) (M = Mg, Ca, Sr, and Ba) after 5 h of photoirradiation. Amount of catalyst: 1.0 g, Solution: H_2O, 1.0L, Concentration of additives: 0.1 M $NaHCO_3$, Flow rate of CO_2: 30 ml/min, Reaction temp. : R.T., Light source: 400 W Hg lamp.

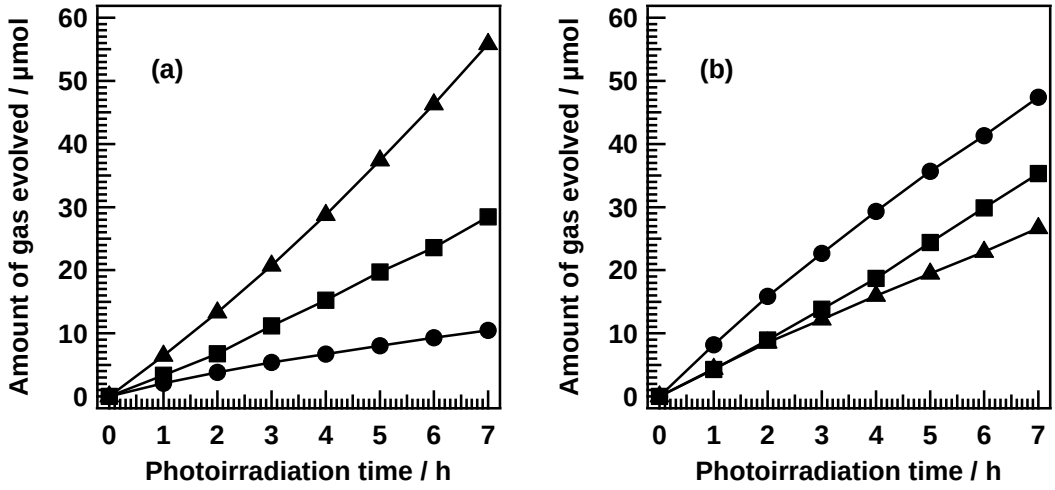

Figure 4 Time course of CO (circle), H_2 (triangle), O_2 (square) evolved for the photocatalytic conversion of CO_2 by H_2O over (a) Ag(3.0wt%)/Ta_2O_5 (*via* IMP) and (b) Ag(3.0wt%)/SrO(0.5mol%)/Ta_2O_5 (*via* IMP).

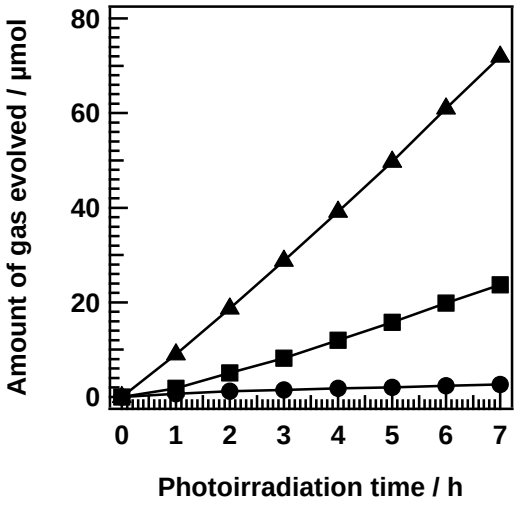

Figure 5 Time course of CO (circle), H_2 (triangle), O_2 (square) evolved for the photocatalytic conversion of CO_2 by H_2O over Ag(3.0wt%)/$Sr_2Ta_2O_7$ (*via* IMP).

We also observed that the selectivity toward CO evolution in the photocatalytic conversion of CO_2 by H_2O depended upon the level of loading of SrO, as indicated in Figure 6, with even minimal quantities of SrO producing an effect on the selectivity toward CO evolution. The amount of electrons generated by charge transfer, which can be estimated by measuring the total amount of H_2 and CO evolved, was comparable to

that observed using Ag(3.0 wt%)/Ta_2O_5 (*via* IMP) alone. However, the photocatalytic activity, as indicated by H_2, O_2, and CO evolution, decreased with increased loading of SrO, most likely because SrO is capable of covering the oxidation sites. The several research groups have already reported that CO_2 can be adsorbed on the isolated metal centers which are located at the surface of metal oxides.[23-26] Symmetrical, unidentate, bidentate carbonates, carboxylate, and bicarbonate are assigned on the surface of the metal oxides by Fourier transform infrared (FT-IR) spectroscopy. We also have studied the structure of adsorbed CO_2 by the FT-IR spectroscopy and proposed that the side-on adsorption-type bidentate carbonate and the bidentate formate are intermediate species for the photocatalytic reduction CO_2 in the presence of H_2 over MgO[8] and Ga_2O_3[10], respectively. Unfortunately, as it now stands, we don't have any information for the detailed structure of SrO on the surface of Ta_2O_5 because of low loading amout; however, expect that the reason for those observations is that SrO plays a role by acting as an adsorbent of CO_2. On the other hand, Ag is a well-known cocatalyst for the photocatalytic and electrochemical conversion of CO_2[18-21,27,28], although in this study we observed that Ag(3.0 wt%)/Ta_2O_5 (*via* IMP) exhibited very little activity in terms of CO evolution. The selectivity toward CO evolution also depended on the loading of Ag cocatalyst for the photocatalytic conversion of CO_2 by H_2O over Ag/SrO(0.5mol%)/Ta_2O_5 (*via* IMP) as shown in Figure 7. In the absence of the Ag cocatalyst, a significant amount of H_2 evolution was observed compared to CO. With the addition of a small quantity of the Ag cocatalyst, H_2 evolution was clearly suppressed, although the expected amount of CO was evolved, resulting in an observed enhancement of the selectivity toward CO evolution. This was a surprising result, as the inclusion of a Ag cocatalyst is known to improve the reduction of CO_2 into CO. It has

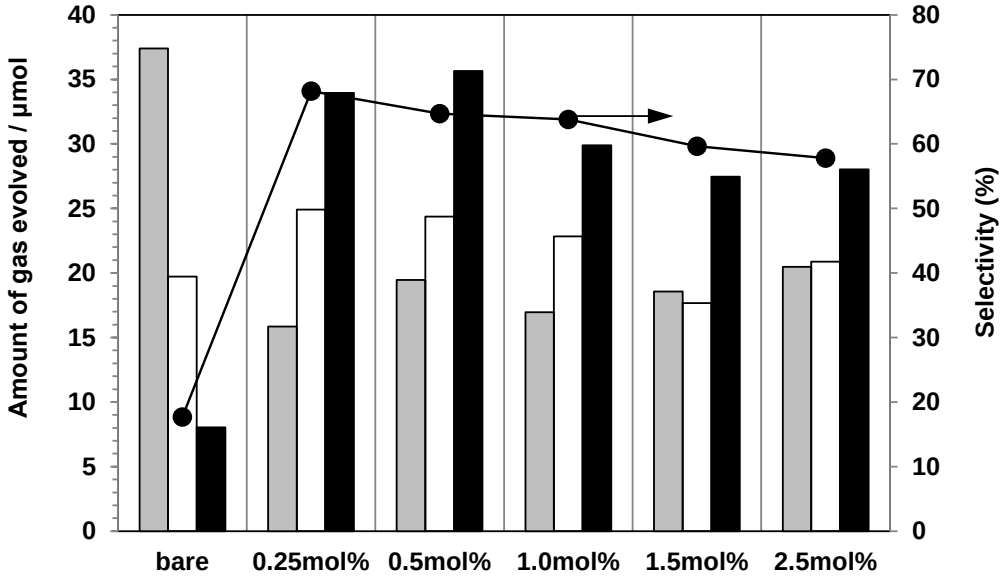

Figure 6 Dependence of evolution of H_2 (gray), O_2 (white) and CO (black) on loading amount of SrO for the photocatalytic conversion of CO_2 by H_2O over Ag(3.0wt%)/SrO/Ta_2O_5 (*via* IMP).

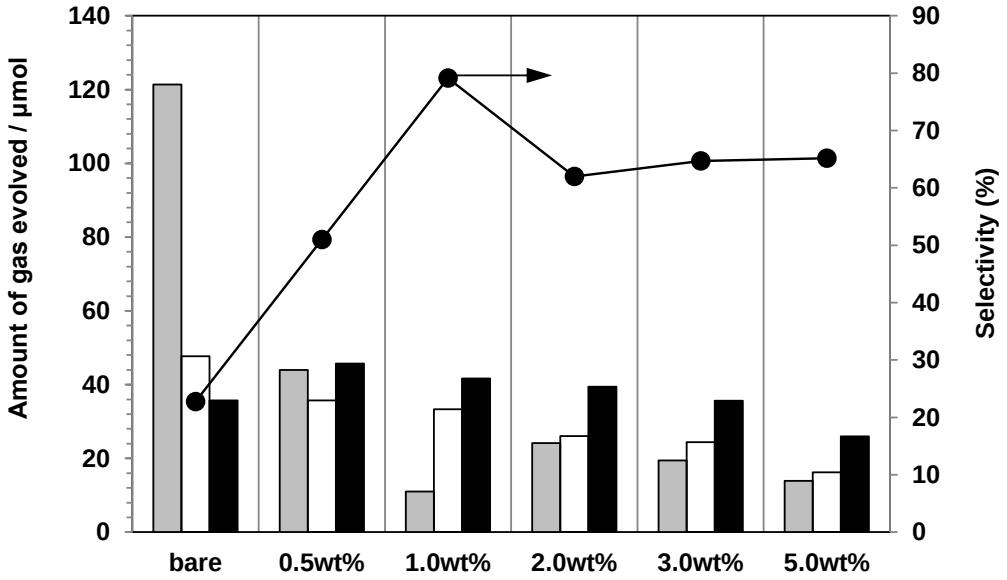

Figure 7 Dependence of evolution of H_2 (gray), O_2 (white) and CO (black) on loading amount of Ag for the photocatalytic conversion of CO_2 by H_2O over Ag/SrO(0.5mol%)/Ta_2O_5 (*via* IMP).

been reported that RuO_2 and NiO-modified Ta_2O_5 exhibits activity for overall water splitting.[29,30] In this study, Ag(3.0 wt%)/Ta_2O_5 (*via* IMP) (Figure 6) exhibited lower

activity than SrO(0.5mol%)/Ta_2O_5 (Figure 7), and so at present, we are driven to believe that the Ag cocatalyst is involved not only in the enhancement of the reduction of CO_2 into CO, but also in the suppression of the production of H_2 from H_2O. However, in this case, we observed only the suppression of the production of H_2 from H_2O and can therefore conclude that Ag is not particularly effective as a promoter to produce CO on Ta_2O_5.

That said, we do not deny that a Ag cocatalyst does improve the reduction of CO_2 into CO. Figure 8 shows the amount of H_2, O_2, and CO evolved for the photocatalytic conversion of CO_2 by H_2O over Ag(3.0 wt%)/SrO(0.5 mol%)/Ta_2O_5 prepared *via* various Ag modification methods after 5 h of photoirradiation. Activity, measured as the total amount of H_2 and CO evolved, and selectivity toward CO evolution were vastly different among the 4 Ag modification methods (*i.e.* IMP, CR, EP, and PD). Ag/SrO/Ta_2O_5 (*via* PD) showed the best activity; however, a stoichiometric amount of O_2 evolution was not recorded. The best selectivity toward CO evolution was 64.7% over a Ag/SrO/Ta_2O_5 system (*via* IMP). In this case, a stoichiometric amount of O_2 was evolved. The use of both Ag/SrO/Ta_2O_5 (*via* CR) and Ag/SrO/Ta_2O_5 (*via* EP) showed relatively lower activity and selectivity toward CO evolution, and O_2 evolution was not stoichiometric, as observed with Ag/SrO/Ta_2O_5 (*via* PD). Accordingly, only Ag/SrO/Ta_2O_5 (*via* IMP) exhibited high selectivity toward CO evolution with the evolution of a stoichiometric amount of O_2. We expect that the difference depends on both the physical and chemical properties of the Ag cocatalyst. TEM images of Ag(3.0 wt%)/SrO(0.5 mol)/Ta_2O_5, shown in Figure 9, clearly demonstrate that there were differences in the size of the Ag nanoparticles on the surface of SrO/Ta_2O_5 among the 4 different kinds of Ag/SrO/Ta_2O_5. Small Ag nanoparticles (<10 nm) were highly

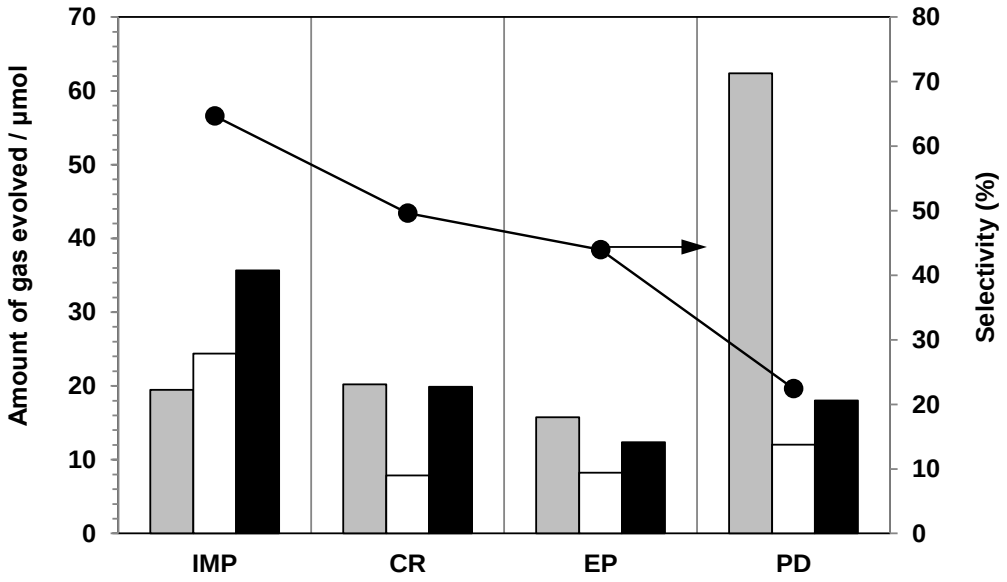

Figure 8 Amount of H_2 (gray), O_2 (white) and CO (black) evolved for the photocatalytic conversion of CO_2 by H_2O over Ag(3.0wt%)/MO(0.5mol%)/Ta_2O_5 by various Ag modification methods after 5 h of photoirradiation.

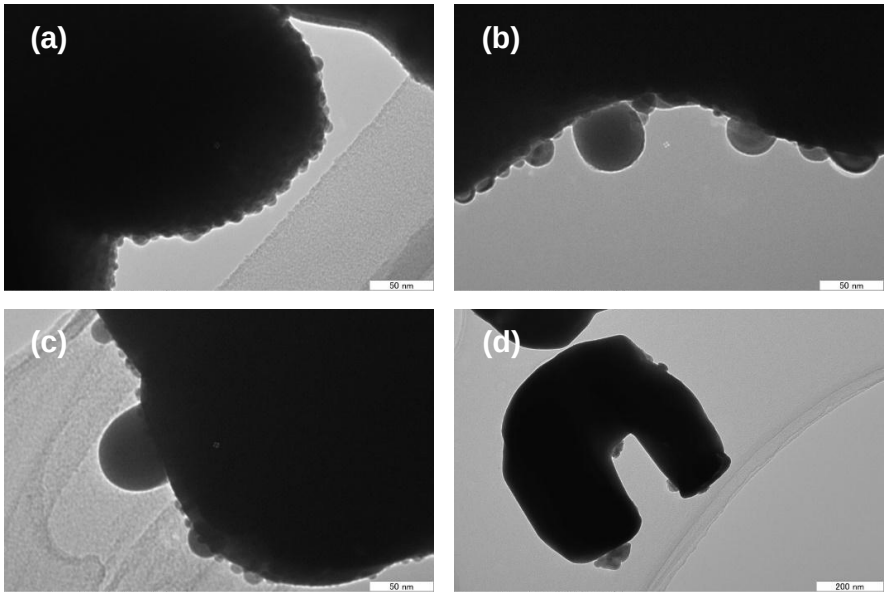

Figure 9 TEM images of Ag(3.0wt%)/SrO(0.5mol)/Ta_2O_5. Ag species were modified by (a) an impregnation method, (b) a chemical reduction method, (c) an electroless plating method, and (d) a photodeposition method.

dispersed in the case of Ag/SrO/Ta_2O_5 (*via* IMP), whereas the PD method gave only aggregated Ag particles (>50 nm) on the surface. In the cases of Ag/SrO/Ta_2O_5 (*via* CR) and Ag/SrO/Ta_2O_5 (*via* EP), both the small Ag nanoparticles and the aggregated Ag particles were observed.

These results were also confirmed by spectroscopic methods. Figure 10 shows the XANES spectra of Ag(3.0 wt%)/SrO(0.5 mol)/Ta_2O_5 with references. The XANES spectra of Ag/SrO/Ta_2O_5 (*via* CR), Ag/SrO/Ta_2O_5 (*via* EP), and Ag/SrO/Ta_2O_5 (*via* PD) were comparable with that of Ag foil, used as a reference. On the other hand, Ag/SrO/Ta_2O_5 (*via* IMP) showed a characteristic XANES spectrum, which was markedly different from those of the Ag foil and from the other Ag/SrO/Ta_2O_5 samples. A sharp absorption edge (as it is called “white line”) was observed at 25521 eV in the case of Ag/SrO/Ta_2O_5 (*via* IMP). The peak of the white line was located at much lower energy than that of Ag foil. Ag/SrO/Ta_2O_5 (*via* IMP) afforded the small amplitude of the EXAFS oscillation derived from the Ag nanoparticles. As a result, the Ag-Ag bond shell of Ag/SrO/Ta_2O_5 (*via* IMP) in the FT of EXAFS spectra was smaller than those of Ag/SrO/Ta_2O_5 (*via* CR), Ag/SrO/Ta_2O_5 (*via* EP), and Ag/SrO/Ta_2O_5 (*via* PD) as shown in Figure 11, indicating that the Ag nanoparticles were well dispersed on the surface of Ag/SrO/Ta_2O_5 (*via* IMP). A series of the XAFS data supported the result of TEM analysis. So far, we have discussed how the Ag cocatalyst improves the reduction of CO_2 into CO and suppresses the production of H_2 from H_2O. However, the aggregated Ag particles were found to actually enhance the evolution of H_2 (Ag/SrO/Ta_2O_5 (*via* PD)). It appears that the expectative effects in regard to the Ag cocatalyst are dependent on the size of Ag particles, and therefore it can be concluded that only the smaller Ag

particles contribute to the high selectivity toward CO evolution and the subsequent evolution of stoichiometric amount of O_2.

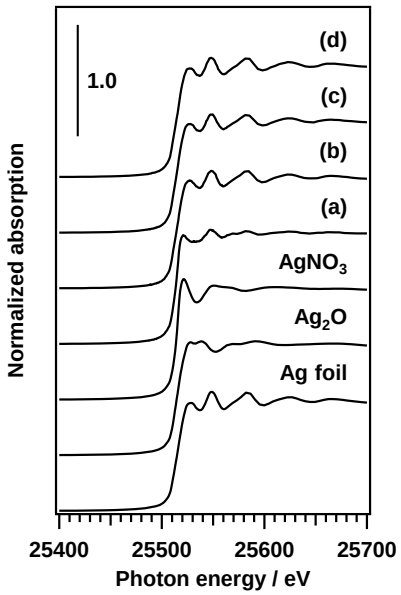

Figure 10 XANES spectra of Ag(3.0wt%)/SrO(0.5mol)/Ta_2O_5 with references. Ag species were modified by (a) an impregnation method, (b) a chemical reduction method, (c) an electroless plating method, and (d) a photodeposition method

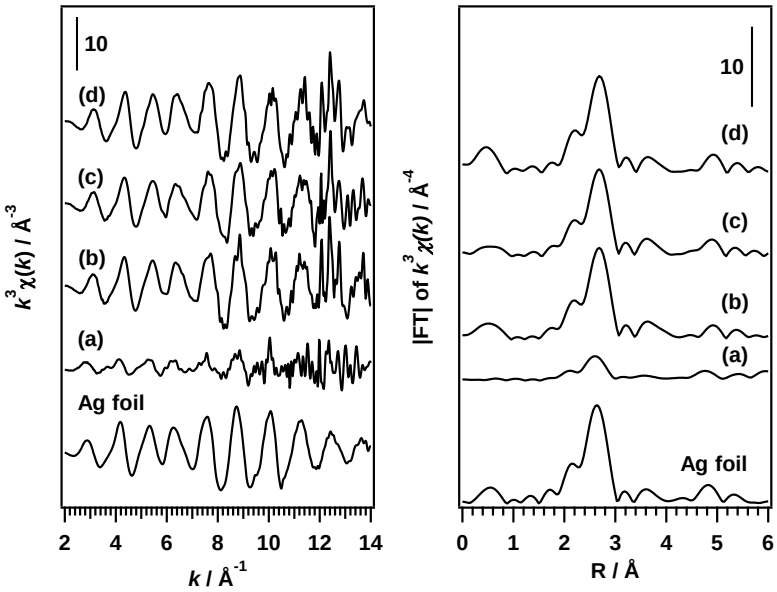

Figure 11 EXAFS spectra (left side) and FT of EXAFS spectra (right side) of Ag(3.0wt%)/SrO(0.5mol)/Ta_2O_5 with that of Ag foil as a reference. Ag species were modified by (a) an impregnation method, (b) a chemical reduction method, (c) an electroless plating method, and (d) a photodeposition method

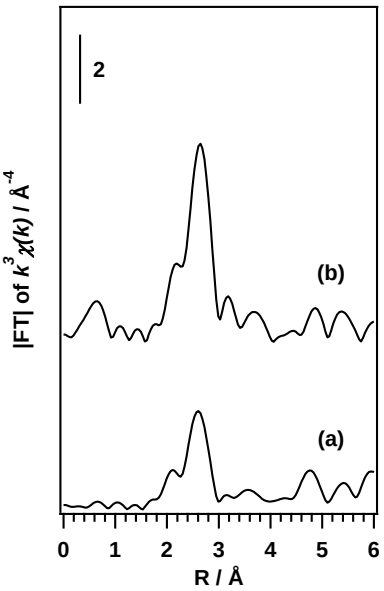

Figure 12 FT of EXAFS spectra of Ag(3.0wt%)/SrO(0.5mol)/Ta_2O_5 modified by an impregnation method (a) before and (b) after the reaction.

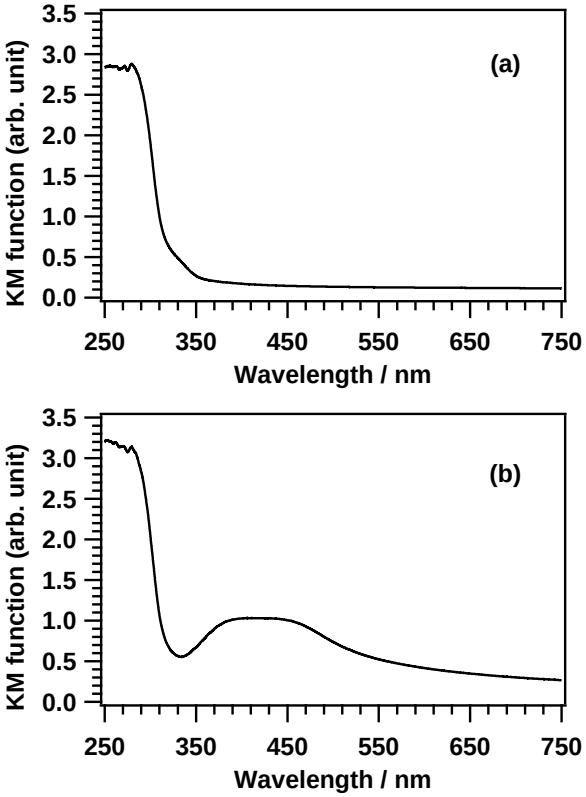

Figure 13 UV-Vis. Diffuse Reflectance spectra of Ag(3.0wt%)/SrO(0.5mol)/Ta_2O_5 modified by an impregnation method (a) before and (b) after the reaction.

As shown in Figure 4(b), the rate of formation of CO gradually decreased with increase of photoirradiation time. This can be also explained by the change in the size of Ag nanoparticles on the surface after the reaction. Figure 12 shows the FT of the EXAFS spectra of Ag(3.0 wt%)/SrO(0.5 mol)/Ta_2O_5 modified by an impregnation method before and after the reaction. The Ag-Ag bond shell increased in size following the reaction, indicating that the smaller Ag particles present before the reaction tend to aggregate into larger particles. The broad peak assigned to plasmon absorption was observed from 350-550 nm after the reaction, whereas before the reaction, no peak was observed (as shown in Figure 13). From our studies, we can therefore conclude that it is essential to prepare and modify robust and small Ag nanoparticles on the surface of SrO/Ta_2O_5 in order to obtain excellent selectivity toward CO evolution, stoichiometric amounts of O_2 evolution, and high conversion of CO_2 throughout the process.

Conclusion

Ag-loaded MO-modified Ta_2O_5 (M = Mg, Ca, Sr, or Ba) exhibited good photocatalytic activity and higher selectivity toward CO than Ag-loaded Ta_2O_5 in the conversion of CO_2 by H_2O to CO and O_2. The evolution of a stoichiometric amount of O_2 was observed in all reactions using Ag/SrO/Ta_2O_5 (prepared *via* IMP). The incorporation of SrO onto the surface of Ta_2O_5 afforded the best selectivity toward CO (65%) for the photocatalytic conversion of CO_2 by H_2O. It was determined that not only the Ag cocatalyst, but also SrO suppressed the reduction of protons into H_2, and as a result, much higher selectivity toward CO evolution was achieved over Ag/SrO/Ta_2O_5. The selectivity toward CO evolution was also dependent on the particle size of the Ag cocatalyst. Smaller Ag nanoparticles prepared *via* an impregnation method enhanced the generation of CO from CO_2 and suppressed the reduction of H^+ to H_2. On the other hand,

aggregated Ag particles prepared *via* a photodeposition method improved the H_2 evolution from H_2O. The systems discussed here could become essential in the fight to reduce CO_2 emissions over the coming years, and thus imperative in tackling one of the main cause of climate change.

References

[1] http://www.ipcc.ch/report/ar5/

[2] P. Markewitz, W. Kuckshinrichs, W. Leitner, J. Linssen, P. Zapp, R. Bongartz, A. Schreiber, T. E. Mueller, *Energy Environ. Sci.* **2012**, *5*, 7281.

[3] A. Sanna, M. Uibu, G. Caramanna, R. Kuusik, M. M. Maroto-Valer, *Chem. Soc. Rev.* **2014**, *43*, 8049.

[4] M. E. Boot-Handford, J. C. Abanades, E. J. Anthony, M. J. Blunt, S. Brandani, N. Mac Dowell, J. R. Fernández, M.-C. Ferrari, R. Gross, J. P. Hallett, R. S. Haszeldine, P. Heptonstall, A. Lyngfelt, Z. Makuch, E. Mangano, R. T. J. Porter, M. Pourkashanian, G. T. Rochelle, N. Shah, J. G. Yao, P. S. Fennell, *Energy Environ. Sci.* **2014**, *7*, 130.

[5] Y. Kohno, T. Tanaka, T. Funabiki, S. Yoshida, *J. Chem. Soc., Faraday Trans.* **1998**, *94*, 1875.

[6] Y. Kohno, T. Tanaka, T. Funabiki, S. Yoshida, *Phys. Chem. Chem. Phys.* **2000**, *2*, 5302.

[7] Y. Kohno, H. Ishikawa, T. Tanaka, T. Funabiki, S. Yoshida, *Phys. Chem. Chem. Phys.* **2001**, *3*, 1108.

[8] K. Teramura, T. Tanaka, H. Ishikawa, Y. Kohno, T. Funabiki, *J. Phys. Chem. B* **2004**, *108*, 346.

[9] K. Teramura, S.-i. Okuoka, H. Tsuneoka, T. Shishido, T. Tanaka, *Appl. Catal. B* **2010**,

96, 565.

[10] H. Tsuneoka, K. Teramura, T. Shishido, T. Tanaka, *J. Phys. Chem. C* **2010**, *114*, 8892.

[11] K. Teramura, S. Iguchi, Y. Mizuno, T. Shishido, T. Tanaka, *Angew. Chem., Int. Ed.* **2012**, *51*, 8008.

[12] S. Iguchi, K. Teramura, S. Hosokawa, T. Tanaka, *Catal. Today* **2014**, Ahead of Print 10.1016/j.cattod.2014.09.005.

[13] S. Xie, Y. Wang, Q. Zhang, W. Fan, W. Deng, Y. Wang, *Chem. Commun.* **2013**, *49*, 2451.

[14] S. Xie, Y. Wang, Q. Zhang, W. Deng, Y. Wang, *ACS Catal.* **2014**, *4*, 3644.

[15] L. Liu, C. Zhao, H. Zhao, D. Pitts, Y. Li, *Chem. Commun.* **2013**, *49*, 3664.

[16] L. Liu, C. Zhao, D. Pitts, H. Zhao, Y. Li, *Catal. Sci. Tech.* **2014**, *4*, 1539.

[17] Q. Li, L. Zong, C. Li, J. Yang, *Appl. Surf. Sci.* **2014**, *314*, 458.

[18] K. Iizuka, T. Wato, Y. Miseki, K. Saito, A. Kudo, *J. Am. Chem. Soc.* **2011**, *133*, 20863.

[19] T. Takayama, K. Tanabe, K. Saito, A. Iwase, A. Kudo, *Phys. Chem. Chem. Phys.* **2014**, *16*, 24417.

[20] K. Teramura, Z. Wang, S. Hosokawa, Y. Sakata, T. Tanaka, *Chem. Eur. J.* **2014**, *20*, 9906.

[21] Z. Wang, K. Teramura, S. Hosokawa, T. Tanaka, *Appl. Catal. B* **2015**, *163*, 241.

[22] A. Kudo, H. Kato, S. Nakagawa, *J. Phys. Chem. B* **2000**, *104*, 571.

[23] G. Busca, V. Lorenzelli, *Mater. Chem.* **1982**, *7*, 89.

[24] N. Ulagappan, H. Frei, *J. Phys. Chem. A* **2000**, *104*, 7834.

[25] M. Santoro, F. Gorelli, J. Haines, O. Cambon, C. Levelut, G. Garbarino, *Proc. Natl.*

Acad. Sci. USA **2011**, *108*, 7689.

[26] J. Baltrusaitis, J. Schuttlefield, E. Zeitler, V. H. Grassian, *Chem. Eng. J.* **2011**, *170*, 471.

[27] Y. Hori, K. Kikuchi, S. Suzuki, *Chem. Lett.* **1985**, 1695.

[28] M. Azuma, K. Hashimoto, M. Hiramoto, M. Watanabe, T. Sakata, *J. Electroanal. Chem. Interfacial Electrochem.* **1989**, *260*, 441.

[29] K. Sayama, H. Arakawa, *J. Photochem. Photobiol. A* **1994**, *77*, 243.

[30] Y. Takahara, J. N. Kondo, T. Takata, D. Lu, K. Domen, *Chem. Mater.* **2001**, *13*, 1194.

Summary

In this thesis, the photocatalytic conversion of CO_2 in and by H_2O over heterogeneous photocatalysts was studied. The general conclusion of this thesis is as follows:

In Chapter 1, we found that Ga_2O_3 photocatalysts exhibit the high conversion of CO_2, modification of Zn species into Ga_2O_3 supresses the H_2 evolution derived from overall water splitting, and consequently, Ag-loaded Zn-modified Ga_2O_3 exhibits higher selectivity toward CO evolution than does Ag-loaded bare Ga_2O_3. We observed stoichiometric amounts of O_2 being evolved together with CO. Mass spectrometry clarified that the carbon source of CO evolved was not the residual carbon species on the photocatalyst surface but was the CO_2 introduced in the gas phase. Modification of the photocatalyst with Zn is expected to establish the surface property that CO_2 can be adsorbed easily.

Chapter 2 describes that the selectivity toward CO evolution between CO and H_2 can be controlled by simply varying the addition of Zn species in the Ag-loaded Zn-modified Ga_2O_3 photocatalyst. The production of H_2 was gradually restrained with an increase of the amount of Zn species from 0.1 to 10.0 mol%, whereas the evolution of CO almost unchanged. The XRD, XAFS, and XPS measurements revealed that a $ZnGa_2O_4$ layer is generated on the surface of Ga_2O_3 by the modification with the Zn species. The formation of the $ZnGa_2O_4$ layer eliminated the proton reduction sites on Ga_2O_3, although the morphology, surface area and crystallinity of Ga_2O_3 did not change.

In Chapter 3, the photocatalytic conversion of CO_2 with H_2O using Ag-loaded Zn-modified Ga_2O_3 in the presence of various additives was investigated. The activity

for CO evolution was largely improved by the addition of Na_3PO_4, $NaHCO_3$, Na_2CO_3, and NaOH. The different alkaline chemicals in the reaction solutions also affected the formation of CO. The increase of $NaHCO_3$ content in the reaction solution dramatically enhanced the activity for the photocatalytic conversion of CO_2 with H_2O over Ag-loaded Zn-modified Ga_2O_3. Therefore, the highest formation rate of CO (171.0 μmol h^{-1}) was obtained in the $NaHCO_3$ solution with the concentration higher than 1.0 mol L^{-1}. According to equilibrium of carbon species (dissolved CO_2, HCO_3^-, and CO_3^{2-}), the major carbon species in the aqueous solutions of Na_3PO_4, $NaHCO_3$, Na_2CO_3, and NaOH was HCO_3^- during the photocatalytic reaction, which was related to the high activity for CO evolution. Moreover, the maintenance of the equilibrium between the dissolved CO_2 molecules and the HCO_3^- species was very important for the photocatalytic conversion of CO_2 with H_2O in the presence of weak acid salt and alkaline additives.

Chapter 4 shows that highly crystalline spinel phase $ZnGa_2O_4$ modified with a Ag cocatalyst exhibited high activity and selectivity toward CO evolution in the photocatalytic conversion of CO_2 using H_2O as a reductant under UV light irradiation. The stoichiometric evolution of CO, H_2, and O_2 clearly indicated that H_2O worked as an electron donor for the photoreduction of CO_2. The catalyst fabrication conditions, such as calcination temperature and duration, had a significant effect on the degree of crystallinity in the $ZnGa_2O_4$ at the expense of surface area, and the photocatalytic activity of the catalyst was maximized by optimizing the balance of these properties. Furthermore, the formation of metallic Ag particles with different sizes and dispersions on the surface of $ZnGa_2O_4$ influenced the evolution of CO. When Ag nanoparticles were loaded onto the $ZnGa_2O_4$ calcined at 1123 K for 40 h using the chemical reduction

method, the highest formation rates of CO, H_2, and O_2 (155.0, 8.5, and 74.3 μmol h^{-1}, respectively) were obtained, and the selectivity toward CO evolution reached 95.0%.

Chapter 5 reported that Ag-modified $La_2Ti_2O_7$ with a layered perovskite structure exhibits activity for the photocatalytic conversion of CO_2 to CO in pure water. The evolution of O_2 proves that H_2O works as an electron donor for the photocatalytic conversion of CO_2. CO was generated as the main product, and CO, H_2, and O_2 were produced in stoichiometric amounts. Maximization of the photocatalytic activity of $La_2Ti_2O_7$ was accomplished by making a trade-off between the crystallite size and surface area. In addition, the loading amount and modification method of the Ag cocatalyst also influenced the amount of CO evolved. An isotope labeling experiment using $^{13}CO_2$ confirmed that the origin of evolved CO was not the residual carbon species on the $La_2Ti_2O_7$ surface, but was rather the CO_2 gas that was introduced during the experimental process.

In Chapter 6, we found that incorporation of alkaline earth metal oxides into Ag-loaded Ta_2O_5 (Ag/Ta_2O_5) suppresses the H_2 production from overall water splitting for the photocatalytic conversion of CO_2 by using H_2O as an electron donor. Four different combinations of the photocatalysts ($Ag/MO/Ta_2O_5$ (M = Mg, Ca, Sr, or Ba)) were utilized; of these, the highest amount of CO was generated over Ag-loaded SrO-modified Ta_2O_5 ($Ag/SrO/Ta_2O_5$) with the evolution of a stoichiometric amount of O_2. It was demonstrated that the presence of low quantities of SrO considerably enhanced the selectivity toward CO evolution. We also confirmed that a Ag cocatalyst increased the selectivity toward CO evolution and relatively small Ag nanoparticles maximized the selectivity toward CO evolution. It was therefore concluded that the particle size of the Ag cocatalysts should be controlled, and alkaline earth metal oxides

should be introduced into Ag/Ta_2O_5 in order to achieve high conversion of CO_2 and good selectivity toward O_2 evolution.

In short, the energy shortage and environmental related problems are becoming the worsening worldwide problems and the great challenges for human in the 21st century. The photocatalytic conversion of CO_2 to useful chemical products is a promising route to impact the global carbon balance. The author found that the photocatalytic conversion of CO_2 in and by water could proceed over Zn-modified Ga_2O_3, $ZnGa_2O_4$, $La_2Ti_2O_7$, and SrO-modified Ta_2O_5 photocatalysts. CO was evolved as the main product for the reduction of CO_2 and H_2 production from overall water splitting was largely suppressed. The simultaneous evolution of O_2 in a stoichiometric ratio proved that H_2O could function as an electron donor during the photocatalytic conversion of CO_2 with H_2O. Among all the photocatalysts, Zn-modified Ga_2O_3 and $ZnGa_2O_4$ exhibited the highest activity and selectivity towards CO evolution. According to the investigation, we demonstrated that the photocatalytic activity and selectivity for the conversion of CO_2 in and by H_2O largely depends on the crystallization and the surface modification of photocatalysts. Generally, these results are expected to contribute to the development of the photocatalytic conversion of CO_2 in and by H_2O, which is considered as the “Artificial Photosynthesis”.

Appendix

Characterization of Cu nanoparticles on TiO_2 photocatalysts fabricated by electroless plating method

Abstract

Cu-modified TiO_2 photocatalysts (Cu/TiO_2) were fabricated by electroless plating and wet impregnation methods. Photocatalytic activity for H_2 production over Cu/TiO_2 by electroless plating method was higher than that over Cu/TiO_2 by impregnation method. Characterization of Cu nanoparticles by HRTEM, STEM-EDX, XRD and XAFS was studied. As compared to the wet impregnation method, the electroless plating method resulted in the formation of Cu nanoparticles with small size and uniform distribution on the TiO_2 surface, which caused the enhancement of H_2 production. XAFS measurement provided the evidences for the chemical state change of Cu species during the photocatalytic reaction. The process that Cu species varied from Cu^{2+} into Cu^0 via Cu^{1+} as the intermediate under photoirradiation is very important for the H_2 production, which indicates that the metallic Cu nanoparticles acted as the active sites and restrained the photogenerated charges recombination.

Introduction

Development of clean renewable energy resources attracts a great deal of attention all over the world due to exhaust of fossil fuels and environmental problems. H_2 is not only an important industrial chemical but also one of the most attractive candidates for the clean renewable energy resources. In addition, solar light is known to be an inexhaustible natural energy source. It is important to convert the solar energy into the chemical energy like H_2 to solve the energy and environmental problems. Photocatalytic splitting of water and reforming of biomass and bio-derivatives are considered as promising ways to realize the sustainable H_2 production.

In this scenario, TiO_2 is certainly one of the most famous photocatalysts for H_2 production, but the photocatalytic efficiency for H_2 production over bare TiO_2 is low, largely owing to the fast recombination of electron and hole pairs.[1] Indeed, the modification of metal nanoparticles, such as Pt, Pd, Au, Rh, Ni, Cu or Ag, on the TiO_2 surface has been proven to restrain charge recombination and enhance photocatalytic activity for H_2 production.[2-6] In comparison to noble metals, Cu is much less costly and shows similar enhancement of TiO_2 activity for the H_2 production.[7,8] Therefore, Cu/TiO_2 exhibits the huge potential for the photocatalytic H_2 production.

The activity of photocatalytic H_2 production over Cu/TiO_2 largely depends on the structure of Cu nanoparticles on the surface of TiO_2.[7,9] Obviously, it is influenced by the fabrication method. Most of Cu/TiO_2 photocatalysts are synthesized by the conventional wet impregnation method,[7,9-11] which usually causes the aggregation of Cu. Electroless plating technique is an important industrial method to generate metal particles or films on various supports with uniform distribution and good physiccochemical properties,[12-14] which is successfully applied in the fabrication of

printed and integrated electronic circuitry and membranes for hydrogen separation. To our knowledge, electroless plating method is seldom utilized to fabricate photocatalysts.

In addition, Cu species on the surface of TiO_2 are composed of multiple chemical states, such as Cu^0, Cu^{1+} and Cu^{2+}. Some reports have investigated the effect of chemical state of Cu species on promoting the photocatalytic H_2 production. Bandara et al.[15] discussed that CuO loaded on TiO_2 functioned as the cocatalyst to promote photocatalytic H_2 production from the water-methanol solution. However, Foo et al.[11] compared the photocatalytic performance of reduced Cu nanoparticles and oxidized Cu nanoparticles on TiO_2. Their data suggested that phase transformation from Cu oxide into metallic Cu affected the activity of H_2 production. Gombac et al.[9] also demonstrated that the CuO_x particles on TiO_2, which were reduced under photoirradiation in the glycerol solution, could facilitate the electrons trapping. Therefore, it is interesting to provide some insights into the chemical state change of nano-sized Cu during the photocatalytic reaction.

In this study, we employ the electroless plating and wet impregnation methods to fabricate Cu/TiO_2 photocatalysts and compare their photocatalytic performances for H_2 production from methanol solution. In particular, by using HRTEM, STEM-EDX, XRD and XAFS measurements, we investigate the structural feature and chemical state change of Cu nanoparticles modified on TiO_2 before, during and after photocatalytic reaction. The relationship of the structure and chemical state of Cu nanoparticles to the photocatalytic activity is also discussed.

Experimental section

Anatase TiO_2 (ST-21) with 50 m^2/g of surface area was supplied by Ishihara Sangyo Kaisya, Ltd. The chemical reagents used in the experiment were analytical

grade and made by Wako Pure Chemical Industries, Ltd. Cu nanoparticles modified onto TiO_2 were prepared by electroless plating and wet impregnation methods. In both samples, the loading amount of Cu is adjusted to 5% by weight.

Electroless plating method is a simple method to deposit metal on the surface of a conductive, semiconductive or nonconductive substrate by an oxidation-reduction reaction without an external electric source. In order to exclude effect of TiO_2 particle size, TiO_2 used as a substrate for the electroless plating process was calcined at 773 K for 3 h in advance. Before the plating Cu nanoparticles on the surface of TiO_2, TiO_2 was subjected to alkaline cleaning (1 M NaOH solution) at 343 K for 15 min, then acid cleaning (25 vol.% H_2SO_4 solution) at 308 K for 15 min, sensitizing (20 g/l $SnCl_2$ and 40 ml/l HCl solution) at 303 K for 10 min, activating (0.25 g/l $PdCl_2$ and 0.5 ml/l HCl solution) at 318 K for 25 min, and finally drying at 383 K for 20 h. The purpose of pretreatment was to make the TiO_2 surface clean and provide catalytic centers on TiO_2 for deposition of Cu nanoparticles.

The pretreated TiO_2 was introduced into the chemical copper plating solution containing 0.04 M $CuSO_4$, 0.08 M EDTA•4Na, 0.08 M HCHO and 5 ppm pyridine. The temperature of plating solution was maintained at 343 K and pH was adjusted to 12.5, with stirring constantly for 30 min. After several rinsing procedures with distilled water, the sample was dried at 383 K for 24 h. The Cu-modified TiO_2 by the electroless plating method is denoted as Cu/TiO_2-EP.

As for the Cu-modified TiO_2 by the wet impregnation method denoted as Cu/TiO_2-IMP, the preparation was carried out as the following procedure. TiO_2 powder was added into $Cu(NO_3)_2$ solution. The suspension was then stirred at 353 K for 1 h followed by evaporation to dryness. Finally, the dried sample was calcined at 773 K for

3 h.

The photocatalytic H_2 production was carried out in a closed circulating system connected to a vacuum line, using Pyrex glass with a flat glass ceiling window for illumination. Pyrex glass can block the irradiation shorter than 300 nm, which causes the decomposition of methanol by photolysis. The prepared Cu/TiO_2 sample (20 mg) was dispersed in 10 vol% methanol solution (4 ml). After being degassed three times with the freeze-pump-thaw method, the suspension was illuminated by a 200 W Hg-Xe lamp (San-Ei Electric Co., Ltd., UVF-204S Type B) equipped with fiber optics, a collective lens, and a mirror. The gas product was analyzed by TCD gas chromatography (GC-8A chromatograph, Shimadzu Corp.) equipped with a Molecular Sieve 5A column.

In order to characterize Cu/TiO_2 after the photocatalytic reaction, the used Cu/TiO_2 was recycled from reaction solution and dried in the air atmosphere at room temperature for two days.

UV-Vis DRS were measured by a JASCO Corporation V-670 diffused reflectance spectrometer equipped with an integrating sphere, using the diffuse reflection method and $BaSO_4$ as a reference to measure all the samples. HRTEM images were obtained with a JEOL JEM-2100F transmission electron microscope (TEM) operating at an accelerating voltage of 200 kV. Samples for the TEM measurement were prepared by depositing drops of a methanol suspension containing small amounts of the powders onto a carbon-coated molybdenum grid (Okenshoji Co. Ltd.) and allowing the methanol to evaporate in air. X-ray diffraction pattern (XRD) of the Cu/TiO_2 photocatalyst was measured by a Rigaku Multi Flex powder X-ray diffractometer.

XAFS (X-ray absorption fine structure spectroscopy) spectra were recorded at

the BL01B1 beamline of the SPring-8 synchrotron radiation facility, Japan. An adequate amount of Cu/TiO_2 photocatalyst was dispersed in a Pyrex glass photoreactor containing 10 vol% methanol solution. After purging the air in the reactor with pure N_2, the suspension was irradiated for different time using a 200 W Hg-Xe lamp. In order to avoid any oxidation of Cu species, the suspension was filtered in a glovebox full of N_2. Then the reduced Cu/TiO_2 was dried and sealed into polyethylene bags under N_2 atmosphere. Cu K-edge XAFS spectra were measured in the fluorescence mode. For Cu/TiO_2 before and after reaction and reference samples (Cu foil, Cu_2O, and CuO), spectra were recorded in the transmission mode. A fixed exit Si(111) double crystal monochromator was used in the measurement and beam intensity was measured before and after samples by ionization chambers. The X-ray energy was calibrated with a spectrum of Cu foil at 8977.7 eV. The XANES and EXAFS analyses were performed by a Rigaku REX2000 program. Pattern fittings of XANES spectra of Cu/TiO_2 irradiated at different time were implemented using the spectra of Cu foil, Cu_2O, and CuO in the energy range of 8950−9010 eV. Fourier transform of EXAFS spectra was carried out in the 3.0-14.0 $Å^{-1}$ regions.

Results and Discussion

Figure 1 shows the time course of H_2 production from methanol solution under UV irradiation in the presence of Cu/TiO_2 photocatalysts fabricated by the electroless plating and wet impregnation methods. A certain difference in the activity of the two samples was observed. In the induction period (the initial 30min), the rate of H_2 production was climbing up step by step for both samples and simultaneously the brown photocatalysts turned into black colour. As compared to Cu/TiO_2-IMP, the amount of evolved H_2 over Cu/TiO_2-EP increased more rapidly in this period. Then the evolution

of H_2 linearly increased with prolonging the irradiation time. The photocatalytic activity of Cu/TiO_2-EP was higher than that of Cu/TiO_2-IMP. After 3 h irradiation, the reaction system was degassed by the freeze-pump-thaw procedure and the UV light illumination started again. It is noted that the induction period disappeared and both photocatalysts showed the linear increment for H_2 production. The activity of Cu/TiO_2-EP reached the former level, while Cu/TiO_2-IMP performed a slight increase in H_2 production after 3 h.

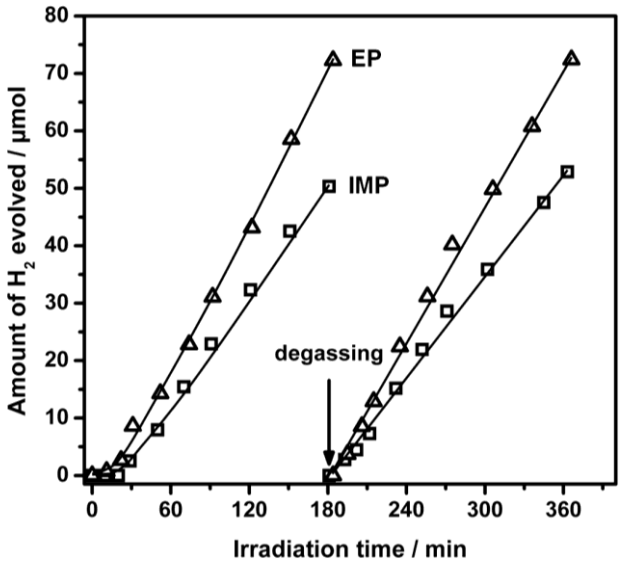

Figure 1 Time course of photocatalytic H_2 production over Cu/TiO_2 fabricated by electroless plating (red triangle) and wet impregnation (blue square) methods.

The similar UV-Vis diffused reflectance spectra before and after the photocatalytic reaction showed that the light absorption could not influence the photocatalytic activity of Cu/TiO_2-EP and Cu/TiO_2-IMP. The surface structure and morphology of Cu-modified photocatalysts before and after the photocatalytic reaction have been investigated by means of HRTEM and STEM-EDX. From the HRTEM image of Cu/TiO_2-EP before reaction shown in Figure 2(a), it is apparent that Cu nanoparticles with semispherical shape were highly dispersed on the surface of TiO_2

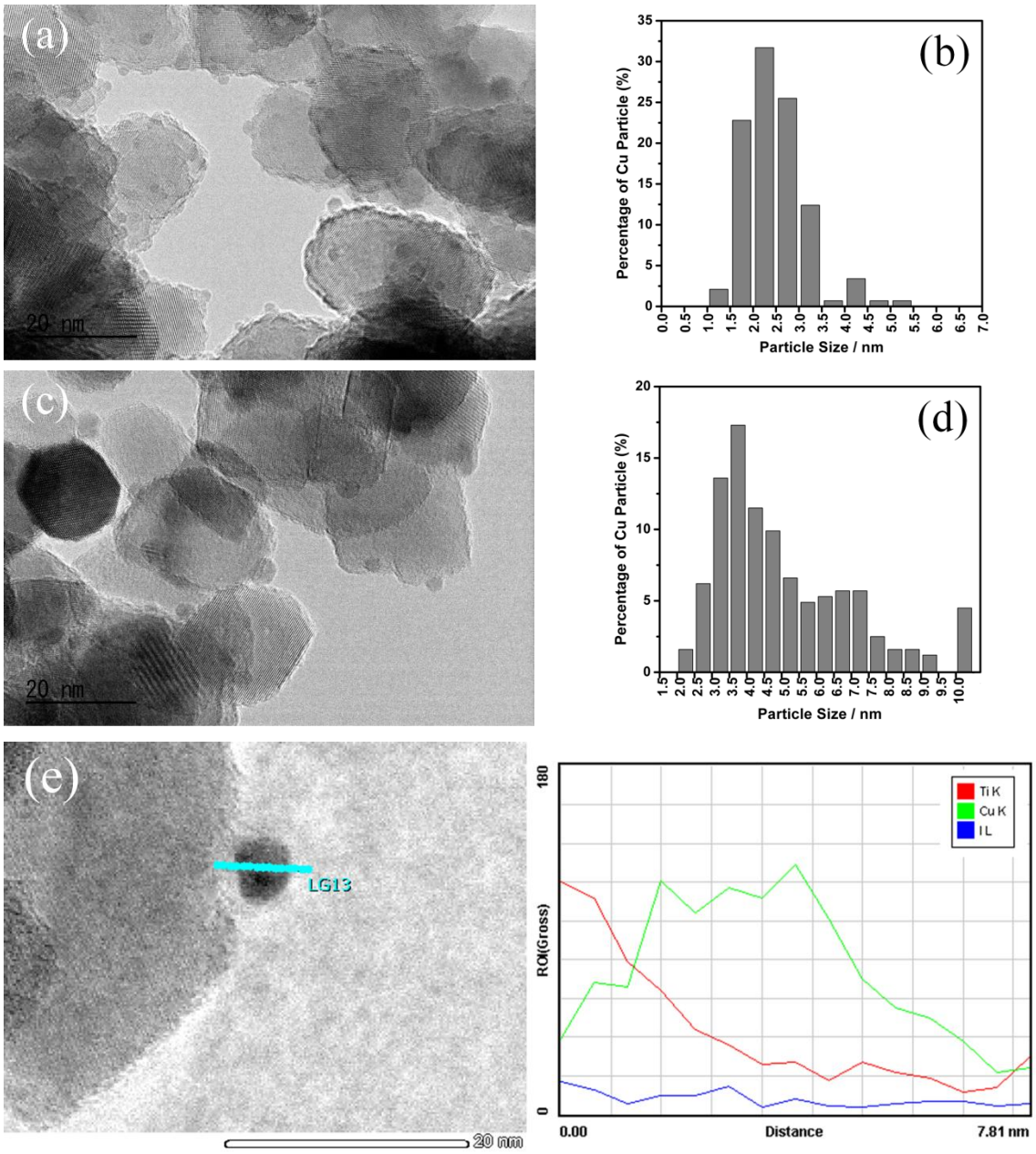

Figure 2 HRTEM images of Cu/TiO2-EP before (a) and after (c) the photocatalytic reaction and the particle size distribution of Cu/TiO_2-EP before (b) and after (d) the reaction. STEM-EDX image of Cu/TiO_2-EP is reported in (e).

particles and contacted well with TiO_2. STEM-EDX image with line scanning mode (Figure 2(e)) also evidences the existence of Cu nanoparticle on TiO_2. Meaningfully, Figure 2(b) summarizes the narrow Cu particle size distribution for Cu/TiO_2-EP, it can be determined that the average Cu particle size was 2.5 nm. Just due to the generation of

Cu nanoparticles with small size and uniform dispersion on the surface of TiO_2 by the electroless plating method, the photocatalytic activity for H_2 production from methanol

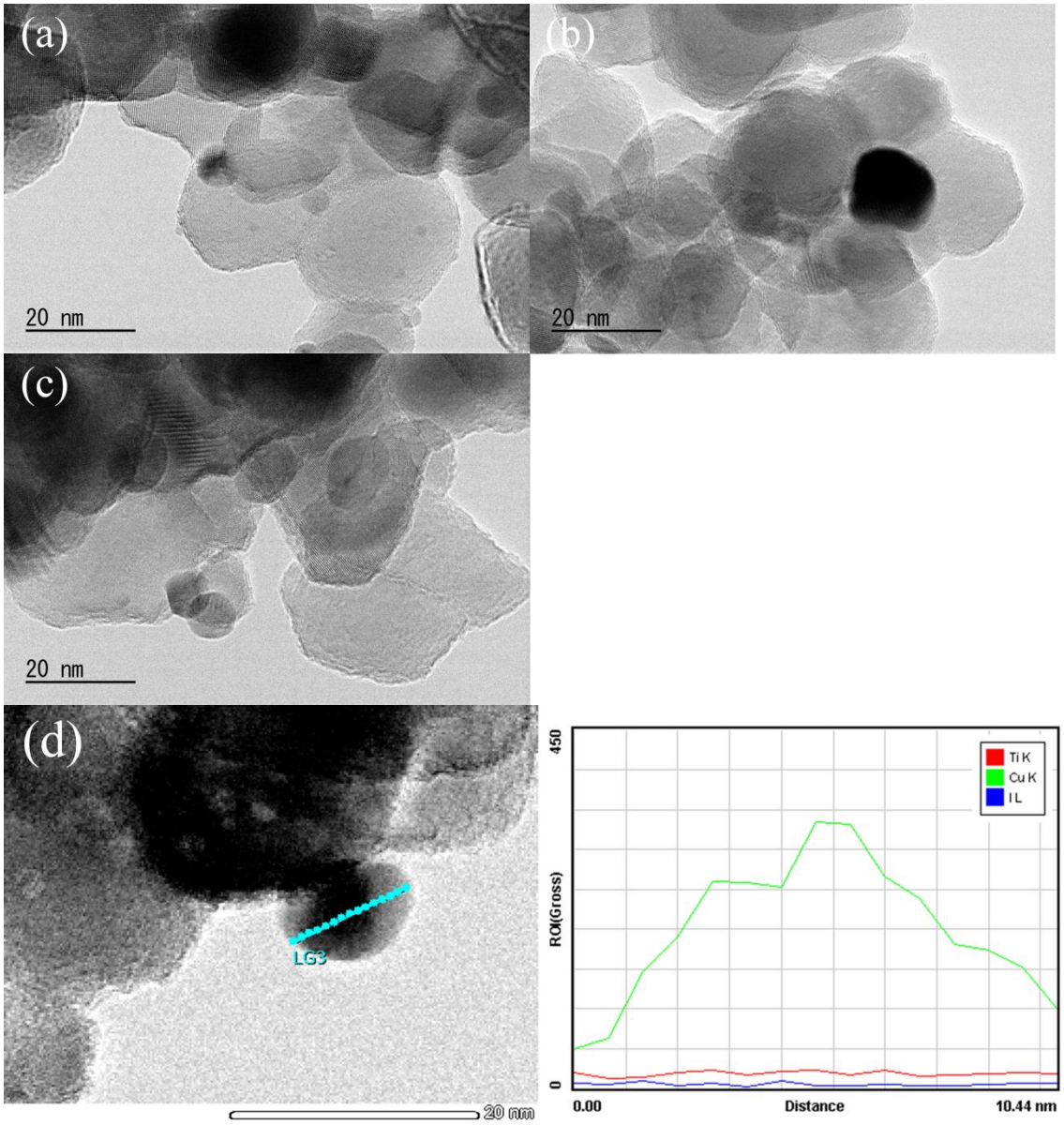

Figure 3 HRTEM images of Cu/TiO_2-IMP before (a,b) and after (c) the photocatalytic reaction and STEM-EDX image (d) of Cu/TiO_2-IMP.

solution was largely improved. Moreover, Cu/TiO_2-EP after reaction still showed well dispersion of small Cu nanoparticles in Figure 2(c), although the Cu particle size distribution became slightly wider than that before reaction and much larger Cu

particles were found (Figure 2(d)). It is believed that electroless plating method could facilitate the formation of stable Cu nanoparticles on photocatalysts. In contrast, HRTEM and STEM-EDX images in Figure 3 show that wet impregnation method resulted in the aggregation of Cu particles and poor Cu dispersion on TiO_2. The Cu particle size of Cu/TiO_2-IMP before and after reaction (Figure 3(a) and (c)) was found to be much bigger as compared with Cu/TiO_2-EP. Occasionally, the particle as large as 16.8 nm was also observed in Figure 3(b). Therefore, Cu/TiO_2-IMP exhibited lower photocatalytic activity than Cu/TiO_2-EP.

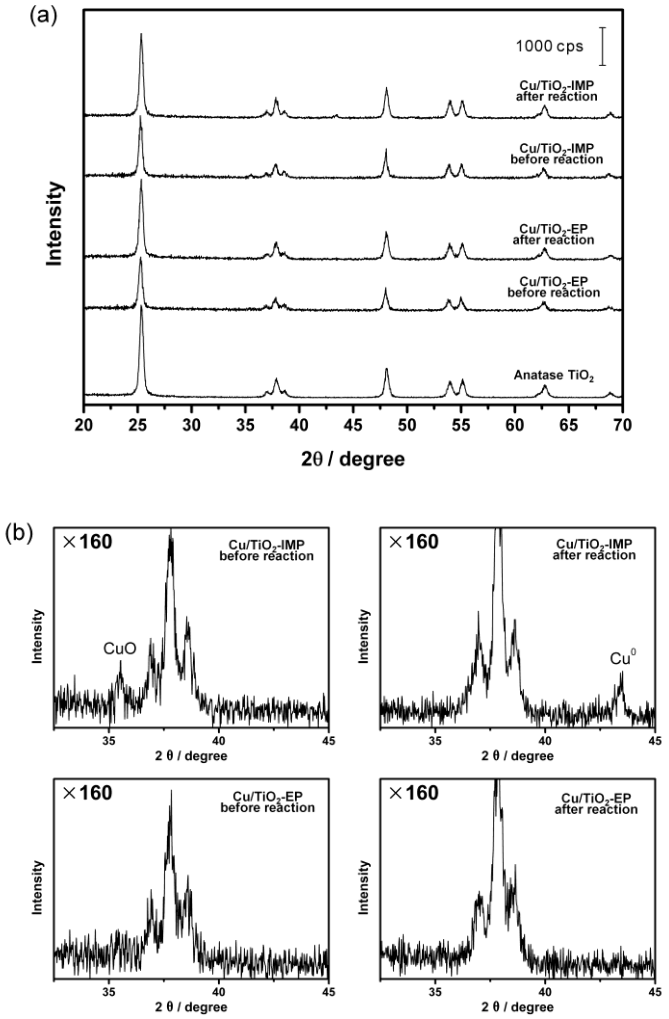

Figure 4 XRD patterns (a) of Cu/TiO_2 photocatalysts and TiO_2 and enlargement (b) of panel a.

XRD patterns of Cu/TiO_2-EP and Cu/TiO_2-IMP before and after the photocatalytic reaction are shown in Figure 4. All samples exhibited the characteristic peaks of anatase TiO_2 (Figure 4(a)). In the Figure 4(b), the diffraction peaks attributed to Cu nanoparticles were not detected for Cu/TiO_2-EP before and after reaction. According to the HRTEM and STEM-EDX results, it was the small size and uniform dispersion of Cu nanoparticles on TiO_2, which caused the low identification from XRD patterns. However, in the patterns of Cu/TiO_2-IMP, a diffraction peak at 35.5 ° ascribed to CuO was observed before the photocatalytic reaction and a diffraction peak at 43.4 ° which can be assigned to metallic Cu appeared after reaction, indicating that Cu particles were aggregated on TiO_2 and experienced the reduction process under UV light irradiation.

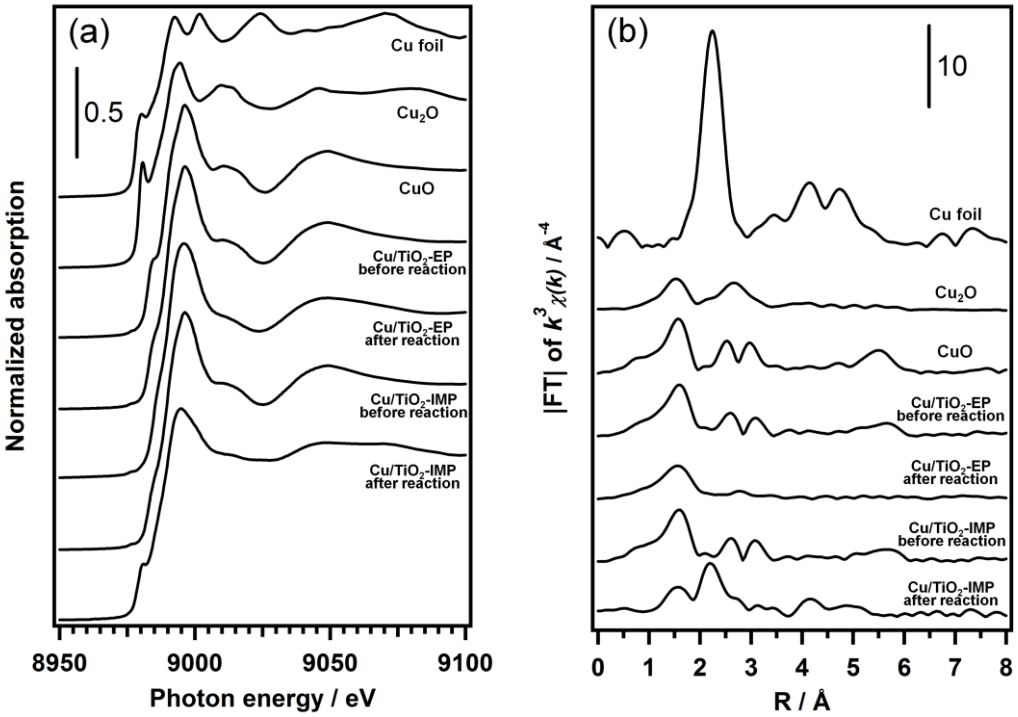

Figure 5 Cu K-edge XANES (a) and Fourier transformed EXAFS (b) spectra of Cu/TiO_2 before and after the photocatalytic reaction.

XAFS measurements were employed to analyze the Cu phases before and after

the photocatalytic reaction and to provide the evidences for the chemical state change of Cu species during the photocatalytic reaction under UV light irradiation. Figure 5 shows the Cu K-edge XANES and Fourier transformed Cu K-edge EXAFS spectra of Cu/TiO_2 before and after the photocatalytic reaction with Cu foil, Cu_2O and CuO as the references. The XANES spectra of Cu/TiO_2-EP before and after reaction were similar to that of CuO. In the corresponding EXAFS, the first Cu-O shell peaks of Cu/TiO_2-EP before and after reaction located at the characteristic distance of bulk CuO. Because the nano-sized Cu species are easy to be deeply oxidized upon exposure to air even at room temperature, Cu nanoparticles synthesized by the electroless plating method showed a CuO phase before and after the photocatalytic reaction. On the other hand, the Cu species in Cu/TiO_2-IMP changed from Cu^{2+} before the reaction into Cu^0/Cu^{2+} after the reaction, which is owing to the reduction of Cu species during the photocatalytic reaction and partial oxidation of the aggregated Cu particles in the air atmosphere after the reaction. The XAFS features of Cu/TiO_2 before and after reaction are well in accordance with HRTEM and XRD results.

The chemical state of Cu species at different irradiation time during the reaction was measured using "in situ" XAFS. Since the valence of Cu is sensitive to the environment, it is necessary to keep the irradiated Cu/TiO_2 samples in N_2 atmosphere during XAFS measurement. Figure 6 shows the Cu K-edge XANES spectra of Cu/TiO_2-EP and Cu/TiO_2-IMP depending on different irradiation time. The XANES spectra of Cu/TiO_2-EP and Cu/TiO_2-IMP at 0 min of photoirradiation were similar to that of CuO. As the irradiation time was prolonged, a discernible shift to lower energy of the absorption edge and a decrease of the white line peak were clearly observed in both cases, indicating that reduction of Cu^{2+} to Cu^0 proceeded gradually under the UV

light irradiation. The XANES spectrum of Cu_2O exhibits an intense pre-edge peak due to the 1s→4p transition around 8980 eV, which is a characteristic of Cu^{1+}.[16,17] This

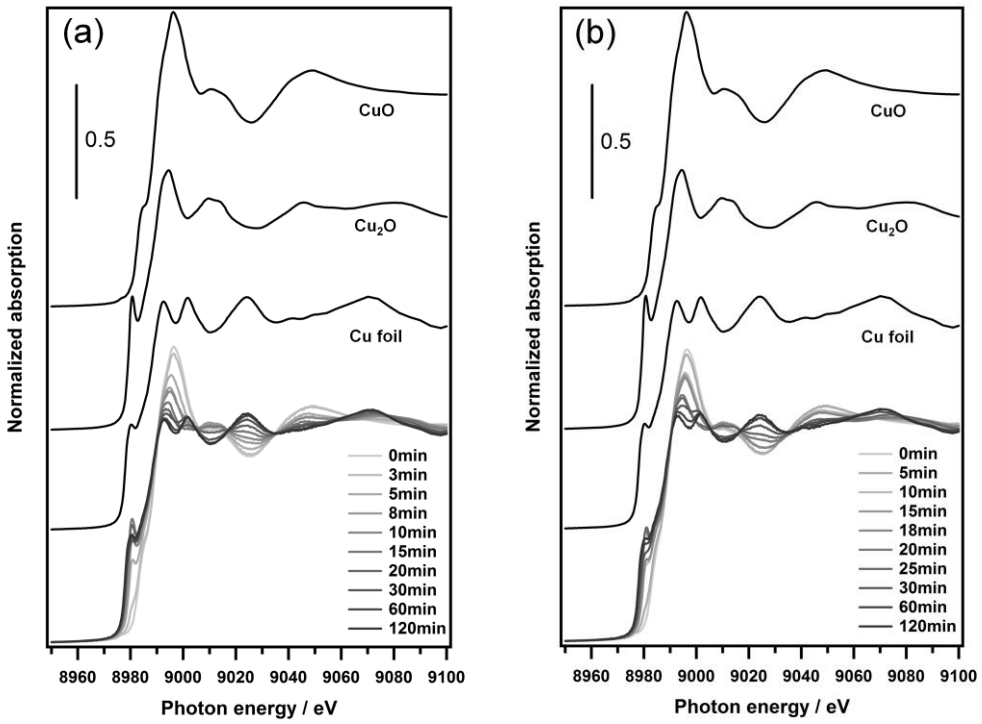

Figure 6 Cu K-edge XANES spectra of Cu/TiO_2-EP (a) and Cu/TiO_2-IMP (b) at different irradiation time.

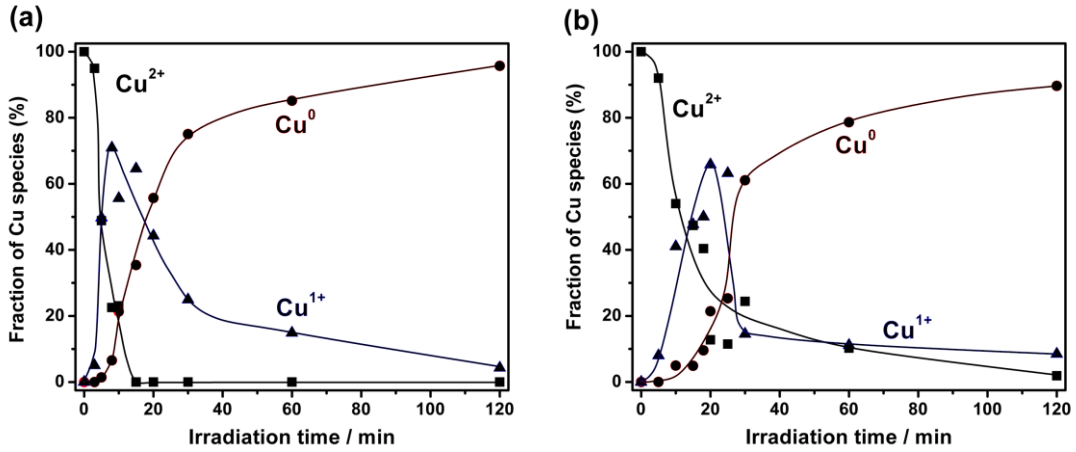

Figure 7 Fractions of Cu species in Cu/TiO_2-EP (a) and Cu/TiO_2-IMP (b) estimated by pattern fittings of the XANES spectra as a function of irradiation time.

feature began to appear after 5 min irradiation for Cu/TiO_2-EP, which was five minutes earlier than that for Cu/TiO_2-IMP. This simply indicates the presence of Cu^{1+} species in

the two samples as an intermediate to Cu^0 species. The first derivative analysis also confirms stepwise reduction of Cu^{2+} to Cu^{1+} and Cu^0 corresponding to the respective irradiation time. The fractions of Cu species in Cu/TiO_2 were then estimated by pattern fitting analysis of the XANES spectra (Figure 7). Significant reduction of CuO to Cu_2O and metallic Cu under photoirradiation occurred from 0 min to 8 min for Cu/TiO_2-EP, then the fraction of CuO disappeared at 15min. When the irradiation time extended from 15 min to 120 min, the fraction of Cu_2O decreased and the portion of metallic Cu rose to the level of 95.7%. In the case of Cu/TiO_2-IMP, the maximum fraction of Cu_2O appeared at 20 min and the portion of metallic Cu increased with a decrease of the fractions of Cu_2O and CuO. At 120 min of photoirradiation, the portion of metallic Cu reached to 89.6% and CuO and Cu_2O still existed in Cu/TiO_2-IMP. Therefore, the change in the fractions as a function of UV light irradiation time represents the stepwise reduction of Cu^{2+} to Cu^0 through Cu^{1+} as the intermediate.

The Fourier-transformed EXAFS spectra of Cu/TiO_2 irradiated for different time are shown in Figure 8. It is clearly observed that, the height of the Cu-O shell peak at the characteristic distance of bulk CuO decreased with an increase of the height of the Cu-Cu shell peak at the characteristic distance of bulk Cu metal. These trends are in accordance with the drawdown of Cu^{2+} fraction and the stepwise rise of the Cu^0 portion represented in Figure 7. The distance of the Cu-O bond slightly decreased with extending the irradiation time. The Fourier-transformed EXAFS of the reference compounds indicate that Cu_2O has a shorter distance of Cu-O shell than CuO. Therefore, the decrease in Cu-O bond length could be attributed to the appearance of Cu_2O. In the spectra of Cu/TiO_2-EP, the Cu-Cu bond of metallic Cu appeared at 8 min of photoirradiation and the Cu-O bond absolutely disappeared after 120 min. As for

Cu/TiO_2-IMP, the Cu-Cu shell peak of metallic Cu emerged at 18 min and the Cu-O shell peak still existed after 120 min. These differences reveal that the reduction of Cu species to metallic Cu in Cu/TiO_2-EP during the photocatalytic reaction proceeded more quickly and deeply than that in Cu/TiO_2-IMP.

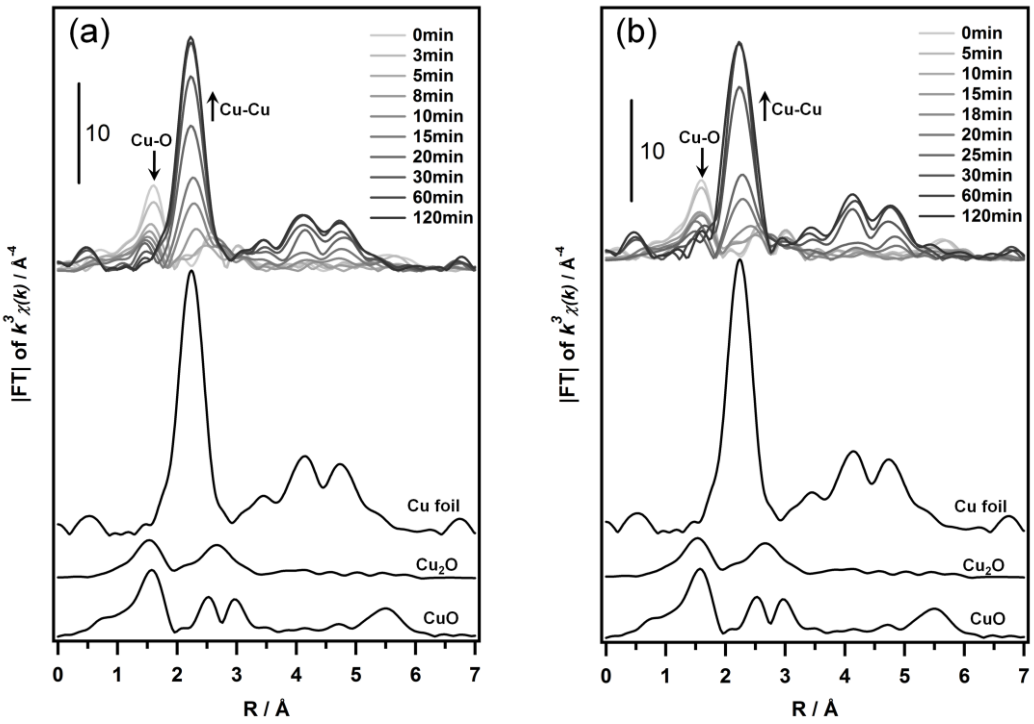

Figure 8 Fourier transformed EXAFS spectra of Cu/TiO_2-EP (a) and Cu/TiO_2-IMP (b) at different irradiation time.

In the photocatalytic H_2 production using Cu-modified TiO_2,[9,10,15] it has been proposed that the absorption of photons by TiO_2 triggers off the reaction, leading to the generation of electron/hole pairs. The separation of electrons and holes is promoted by the capture of electrons in Cu cocatalyst and by the interaction of holes with sacrificial reagents, such as methanol. The electrons trapped in the Cu cocatalyst subsequently reduce H^+ to H_2. In this study, it is known that the Cu species prepared by the electroless plating and impregnation methods experienced the reduction process from Cu^{2+} to Cu^0 via Cu^{1+} as the intermediate under photoirradiation during the

photocatalytic reaction. Therefore, a number of photogenerated electrons were consumed by the reduction of Cu species in the induction period. Once the metallic Cu appeared on TiO_2, the large amount of H_2 was produced steadily on Cu^0 site. The disappearance of the induction period and the slight increase of H_2 production in the second run also confirm that the metallic Cu functioned as the active sites. In addition, our Cu/TiO_2-EP photocatalyst showed the higher activity for H_2 production than Cu/TiO2-IMP. It is noted that the electroless plating method facilitated the formation of Cu nanoparticles with small size and uniform distribution as compared to the impregnation method. Hence, the well-dispersed Cu nanoparticles were easily reduced into metallic Cu under photoirradiation and exposed a significant number of Cu^0 sites for H_2 production. Accordingly, both the chemical state change of Cu species and the structure of Cu nanoparticles could affect the photocatalytic activity of Cu-modified TiO_2.

Conclusion

We fabricated Cu/TiO_2 photocatalysts by electroless plating and wet impregnation methods. Cu/TiO_2-EP exhibited higher photocatalytic activity for H_2 production than Cu/TiO_2-IMP. HRTEM, STEM-EDX and XRD show that the electroless plating method resulted in the formation of Cu nanoparticles with small size and uniform distribution on the TiO_2 surface, while the impregnation method caused the aggregation of Cu particles. XAFS measurement proves that the chemical state of Cu species varied from Cu^{2+} into Cu^0 via Cu^{1+} as the intermediate under photoirradiation during the photocatalytic reaction, which indicates that the metallic Cu acted as the active sites and restrained the photogenerated charges recombination. In general, the nano-sized and well-dispersed Cu species were easily reduced into metallic Cu and

enhanced the photocatalytic activity for H_2 production.

References and Notes

[1] M. Ni, M.K.H. Leung, D.Y.C. Leung, K. Sumathy, *Renew. Sust. Energ. Rev.* **2007**, *11*, 401.

[2] Y.Z. Yang, C.H. Chang, H. Idriss, *Appl. Catal. B* **2006**, *67*, 217.

[3] T. Sreethawong, S. Yoshikawa, *Catal. Commun.* **2005**, *6*, 661.

[4] T. Sreethawong, Y. Suzuki, S. Yoshikawa, *Int. J. Hydrogen Energy* **2005**, *30*, 1053.

[5] G. Colón, M. Maicu, M.C. Hidalgo, J.A. Navío, *Appl. Catal. B* **2006**, *67*, 41.

[6] N. Alenzi, W-S. Liao, P. S. Cremer, V. Sanchez-Torres, T. K. Wood, C. Ehlig-Economides, Z. Cheng, *Int. J. Hydrogen Energy* **2010**, *35*, 11768.

[7] S.P. Xu, J.W. Ng, X.W. Zhang, H.W. Bai, D. D. Sun, *Int. J. Hydrogen Energy* **2010**, *35*, 5254.

[8] J.G. Yu, J.R. Ran, *Energy Environ. Sci.* **2011**, *4*, 1364.

[9] V. Gombac, L. Sordelli, T. Montini, J. J. Delgado, A. Adamski, G. Adami, M. Cargnello, S. Bernal, P. Fornasiero, *J. Phys. Chem. A* **2010**, *114*, 3916.

[10] H.J. Choi, M. Kang, *Int. J. Hydrogen Energy* **2007**, *32*, 3841.

[11] W.J. Foo, C. Zhang, G.W. Ho, *Nanoscale* **2013**, *5*, 759.

[12] E. Natividad, E. Lataste, M. Lahaye, *Surf. Sci.* **2004**, *557*, 129.

[13] H.F. Chang, M. A. Saleque, W.S. Hsu, W.H. Lin, *J. Mol. Catal. A* **1996**, *109*, 249.

[14] C. Fukuhara, Y. Kamata, A. Igarashi, *Appl. Catal. A* **2005**, *296*, 100.

[15] J. Bandara, C.P.K. Udawatta, C.S.K. Rajapakse, *Photochem. Photobiol. Sci.* **2005**, *4*, 857.

[16] L.S. Kau, D.J. Spirasolomon, J. E. Penner-Hahn, K. O. Hodgson, E. I. Solomon, *J. Am. Chem. Soc.* **1987**, *109*, 6433.

[17] N. Kosugi, H. Kondoh, H. Tajima, H. Kuroda. *Chem. Phys.* **1989**, *135*, 149.

List of Publications

Chapter 1

A Doping Technique Suppressing Undesirable H_2 Evolution Derived from Overall Water Splitting in Highly Selective Photocatalytic Conversion of CO_2 in and by Water

Kentaro Teramura, **Zheng Wang**, Saburo Hosokawa, Yoshihisa Sakata, Tsunehiro Tanaka

Chemistry-A European Journal, **2014**, *20*, 9906-9909

Chapter 2

Tuning the selectivity toward CO evolution in the photocatalytic conversion of CO_2 by H_2O through the modification of Ag-loaded Ga_2O_3 with a $ZnGa_2O_4$ layer

Zheng Wang, Kentaro Teramura, Saburo Hosokawa, Yoshihisa Sakata, Tsunehiro Tanaka

Submitted to Chemical Science

Chapter 3

Effect of additives on the photocatalytic conversion of CO_2 by H_2O over Ag-loaded Zn-modified Ga_2O_3

Zheng Wang, Kentaro Teramura, Saburo Hosokawa, Tsunehiro Tanaka

Submitted to Catalysis Science & Technology

Chapter 4

Highly efficient photocatalytic conversion of CO_2 into CO using H_2O as a reductant over Ag-modified $ZnGa_2O_4$

Zheng Wang, Kentaro Teramura, Saburo Hosokawa, Tsunehiro Tanaka

Submitted to Chemical Science.

Chapter 5

Photocatalytic conversion of CO_2 in water over Ag-modified $La_2Ti_2O_7$

Zheng Wang, Kentaro Teramura, Saburo Hosokawa, Tsunehiro Tanaka

Applied Catalysis B: Environmental, **2015**, *163*, 241-247.

Chapter 6

Photocatalytic Conversion of CO_2 by H_2O over Ag-loaded SrO-modified Ta_2O_5

Kentaro Teramura, Hiroyuki Tatsumi, **Zheng Wang**, Saburo Hosokawa, TsunehiroTanaka

Bulletin of the Chemical Society of Japan, doi:10.1246/bcsj.20140385.

Appendix

Characterization of Cu Nanoparticles on TiO_2 Photocatalysts Fabricated by Electroless Plating Method

Zheng Wang, Kentaro Teramura, Tetsuya Shishido, Tsunehiro Tanaka

Topic in Catalysis, **2014**, *57*, 975-983.